The double-edge effect of second-phase particles on the recrystallization behaviour and associated mechanical properties of metallic materials

Ke Huang [1]*, Knut Marthinsen[2], Qinglong Zhao[3], Roland E. Logé[1]

[1] Thermomechanical Metallurgy Laboratory – PX Group Chair, Ecole Polytechnique Fédérale de Lausanne (EPFL), CH-2002 Neuchâtel, Switzerland

[2] Department of Materials Science and Engineering, Norwegian University of Science and Technology, N-7491 Trondheim, Norway

[3] Key Laboratory of Automobile Materials, Ministry of Education and Department of Materials Science and Engineering, Jilin University, Changchun 130025, PR China

*Corresponding author: Email address: huangke0729@hotmail.com (K. Huang)

This paper has now been formally published:

Progress in Materials Science

Volume 92, March 2018, Pages 284-359

https://doi.org/10.1016/j.pmatsci.2017.10.004

Abstract

Most industrial alloys contain a matrix phase and dispersed second-phase particles. Several thermomechanical processing (TMP) steps are usually needed to produce a final product, during which recrystallization and its related phenomena may take place. Second-phase particles may *retard* or *accelerate* recrystallization, depending on their size and spatial distribution, the TMP conditions, among others. Besides their effect on recrystallization kinetics, the introduction of second-phase particles creates additional interfaces within the matrix, it also modifies the grain structure and crystallographic texture after recrystallization, which then either *improves* or *deteriorates* the associated mechanical properties of the investigated materials. The interactions between second-phase particles and recrystallization are further complicated when these particles are not stable. In addition to particle coarsening, they can also precipitate out or dissolve into the matrix before, simultaneously with or after recrystallization. This review article attempts to summarize the recent progresses on the complex interaction between second-phase particles and recrystallization and the science behind them. This double-edge effect of second-phase particles on recrystallization behaviour and mechanical properties of metallic materials is still far from being clear. A better understanding of this issue is of high academic and industrial interests, since it provides potential freedom for TMP design and microstructure control.

Keywords: Recrystallization, Second-phase particles, Precipitation, Nucleation, Crystallographic texture, Mechanical properties

Table of Contents

TABLE OF CONTENTS **3**

1. INTRODUCTION **5**

2. CHARACTERIZATION OF SECOND-PHASE PARTICLES AND RECRYSTALLIZATION **8**

2.1 SECOND-PHASE PARTICLES 8

2.1.1 Classification of second-phase particles *8*

2.1.2 Characterization of particles *9*

2.1.3 Solute, voids, pores/gas bubbles *12*

2.2 RECRYSTALLIZATION 12

2.2.1 Classification of recrystallization *13*

2.2.2 Characterization of recrystallization *15*

2.3 HOW SECOND-PHASE PARTICLES AFFECT RECRYSTALLIZATION 18

3. THE EFFECT OF SECOND-PHASE PARTICLES ON DEFORMATION MICROSTRUCTURE AND TEXTURE **20**

3.1 EFFECT OF SECOND-PHASE PARTICLES ON DEFORMATION MICROSTRUCTURE 20

3.2 EFFECT OF SECOND-PHASE PARTICLES ON DEFORMATION TEXTURE 24

3.3 EFFECT OF SECOND-PHASE PARTICLES ON SEVERE PLASTIC DEFORMATION AT ROOM TEMPERATURE 26

3.4 DEFORMATION INDUCED EVOLUTION OF SECOND-PHASE PARTICLES 30

3.5 NUMERICAL MODELLING 34

4. THE EFFECT OF SECOND-PHASE PARTICLES ON RECRYSTALLIZATION **37**

4.1 EFFECT OF FINE DISPERSOIDS ON RECRYSTALLIZATION 37

4.1.1 Zener pinning principle *37*

4.1.2 On grain boundary migration during recrystallization *40*

4.1.3 On nucleation of recrystallization *49*

4.2 EFFECT OF COARSE PARTICLES ON RECRYSTALLIZATION 54

4.2.1 Mechanism of Particle Stimulated Nucleation (PSN) *54*

4.2.2 Acceleration of recrystallization and grain refinement by PSN *60*

4.2.3 Orientation of PSN nucleated grains *62*

4.3 BIMODAL SECOND-PHASE PARTICLES STRUCTURE 65

4.3.1 On grain size *65*

4.3.2 On recrystallization kinetics *70*
4.4 Interaction between recrystallization and precipitation 72
4.4.1 Precipitation prior to recrystallization *73*
4.4.2 Concurrent precipitation *76*
4.4.3 Precipitation after recrystallization *79*
4.5 Effect of unstable second-phase particles 80
4.5.1 Dissolution and coarsening of second-phase particles *81*
4.5.2 Change of particle/matrix coherency *83*
4.6 Numerical modelling 90
4.6.1 Recrystallization with bimodal particle structures *90*
4.6.2 Recrystallization with concurrent precipitation *94*
5. THE EFFECT OF SECOND-PHASE PARTICLES AND RECRYSTALLIZATION ON MECHANICAL PROPERTIES 98
5.1 Mechanical properties associated with second-phase particles and recrystallization 98
5.1.1 Yield strength *98*
5.1.2 Ductility *101*
5.1.3 Other properties *105*
5.2 Controlling mechanical properties of particle-containing metallic materials 109
5.2.1 Control of grain size *109*
5.2.2 Control of crystallographic texture *112*
5.2.3 Control of particles *114*
6. INDUSTRIAL APPLICATIONS 117
6.1 High temperature alloys 117
6.2 Additive manufacturing 121
6.3 Superplastic metallic materials with ultrafine-grained structure 124
6.4 Traditional applications 127
7. SUMMARY AND FUTURE WORK 131
7.1 Summary 131
7.2 Existing unresolved problems and future outlooks 132
ACKNOWLEDGEMENTS 134
APPENDIX A. ABBREVIATIONS 135
APPENDIX B. SYMBOLS 138
REFERENCES 142

1. Introduction

A very large part of metallic materials, which often contain a matrix phase and dispersed second-phase particles, are used in the wrought form. Several thermomechanical processing (TMP) steps are usually needed to produce an intermediate or final product for these materials, during which recrystallization and its related phenomena such as work hardening, recovery and grain growth may take place, all of which are strongly affected by second-phase particles. These interconnected metallurgical reactions, occurring concurrently or sequentially, need to be carefully controlled to obtain desired microstructures, which dictate the mechanical properties of the final products.

Recrystallization was defined by Doherty et al. [1] as "the formation of a new grain structure in a deformed material by the formation and migration of high angle grain boundaries driven by the stored energy of deformation". Second-phase particles may modify the stored energy of deformation and hence the driving force for recrystallization, they can also significantly alter the formation and migration of high angle grain boundaries (HAGBs) [2]. These particles, either stable or unstable, formed prior to, after or concurrently with the recrystallization, leading to complex interactions with the recrystallization process.

Recrystallization and its interaction with second-phase particles is not a recently-discovered phenomenon, a considerable amount of data is available in the literature on this topic. The publications on the interaction between second-phase particles and recrystallization are steadily increasing, with more than 300 papers published last year, according to Web of Science. The most comprehensive review on recrystallization was performed by top experts in this field in 1997 [1]. The effect of second-phase particles on recrystallization was summarized in great details in the excellent textbook on recrystallization by Humphreys and Hatherly in 2004 [2]. Since then, new characterization techniques [3,4], as well as multi scale numerical modelling schemes [4,5,6], have greatly advanced our understanding on this topic. Apart from its academic value, the interaction of recrystallization with second-phase particles has also come to be of considerable industrial importance, as will be further discussed in the later sections. This topic clearly merits an updated review paper covering the significant progress that has been made

during the last decade. Recrystallization and its related phenomena were recently summarized by Raabe [4] as a chapter in the fifth edition of Physical Metallurgy published in 2014, however the effect of second-phase particles on recrystallization was only briefly mentioned. Detailed review papers subsequently highlighted static [7,8] and dynamic recrystallization [9,10], respectively, with influences from second-phase particles again not thoroughly considered. It follows that the effect of second-phase particles on recrystallization and mechanical properties has not been systematically emphasized by any of these later mentioned textbooks and review papers.

Due to its complexity, the effect of second-phase particles on recrystallization behaviour is usually analysed in a simplified fashion. In terms of finely dispersed particles, their effect on recrystallization is routinely considered by applying a dragging force on grain boundary migration using the classical Zener pinning theory [11], assuming spherical and randomly distributed stable particles. Improved Zener pinning theories are occasionally employed, but recent publications with this effect being totally neglected can still be found. The effects of these fine particles on nucleation of recrystallization, on the driving force for recrystallization, as well as on the mechanical properties of the material after recrystallization have not been equally emphasized. On the other hand, the effect of coarse second-phase particles (>1μm) on recrystallization has been almost exclusively focused on particle stimulated nucleation (PSN), which usually results in accelerated recrystallization kinetics, fine grain size and a near random texture. Apart from its effect on microstructure evolution, the introduced particle-matrix interface also affects the mechanical properties such as strength, elongation and fracture. The mixture of both fine and coarse particles in the same material, which is usually the case in commercial alloys, makes it difficult to identify their individual contribution on recrystallization behaviour. An appropriate control of these two different types of particles during recrystallization could in principle lead to tailored microstructures. However, this is still not the case, due to our incomplete understanding on the complex effect of second-phase particles on recrystallization. A better understanding of their effect on recrystallization could provide potential freedom for thermo-mechanical process design and microstructure control in particle-containing metallic materials. Related work focusing on other types of materials such as intermetallic compounds [2,12] and mineral materials [13, 14] could also provide valuable information to help understanding the topic. The scale of this review, however, does not allow us to cover also these materials. For the same reason, recrystallization in dual-phase or composite

materials is not discussed, conventional alloys with low volume fraction of particles (<5%) is instead assumed unless specifically stated.

The objective of this review is to explore the recent progress on the double-edge effect of second-phase particles on recrystallization behaviour and associated mechanical properties of metallic materials, i.e., the retarding or acceleration effect on recrystallization kinetics, and the detrimental or beneficial effect on mechanical properties. Therefore, this review is substantially different from most available review papers focusing mainly on recrystallization [1,7,8,9,10]. As the first of its kind, we aim to cover not only the current state of this topic, but also its future trajectory. When required and appropriate it also includes more classical results, as a basis for discussing more recent progress.

This review paper is organized as follows. The characterization of second-phase particles and recrystallization is presented in Section 2. The interaction between second-phase particles with work hardening and recovery, which take place before the onset of recrystallization, is treated in Section 3. A detailed discussion on the interactions between second-phase particles and recrystallization is then given in Section 4. Section 5 is devoted to the mechanical properties associated with the second-phase particles and recrystallization; it also includes the tailoring of mechanical properties through control of the interactions between second-phase particles and recrystallization. Relevant examples of industrial applications guided by the above mentioned theory are provided in Section 6. Further studies within this topic are suggested in Section 7 before the final summary section. Numerical modelling efforts are also included in each section whenever relevant and available.

2. Characterization of second-phase particles and recrystallization

Before elaborating the details of the interaction between second-phase particles and recrystallization, it is convenient to briefly summarize the characterizations of second-phase particles and recrystallization, which could also serve as an introduction to this topic. Different terminologies used in this field are also explained.

2.1 Second-phase particles

2.1.1 Classification of second-phase particles

Second-phase particles can be dispersed into the matrix in different ways: coarse particles can be formed already during solidification [2, 15], while fine particles can be precipitated from the supersaturated solute atoms in the subsequent thermo-mechanical processing steps [16,17], or by internal oxidation [18,19], mechanical alloying [20] etc. Second-phase particles are classified into different categories, when discussed related to recrystallization, according to their characteristics such as size and spatial distribution, interface with host lattice, mechanical property effects etc.

The most common classification of second-phase particles with respect to recrystallization is made according to their sizes. In this classification, particles are separated into two groups: i) Coarse particles of size typically >1 μm; ii) Fine dispersoids of size ~10nm-300nm. These two classes of particles have strong effects on the recrystallization behaviour, with the coarser ones accelerating recrystallization through PSN and the finer ones retarding or even suppressing recrystallization, the details of which will be provided in later sections.

Particles are also frequently classified according to their spatial distributions. In many cases, particles are more or less randomly distributed within the matrix, a good example is the heat treatable Al-Cu system [21]. Particles can also be heterogeneously positioned at grain boundaries [22] and dislocations [23, 24], such regions usually have a higher free energy such that the formation of second-phase particles there minimizes the increase in surface energy. The lower activation energy for diffusion in these regions, as compared to bulk lattice diffusion, is another reason. Even when the size and volume fraction of particles are the same, the difference in spatial distribution of particles alone can lead to different pinning effects on moving boundaries [2,25].

A third classification is based on the interface characteristics between the particles and the host lattice. A coherent interface is formed when the particle and the matrix have a good atomic structure matching and the two lattices are continuous across the interface [26]. More often, the matching at the interface is not perfect, coherency is however maintained by a misfit strain (with a small surface energy) between the matrix and the particle, which gives rise to stress fields that hinder the movement of gliding dislocations. When the misfit strain becomes high enough, it is energetically favourable to form a semi-coherent interface with the particle where the mismatch is periodically taken up by misfit dislocations. As the size of particles further increases (~10nm-1μm), an incoherent interface usually forms where there is no matching at the interface. Coherent particles are more effective in pinning boundaries than incoherent ones [25, 27].

During deformation of particle-containing alloys, whether or not the particles are deformable is an important aspect related to the work hardening behaviour, as well as the subsequent recrystallization behaviour. During deformation of materials with non-deformable particles, dislocations start to bow around the encountered particles, a maximum shear stress is reached when the dislocation reaches the semi-circular configuration, after which the dislocation becomes unstable and tends to expand until an Orowan loop around the particles is formed. If the particle is not strong enough to withstand the shear stress applied on it by the incoming dislocation, then its size on the slip plane is reduced by the Burgers vector **b** of the dislocation due to the shear deformation, and subsequent dislocations tend to concentrate on the same plane.

While most of the particles encountered in metallic materials are crystalline and solid, amorphous [28] or liquid [29, 30] particles are also reported. One characteristic feature of these particles is that they may be mobile, i.e., they can travel with the migrating boundaries, especially at very high temperatures [28] and low driving force [31]. On the contrary, crystalline particles do not show measurable mobility up to the melting point of the matrix [28].

2.1.2 Characterization of particles

The quantitative characterization of second-phase particles was reported by Richmond et al. [32] in 1985 and the characterization of inclusions/particles in steels was detailed by Atkinson and Shi [33] in 2003. While the principles described in these earlier review papers are still valid, the fast development in characterization techniques since then calls for an update on this topic. However, we do not attempt here to describe the principles of each technique in details, as this is

out of the scope of this review. More thorough treatments can easily be found in standard textbooks as well as in the provided references in this section.

The most important particle parameters related to the recrystallization behaviour are their volume fraction, size, shape and spacing, which require direct quantitative characterization with image analysis methods. Optical microscopes can only be used to track relatively large second-phase particles due to their limited resolution (>0.2μm). In order to reveal finer particles, a scanning electron microscope (SEM) equipped with a backscattered electron (BSE) detector is frequently used. This is because the particles usually contain elements that have a different atomic number Z than the matrix, which results in recognizable dark and white areas and thus makes it possible to distinguish different phases. Particles can also be extracted from the matrix by using chemical or electrochemical methods [34]. If the spatial resolution offered by conventional SEM is still not satisfactory, a transmission electron microscope (TEM) must be used [e.g. 35]. Even though the measurements taken by SEM/BSE and TEM are usually considered as 2D in nature, the particles slightly below the examined surface can also be revealed by both techniques, since the electron beam can penetrate a thin layer in the sample. These techniques can be combined with automated focused ion beam (FIB) [36,37] or controlled serial sectioning [38,39, 40] to reveal the particles in full 3D; most of these methods are limited to a spatial resolution of ~50 nm and they are destructive. The spatial resolution of X-ray-based non-destructive methods [e.g. 41, 42] is even worse, i.e., 1-2μm [36], they are thus not appropriate for fine particle characterization. The atom probe tomography (APT) [43, 44] technique is the only one which allows single atom mapping in a 3D structure, its high accuracy, however, comes along with its limitation in sample dimension: only a few hundred nanometers [45].

Besides the above mentioned direct characterization of particle parameters, other quick but indirect techniques are often used to estimate the volume fraction and/or average size of particles with the sacrifice of their spatial distribution information. Differential scanning calorimetry (DSC) and isothermal calorimetry have been widely used to characterize precipitation of particles, its advantages and disadvantages are well summarized in Ref [46]. Another conventional way to estimate the volume fraction of particles consists in measuring the electrical resistivity of the investigated material [35, 47,48,49], in view that the precipitation of (incoherent) second-phase particles reduces the lattice distortion from solute atoms and thus decreases the

electrical resistivity. The effect of precipitated particles with spacing larger than 100 nm has negligible effect on electrical resistivity in aluminium alloys [50], i.e., this method becomes less accurate once dense fine dispersoids (<100 nm) are involved. Small-angle neutron/X-ray scattering (SANS/SAXS) [51,52,53,54,55] is very useful to obtain statistically reliable data on the average particle size (1-100 nm [56]), and number density and composition from a bulk specimen volume [57]. The SANS and SAXS techniques are similar in many ways, the main difference is that SAXS is easier to access and operate, and SANS is sensitive to light elements and is able to label isotopes which is useful in cases where the particles have similar atomic numbers with the matrix. They are mostly applied to alloy systems involving only one type of particle since a separation of the scattering contributions from different types of precipitates is difficult, even though a method to characterize particles for cases with several populations of particles has been proposed [58,59].

It should be pointed out, with regard to the interaction between particles and recrystallization, that "neither the theories nor the experimental results are currently of sufficient accuracy to warrant the use of very complicated parameters" [2]. Only one particle parameter is further discussed, i.e., its coherency with the host matrix, which is closely related to the recrystallization behaviour [60, 61, 62] and can be characterized by high resolution TEM [63,64]. For more details on the characterization of the coherency with the host matrix, the readers are referred to Refs [65,66]. The misfit strain between the coherent particle and host lattice is usually quite small and thus challenging to measure accurately, the effect of misfit generated elastic energy from coherent particles on grain boundary migration has been numerically studied [67]. A recent attempt has been made on the measurement of the misfit between β" particles and the Al matrix in the Al-Mg-Si alloy system using distortion-corrected high-resolution scanning transmission electron microscopy images [68]. The chemical composition of particles can also be determined, but this is not further discussed in the present review since it is not supposed to have a significant effect on the recrystallization behaviour.

More information can be obtained if the particles are characterized in-situ [57] or using appropriate combinations of the above mentioned techniques [59, 69,70]. For example, APT and SANS techniques [71, 72] can be complementary in that the former provides reliable data on particle composition and spatial distribution in a small volume, while the latter yields average particle parameters in larger bulk samples.

2.1.3 Solute, voids, pores/gas bubbles

While the focus of this review paper is on second-phase particles, other obstacles which have similar effect as second-phase particles on recrystallization and mechanical properties evolution are also briefly summarized in this section.

Solute elements are almost always present in most particle-containing conventional alloys, such as microalloyed steels [73,74], Al-Mg [75] or Al-Zn [76] alloys, Ni-S [77] or Ni-Fe alloys [78], Ni-based superalloys [79,80], Cu-Sn alloys [81] etc. They can interact with dislocations [82,83], lead to a sharp decrease in grain boundary apparent mobility [84, 85,86,87,88, 89, 90], affect the stacking fault energy of the materials [91], favour the formation of shear banding [92], and modify the recrystallization texture by promoting faster migration rate of special boundaries (i.e. boundaries of high structural order, so-called coincident site lattice (CSL) boundaries), which are less susceptible to the effects of solutes than random boundaries [2]. The effect of rare earth (RE) elements solutes on recrystallization and mechanical properties of Mg alloys are currently being extensively studied [93, 94, 95, 96, 97]. Another hot topic in this regard is related to the effect of solute on recrystallization and mechanical properties of high entropy alloys [98,99]. In general, recrystallization is retarded by the presence of solute elements, but a much stronger retardation of recrystallization can be observed when precipitates are formed [100].

Pores/voids or gas bubbles, formed during solidification, powder consolidation or additive manufacturing, are found to exert similar pinning effects on boundaries as those associated to second-phase particles [2, 101]. Deformation on materials containing pores/voids and gas bubbles does not lead to significant increase of overall dislocation density since no geometrically necessary dislocations are formed around them. However, the dispersed pores/voids can contribute to strengthening by a dislocation pinning mechanism [102,103].

2.2 Recrystallization

Different aspects of recrystallization phenomena have been summarized in existing review papers [1,7,8, 9,10] and excellent textbook by Humphreys and Hatherly [2] and in the book chapter by Raabe [4]. A brief introduction is probably appropriate before going to the details in the following sections.

2.2.1 Classification of recrystallization

Different classifications of recrystallization processes are often used in the literature, and many of the terminologies used in this field are "a bit imprecise at first view" [4]. Therefore, they are clarified below, together with some related terminologies in this field.

Defects like dislocations and interfaces accumulate during plastic straining, regardless of hot or cold deformation, leading to a thermodynamically unstable state for the material and changes in a number of properties, such as strength and electrical resistivity. When the deformed material is exposed to higher temperatures (with respect to the melting temperature of the material), the microstructure and also its associated properties can be partially and homogeneously restored to their original values through **recovery**, i.e., thermally activated annihilation and rearrangement of dislocations. Static recovery (SRV) and dynamic recovery (DRV) refer to the recovery processes taking place during annealing and deformation, respectively. A characteristic feature of the recovery process is that it generally does not involve the migration of HAGBs between the deformed grains [1], the corresponding crystallographic texture is thus not supposed to be significantly modified, possibly just a moderate sharpening.

The "formation of a new grain structure in a deformed material by the formation and migration of HAGBs driven by the stored energy" introduced by plastic deformation is termed as **recrystallization** [1]. **Static recrystallization** (SRX), which has been most widely studied, refers to the recrystallization process during annealing. If recrystallization is occurring during deformation at elevated temperatures, it is then called **dynamic recrystallization** (DRX). During recrystallization, material properties such as the strength and hardness often change at much higher rates than during recovery.

Recrystallization may take place with two clear steps: nucleation and growth stages, i.e. in a discontinuous way, which is the most studied recrystallization case. In this regard, it has been well accepted now that the nuclei of recrystallization are small volumes that already exist in the deformed microstructure [2], instead of being formed by random atomic fluctuations (classical nucleation theory) as for the case of phase transformations. When these small volumes (usually subgrains) satisfy the necessary condition of both a high angle misorientation and a driving force advantage, they can further grow and become successful new grains. A good example confirming this theory is the classical strain induced grain boundary motion (SIBM) experiments, where the high angle misorientation condition is met, performed by Beck and

Sperry [104]. During SRX, the size and energy advantage can be obtained at the SRV stage by subgrain growth [105] or subgrain coalescence [106,107,108]. The initiation of recrystallization *during SRX*, termed as **incubation time**, refers to the time needed to form large enough subgrains with sufficient surrounding stored energy to overcome the opposing pressure from boundary curvature, according to the seminal work of Bailey and Hirsch [109]. This definition is no longer appropriate for DRX, and the **critical dislocation density** or **critical strain** is often used to replace incubation time.

The deformed microstructure can also be progressively recrystallized with no clear nucleation and growth stages, exhibiting a continuous character. In terms of SRX, a good example is when deformed Al alloys with a subgrain structure pinned by fine dispersoids are annealed at elevated temperatures, where homogeneous subgrain growth occurs due to the gradual coarsening of dispersoids (with reduced pinning force) and misorientations of low angle grain boundaries (LAGBs) increase progressively until they are transformed into high angle grain boundaries (HAGBs) [110]. During plastic straining, cell or subgrain structures with LAGBs are readily formed for high stacking fault energy (SFE) materials due to their efficient dynamic recovery. LAGBs can progressively transform to HAGBs at larger deformations, a process which is commonly known as continuous dynamic recrystallization (CDRX) [2,111]. Another relatively similar concept is the geometric dynamic recrystallization (GDRX) [112,113], which is often observed when deforming high SFE materials to large strains at elevated temperatures. In this case, the initial grains are deformed in a way such that the separation of original HAGBs keeps decreasing during deformation, e.g., hot rolling or hot torsion. A more or less equiaxed grain structure is obtained when the separation of original HAGBs finally reaches the size of ~1-2 subgrains and the developed serrations become pinched off. If the hot plastic deformation is interrupted, nuclei with small internal stored energy will immediately form in the material while high temperature is kept on purpose or unintentionally (e.g., quench delay). These dynamically formed fresh nuclei can quickly grow into the deformed matrix without any incubation time. This phenomenon is commonly referred to as post-dynamic recrystallization (PDRX) or metadynamic recrystallization (MDRX) [9].

2.2.2 Characterization of recrystallization

After defining the key terminology related to recrystallization, the techniques used to characterize recrystallization are now summarized in the following section. It will be seen that many techniques used to characterize particles can also be applied to recrystallization studies. The experimental methods to study recovery and recrystallization were detailed in Humphrey and Hatherly's textbook [2] and a recent update was presented by Raabe [4], while characterization of materials in general [3] was given by a group of top experts in this field quite recently.

Nucleation of recrystallization is never a homogeneous process in any sense. It takes place in regions that contain microstructural heterogeneities such as grain boundaries, micro or shear bands, or around large second-phase particles, i.e., it is difficult to predict where it will occur. The recrystallization process can be strongly affected by a large number of factors such as deformation structure inherited from prior thermomechanical processing steps, nucleation mechanisms, impurities, grain/grain boundary crystallographic orientation etc. The problem is further complicated since it always takes place at small length scales close to the subgrain scale. Moreover, the fast progress of recrystallization consumes the deformation substructure leading to lost evidence. Microstructure features relevant to recrystallization studies are: deformed microstructure in terms of substructure, dislocations and heterogeneity sites, crystallographic orientation of grains and their boundaries, grain size and shape, recrystallized fraction etc.

Electron backscattering diffraction (EBSD) is a powerful technique for microstructure characterization related to recrystallization. It provides important information on crystallographic features such as (sub)grain orientation and (sub)grain boundary misorientations, local phases, which are important aspects for studying recrystallization. Average values and distribution of grain size, crystallographic texture and boundary misorientation can easily be obtained. Whether a grain is recrystallized or not, either dynamically or statically, could be determined by a combined analysis of its internal energy, grain boundary misorientation, grain size and shape etc. At present, individual dislocations cannot be resolved by EBSD (with the exception of using the electron channelling contrast imaging [114]), even though geometrically necessary dislocations density can be estimated [115,116,117,118]. The transmission EBSD (T-EBSD) [119] or transmission Kikuchi diffraction (TKD) [120] technique, with spatial resolution <10 nm has recently been developed to characterize material at nanoscale. The technical challenges and

applications of this technique were summarized in Ref [121]. While EBSD seems to be a routine technique for studying recrystallization nowadays, it should not be ignored that optical microscopy is still the only accessible tool for characterization of recrystallization in some universities and many industrial research centres. This easy-to-use and cheap technique provides information such as grain structure, particle morphology, recrystallization fraction (based on size and shape of recrystallized grains), it can even be used in certain cases to study dislocations using the etch-pit method [122]. X-ray diffraction (XRD) is commonly used for crystallographic texture analysis. Since the lattice distortions due to dislocations lead to a broadening of XRD peaks, laboratory scale XRD is also widely used to measure stored energy. If these techniques are not sufficient to reach desired spatial resolution, TEM has to be used. The high spatial and angular resolution of TEM renders it appropriate for studying individual crystal defects such as dislocations, stacking faults, thin twins etc. Crystals, i.e. grains or subgrains, and boundary misorientation angles can also be obtained using Kikuchi pattern analysis techniques [123,124]. The automated crystal orientation mapping technique based on TEM (ACOM or ASTAR-TEM) [125,126,127] is extremely powerful in cases where the conventional EBSD technique is insufficient, e.g., materials with sizes or features close to EBSD spatial resolution limit [128,129] or severely deformed materials with poor Kikuchi patterns quality for indexable EBSD data [51,130,131]. However, TEM techniques are limited by difficult and time consuming sample preparation, artefacts associated with the thin foil, and relatively small observation areas, making it difficult to collect statistically reliable quantitative information on microstructure required in many topics in materials science. These four characterization methods are perhaps the most used ones in the field of recrystallization. Other less used methods for characterization of recrystallization and related phenomena include calorimetry [132,133,134], laser ultrasonics [135, 136,137], resistivity measurements [138], and electron channelling contrast imaging (ECCI) [114,139,140].

While characterizations in 2D by EBSD, TEM etc. give valuable information on recrystallization behaviour, the 2D micrographs obtained in this way only reveal the complex 3D microstructure in an oversimplified way. Recent advances in available characterization techniques make it possible to study recrystallization in 3D. This is typically realized by automated serial sectioning using FIB combined with EBSD analysis, which is referred to as 3D EBSD [3,4, 36,141,142, 143]. A great advantage of this method is its achievable low spatial

resolution of ~50×50×50 nm^3 [4]. When FIB is not available, manual or other (semi)automated sectioning techniques [38,144, 145, 146,147] can also be used. This is compensated, however, by reduced spatial resolution due to difficulties in precise depth removal and re-localization of the focused area in the subsequent layers. Data processing is needed to decrease the misalignment between the sections during serial sectioning before the reconstruction of the 3D microstructure [146,148,149,150]. This enables new and/or more complete microstructure information to be collected, e.g., five-dimensional grain boundaries [151], PSN around large particles [36], and GND dislocation density [152]. Besides 2D TEM analysis, 3D grain orientation mapping of mono- and multiphase nanocrystalline materials in the TEM has also been developed [153].

Significant advances in characterization of recrystallization in recent years are often gained by non-destructive techniques focusing on direct observation of the deformation behaviour [154,155], nucleation process [156,157] and subsequent growth [158] of individual grains in a bulk sample by 3DXRD [159] using a monochromatic high-energy synchrotron beam, see e.g. Fig.1. These experiments are, however, limited by a relatively low spatial resolution (≥4μm) for characterization of finer scale deformation structures at which nucleation usually takes place. Higher spatial and angular resolution, 1.5×1.5×1.5 μm^3 and 0.01°, respectively, were achieved to advance the direct observation of nucleation in cold deformed high purity aluminium [160] using differential aperture X-ray microscopy (DAXM) [161] with polychromatic synchrotron X-ray microbeams. This experiment concluded that nuclei indeed develop at sites of high stored energy and they form with orientations that are already present in the deformed matrix [160].

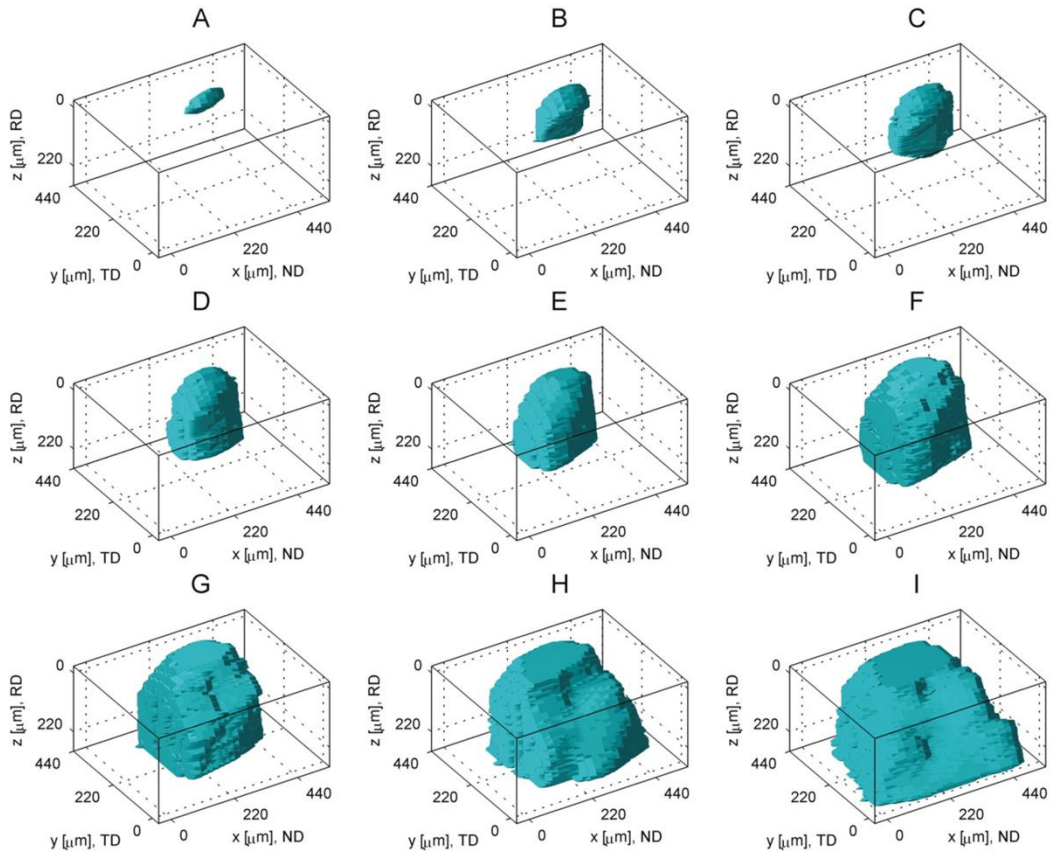

Fig. 1 Direct observation of the growth of a grain during recrystallization in the bulk of a deformed sample by 3D-XRD from [158]. The total annealing time from A to I was 30 hours, the annealing temperature was between 280°C to 290°C from A to H, it was raised to 310°C in I. Reprinted with permission from AAAS.

2.3 How second-phase particles affect recrystallization

After a separate summary on second-phase particles (**Section 2.1**) and recrystallization (**Section 2.2**), we are now ready to introduce their mutual interaction, which is the main focus of this review paper.

First, second-phase particles modify the deformation structure in terms of stored energy and heterogeneity sites, which may have significant influence on the subsequent recrystallization process. A better understanding of the recrystallization behaviour of a material must be based on a detailed knowledge of the deformed state. It should be recognized that deformation in return may also lead to the evolution of second-phase particles. The interface boundary migration

(during either growth or dissolution of particles) in return is likely to modify partcle shapes as well as deformation. The details on this topic are given in **Section 3**.

Second, second phase particles have direct interactions with recrystallization in different manners. They may retard or accelerate nucleation of recrystallization, influence the orientations of recrystallized grains, pin the growth of recrystallized grains or become unstable during recrystallization by coarsening, dissolution or re-precipitation. **Section 4** is devoted to all these related phenomena.

Third, the grain growth process after the completion of recrystallization is also affected by second-phase particles. Second-phase particles affect the kinetics of grain growth, lead to a limiting grain size and may induce abnormal grain growth. However, the scope of this review paper does not allow us to cover these grain growth aspects, the interested readers are referred to Refs [2, 162,163] for more details.

Last but not least, the complex interactions between second-phase particles also bring opportunities for tailoring microstructures and mechanical properties of particle containing metallic materials. Notable examples include controlling the grain size and crystallographic texture of investigated materials, as well as the particle structures, details of which are presented in **Section 5** and **Section 6**.

3. The effect of second-phase particles on deformation microstructure and texture

The presence of second-phase particles has important influences on the deformation structures, which may significantly affect subsequent recrystallization behaviour. First, they tend to increase the overall dislocation density. Second, large scale microstructural heterogeneities of deformation such as shear bands may occur. Third, larger orientation gradients are usually observed around large particles than that of the deformed matrix. Fourth, deformation textures and deformation modes may be affected by second-phase particles. Last but not least, deformation in return can change the second-phase particle structures such as fragmentation of coarse particles, dynamic precipitation of fine dispersoids etc. The use of numerical models for describing the deformation or work hardening behaviour of particle-containing materials is a challenging task, recent development on this topic is included at the end of this section. The large amount of literature focusing solely on improving material strength or ductility, e.g., by low temperature aging treatment [e.g. 164, 165], is not covered here since it is unlikely that a recrystallization treatment at higher temperatures, which is the key topic of this paper, will be subsequently performed. Excellent review papers [26, 166] already published on this topic also justify this omission. Despite these restrictions, we are of the opinion that many of the conclusions reached in this paper regarding deformation can be applied with appropriate modifications to these alloy systems as well. Emphasis in this review is placed on work that elaborates deformation structures which strongly affect the subsequent recrystallization behaviour. Since the effect of particles on recrystallization will be detailed later, only deformation conditions without recrystallization, i.e., cold deformation up to large strains and/or hot deformation to small strain levels, are discussed in this section.

3.1 Effect of second-phase particles on deformation microstructure

The increase of the overall dislocation density by the introduction of second-phase particles depends on whether they are deformable or not. For alloy systems with non-deformable fine particles (typically ~100nm in diameter), the dislocations will bow around the particle during deformation (see Figs. 2a and b) under the Orowan stress (τ_0) with respect to particle spacing (λ), given by

$$\tau_0 = \frac{\mu b}{\lambda} \tag{1}$$

where μ and b are shear modulus and Burgers vector, respectively. The value of λ is usually taken as the distance between particles (arranged on a square grid in the slip plane). Later improvements on this equation will be further addressed in Section 5.1.1. The dislocation under the applied stress encircles the particle, leaving an Orowan loop (see Fig.2c) and exerting a shear stress on the particle (with radius of r) given by

$$\tau = \frac{\mu b}{2r} \tag{2}$$

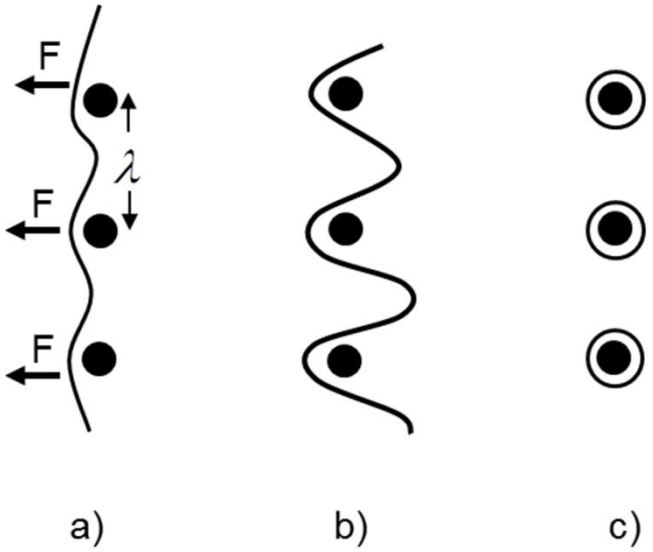

Fig.2 The formation sequence of Orowan loops. Reproduced from [2], with permission from Elsevier.

If the fine particles deform with deformation, either due to their small sizes or low strength, they are then sheared by moving dislocations which reduce the strength of the particles by decreasing their sizes on the slip plane (see Fig.3b), leading to preferred planar slip on a few slip planes (Fig.3d). The strong slip localization can penetrate into neighbouring grains, particularly in high strength precipitation hardened alloys, finally leading to the formation of shear bands [167,168,169, 170]. This effect is most pronounced in alloys strengthened by precipitates of ordered atomic structure (order strengthening) such as Ni-Al and Al-Li alloys [171], Ti alloys with α_2 (Ti_3Al) precipitation [172] etc. More homogeneous slip is usually observed for alloys containing only non-deformable particles [173,174], see Fig.3c and Fig.3e.

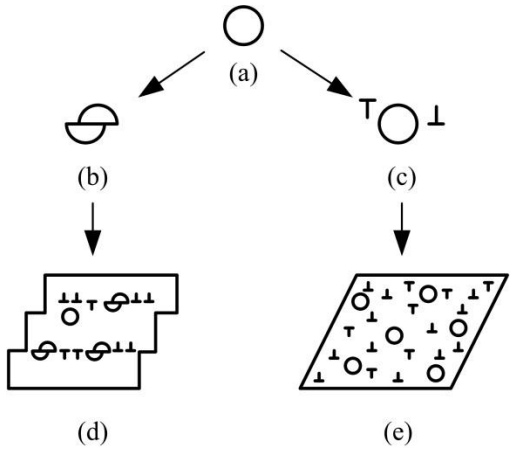

Fig. 3 The effect of particle strength on the distribution of slip. A deformable particle (b) leads to slip concentration, as shown in (d). A non-deformable particle (c) results in more homogeneous slip, as can be seen in (e). Reproduced from [2] with permission from Elsevier.

The real situation is of course more complex than those shown in Fig.2 and Fig.3. In fact, during continued deformation, more loops are formed around non-deformable particles, which increases the stress level and finally leads to localized plastic flow. The strain incompatibility between the matrix and particles, due to the differences in the elasticity and plasticity of dispersoids and matrix, can be accommodated by the generation of geometrically necessary dislocations (GNDs) [175, 176] or even the formation of voids [37]. A statistical analysis suggests that Orowan loops or prismatic loops (i.e. Burgers vector is not in the plane of the loop) formed by cross slip [177] around dispersoids are required for compatible deformation [175], where the density of the GNDs introduced by spherical non-deformable particles can be calculated as [175]:

$$\rho_G = \frac{4 f_V \gamma}{rb} \tag{3}$$

where γ is the shear strain, f_V and r are volume fraction and size of the particles, respectively. This equation predicts a linear increase of GNDs with shear strain. However, it has been concluded that a large increase in dislocation density for alloys containing fine non-deformable particles are only significant at small strains. Dynamic recovery reduces the accumulation of dislocations at larger strains that become important for recrystallization, leading to a dislocation density significantly less than that predicted theoretically, even though it is still slightly higher than that of its single-phase counterpart [2, 178]. A slightly higher dislocation density is observed since most dislocations still interact with precipitates before annihilation at a later stage

during recovery, as demonstrated during static recovery [179]. It is reasonable to believe this difference in dislocation density will be larger for alloys with slow recovery activity (alloys with low stacking fault energy), as was reported in a copper alloy [180].

In metals with high stacking fault energy like aluminium, dislocation loops are unstable due to dynamic recovery. Tangled dislocations around dispersoids are usually observed rather than loops in pure copper [181,182]. The local lattice rotations at non-deformable second phase particles ranging from 0.02 to 5μm, in aluminium and copper single crystals have been examined during cold deformation up to a tensile strain of 0.5 [183]. It was found that the misorientation close to the particle decreases with decreasing particle size and becomes very small for particles less than ~0.1μm. The high density of tangled dislocations enhances the tendency for cell formation [173, 184], but a pinning effect on moving dislocations from fine dispersoids also exists. Therefore, the net effect of introducing dispersoids on the cell size and misorientations is actually not straightforward for conventional alloys containing a large number of second-phase particles. Even though quite contradicting results have been reported in the literature, it is now generally accepted that both the cell size and misorientations are not significantly different from that of particle-free alloys, with the exception of misorientations being much smaller when the particle spacing is similar to the cell size, i.e., homogenization of the deformation microstructure [2].

The experimental and theoretical research by Humphreys and his co-workers have established the fundamental understanding of the deformation structure around coarse particles, which has been comprehensively summarized in [2]. Fine subgrains and orientation gradients are formed in the deformation zone around coarse particles, which are critical for PSN. It is now generally accepted that the misorientation decreases when the distance from the coarse particle increases, the misorientation around particles increases with particle size up to ~2.5μm and only increases with strain thereafter [2]. The fact that many conventional alloys contain both small and large particles makes the analysis on their influence on deformation structure more complex. We will further discuss these topics when dealing with the effect of second-phase particles on nucleation of recrystallization (**Section 4.1.3**).

3.2 Effect of second-phase particles on deformation texture

As detailed in Section 3.1, the second-phase particles affect deformation structures, it is thus not surprising that they also influence deformation textures. Many mechanical and physical properties of materials are dependent on their crystallographic texture [2], which is primarily the reason for investigating the effect of particles on deformation texture. Their influence on deformation texture is further of high interest in that subsequent recrystallization behaviour, both by oriented nucleation and oriented growth, which will be detailed in Section 4, also strongly depends on the orientations of the deformed grains. Recrystallization by nucleation at sites introduced during deformation by second-phase particles, such as shear bands caused by deformable fine dispersoids and deformation zones near coarse particles after deformation, offers a potential way to randomize recrystallization texture [2,185,186, 187]. The different approaches to modify the texture of Al and Mg alloys are reviewed in Ref [188], focus here will only be given to the texture engineering by second-phase particles.

Aluminium alloys are perhaps the most widely studied particle-containing metals, rolling texture of single-phase aluminium (with random starting texture) increases in strength with deformation and is typically of β-fibre form, running from the Copper orientation {112}<111>, via S {123}<634> to Brass {011}<211>, with relatively uniform orientation densities along this fibre [2].

However, coarse particles in conventional alloys have little effect on the overall deformation texture due to their low volume fraction (<5%) [2], a comparison of the development of deformation texture during rolling of single- and two-phase Al-Cu single crystals can be found in Ref [189]. When a large number of coarse particles are present, a weakened deformation texture can be found due to the inhomogeneous deformation around the large particles [169, 190]. However, the intensity of the rolling texture could increase at ultra-high strain levels (>9.6) for alloy systems containing coarse particles, if deformation induced reprecipitation of fine particles, which favour homogeneous deformation, is present in the grain interiors [190]. CPFEM suggests that the microtexture in the deformation zones around spherical and cuboidal particles are not random, but depends on the location and strain state [191]. Recrystallization texture components such as ND-rotated Cube {001}<310> and P {011}<566> orientation have been found in the deformation zone after rolling [191].

The cutting of deformable precipitates causes strain localization and leads to strong shear band formation, typical materials include Al-Cu, Al-Mg-Si, Al-Li etc. Rolled samples with a small amount of fine shearable particles exhibit an increase in Goss {110}<001> and Brass orientations [167,169]. The shear band sensitivity increases with the number of shearable particles, a significant reduction in the sharpness of deformation texture can be obtained with a large number of shearable particles [169]. In this case, no sharp rolling texture is thus formed as seen in its single-phase counterpart, except a somewhat increased strength of the Brass orientation. It has been noted that rolling textures of aluminium containing dispersoids are closer to the prediction by the full constraint (FC) Taylor model, while the texture of single-phase aluminium is more close to the prediction of the relaxed constraint (RC) Taylor model [182]. During hot deformation of Al alloys there are also strong evidence that the dominating Brass texture component can be formed due to selective dynamic grain growth [192,193], where the grain orientation dependent stored energy and pinning effect from fine particles were held responsible. Small second-phase particles have been reported to reduce the strength of texture components by breaking up slip patterns [194].

Second-phase particles are also used to modify the deformation modes, this is especially important for HCP metals with large variation in activation stresses for the various deformation modes, e.g., as in magnesium alloys. Wrought Mg alloys form strong deformation textures (basal-type textures) which are difficult to change by an annealing treatment. There is usually a significant tension-compression asymmetry [e.g. 195,196] which is a detrimental property. A large number of second-phase particles can be easily produced in commercial Mg alloys such as the AZ series (Mg-Al alloys contain Zn as a secondary alloying element) by aging. These precipitated particles can be used to modify the deformation modes (basal slip, prismatic slip and $\{10\bar{1}2\}$ twinning modes) by selective hardening of the different deformation modes, and thus reducing the yield asymmetry [197, 198]. The modification of deformation mode by fine precipitates [199] and inhomogeneous deformation caused by coarse particles [200] could also affect subsequent dynamic recrystallization behaviour if deformation is conducted at high temperatures, leading to different deformation texture.

3.3 Effect of second-phase particles on severe plastic deformation at room temperature

The effect of second-phase particles on deformation structure is perhaps best manifested during severe plastic deformation (SPD) at room temperature. While most conventional alloys contain, to different extent, both fine and coarse second-phase particles, it is convenient in this context to first analyse their separate effects on deformation structure after large deformation using model alloys. The reason is that it is difficult to distinguish their individual contribution from the final microstructures which are the result of the net effects from the two types of particles, regardless of whether their effects are additive or contradictive. If the deformation of particle-containing materials is conducted at high temperature, e.g. as in Ref [201], dynamic recrystallization during deformation and static recrystallization during interpass time further complicate the analysis of the role of second-phase particles.

The effect of fine dispersoids on microstructure evolution has been investigated during heavy deformation of a single-phase Al-0.13%Mg alloy and a binary Al-0.2%Sc alloy by Apps et al. [174]. The Al–0.2%Sc alloy contains fine coherent Al_3Sc dispersoids (~20 nm in diameter and ~100 nm spacing). These two alloys have been deformed at room temperature by equal channel angular extrusion (ECAE) to an effective strain of 10 under the same deformation condition, see Fig.4. It was found that the presence of fine, non-shearable, dispersoids in the Al-0.2%Sc alloy leads to homogenized slip, as compared to the single-phase counterpart where the formation of high misorientation boundaries is assisted by microshear bands, as well as in crystallographically unstable grains. These fine dispersoids also inhibit the formation of a cellular substructure and dense dislocation walls (which are observed in the Al-0.13%Mg alloy), with weakly misoriented and diffuse boundaries. All these factors act together to reduce the rate of HAGB generation at low to medium strains, making it more difficult to get a submicron grain structure at higher strains during severe plastic deformation. This adds some difficulties to develop thermally stable submicron grained alloys by severe plastic deformation of alloys containing stable fine dispersoids. An alternative way to achieve this has already been proposed by an ingenious control of second phase particles, the details of which will be discussed in **Section 5.2.3**. However, there is still some confusion in the literature about the effect of fine dispersoids on grain refinement. Accelerated grain refinement by nanoparticle reinforcement during accumulative roll bonding of commercial purity AA1050 alloy was reported [202], but all the

crystals were considered by these authors as grains regardless of their boundary misorientations since only BSE micrographs were used to characterize the "grain size". Fine alumina particles (3.8 vol.%) in an Al alloy were found by Barlow et al. [194] to accelerate the development of subgrain structure as compared to particle-free materials. No quantitative data for the grain size evolution was given since all the characterization was performed by TEM. The alumina particles used in their study were in the form of platelets and most of them were in clusters aligned with the extrusion direction, i.e. not evenly distributed. A small volume fraction of large $FeAl_3$ particles up to a few microns in diameter were also present. Acceleration of grain refinement by nanosized precipitates during accumulative continuous extrusion forming in an Al-0.2Sc-0.1Zr alloy was reported by Shen et al. [203] using EBSD. The comparison was based on two variants of the same Al-0.2Sc-0.1Zr alloy but with f_V / d (f_V and d are volume fraction and average diameter of second phase particles, respectively) of 1.59×10^{-5} nm^{-1} and 1.85×10^{-5} nm^{-1}, respectively, together with a pure Al. In fact, a single phase Al alloy, instead of a pure Al, would have been more appropriate for quantitative comparison, as was done by Apps et al. [174]. The reason is that pure metal has higher grain boundary mobility and could easily lead to larger grain size. Since the temperature of the deformed sample after each pass can reach more than 300°C, SRX must have been activated during the inter-pass time (at least for the pure Al sample), i.e., the measured grain size is not only due to grain refinement by deformation. If SRX is involved, lower f_V / d also signifies smaller Zener pinning, which can in principle also lead to larger final recrystallized grain size. All these factors were not discussed in Ref [203], which makes their conclusion less convincing.

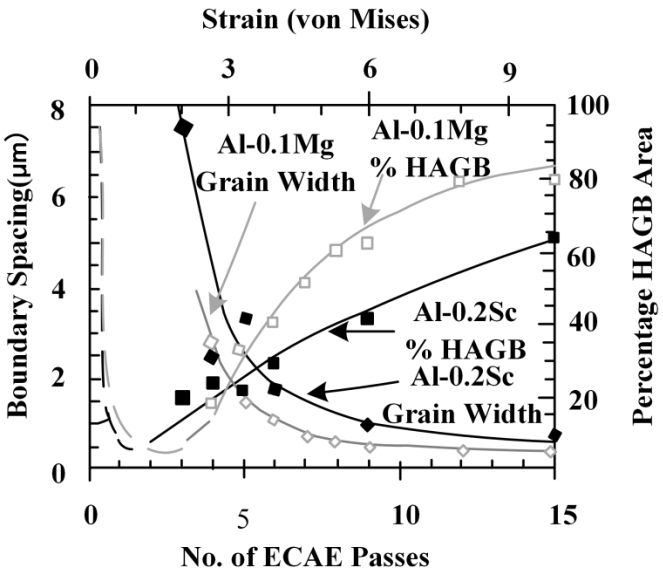

Fig. 4 The average transverse HAGB spacing and HAGB area fraction (%), as a function of ECAE passes or von Mises strain, during ECAE processing of the Al–0.2Sc and single-phase Al–0.13Mg alloys, deformed under the same conditions. Reprinted from [174], with permission from Elsevier.

Using the same approach, the effect of coarse second-phase particles on microstructure evolution during severe deformation processing has also been investigated by the same research group [204]. The single-phase Al-0.13% Mg alloy and an AA8079 two-phase Al alloy with 2.5 vol.% of ~2 μm $Al_{13}Fe_4$ particles were deformed at room temperature to an effective strain of 10 by ECAE under identical conditions. A careful examination of the microstructures revealed that grain refinement was significantly higher in the particle-containing AA8079 alloy: a submicron grained structure could already be obtained at an effective strain of five in the particle-containing AA8079 alloy, while a larger strain of 10 was needed to reach a similar grain structure in the single-phase Al-0.13% Mg alloy, see Fig.5. It should be noted that further deformation of the AA8079 alloy from a strain of 5-10 did not lead to any significant microstructural changes, as shown in Fig.5. The deformation structures of both materials in terms of boundary spacing and percentage of HAGB area tend to converge, even though the grain width of the particle-containing alloy is slightly lower. More affecting factors on the saturation grain size can be found in Ref [205]. The reason for the acceleration of grain refinement in AA8079 was found to be closely related to the development of deformation zones around the coarse second-phase particles, where highly misoriented boundaries with higher density are formed at low strains. A submicron grained microstructure is rapidly formed at higher strains as a result of high particle

volume fraction and the associated heterogeneities in plastic flow, which disturb the regular lamellar boundary structures that was seen in the single-phase Al-0.13% Mg alloy and accelerate grain refinement. The acceleration of grain refinement by coarse second-phase particles was also reported in Al-7%Si alloy [206] and Al-Fe-Mn alloy [207] during severe plastic deformation.

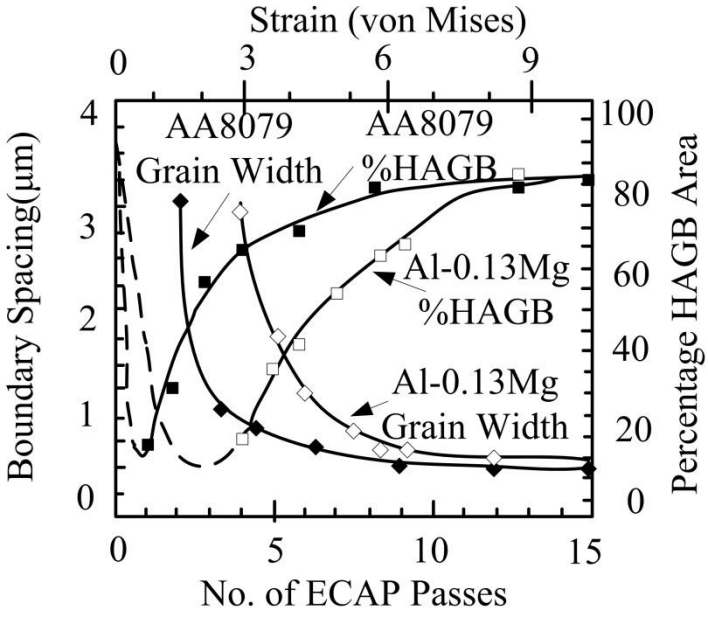

Fig. 5 The average transverse HAGB spacing and HAGB area fraction (%), in the Al-0.13%Mg and AA8079 alloys, as a function of von Mises strain during ECAE processing. Reprinted from [204], with permission from Elsevier.

With a good understanding of the individual effect of both coarse and fine second-phase particles on microstructure evolution during severe plastic deformation, it is possible to treat more complex alloy systems. The effect of mixed coarse second-phase particles and fine precipitates on microstructure refinement and mechanical properties of a severely deformed Al alloy was investigated by Gutierrez-Urrutia et al. [208]. The acceleration of microstructure refinement by coarse particles was confirmed, while the fine precipitates were believed to be sheared during deformation and then dissolved in the matrix. If not, it is expected that they would have led to a slower grain refinement process.

Not yet mentioned here is the effect of second-phase particles on ductility. It will be discussed in **Section 5.1.2** that second-phase particles are the main source for fracture. In this context, the work by Zha et al. [209] on grain refinement during ECAP using soft particles that are less prone to void formation is of high interest.

3.4 Deformation induced evolution of second-phase particles

The effect of stable second-phase particles on microstructure evolution during deformation has been extensively investigated, less work can be found in the literature on unstable particles. Besides cutting deformable fine particles, which lead to the formation of shear bands, deformation also affects the evolution of second-phase particles in other aspects. Among them, the change of deformable particles in shape and coherency, the fragmentation of coarse particles, and deformation induced dynamic precipitation or dissolution of precipitates are perhaps the most important ones. The evolution of second-phase particles modifies deformation structures and can have an important role in subsequent recrystallization behaviour.

Let us start with simple cases where the particles are present before deformation. A very comprehensive study on this topic was recently reported by Tsuchiyama et al. [210], where the plastic deformation and dissolution of FCC ε-Cu particles (35nm) during cold rolling of a Fe-2%Cu alloy (Cu steel) were compared to a Fe-V-C alloy (VC steel) with hard particles of similar sizes, as well as dispersion particle free pure iron. It was found that soft Cu particles are plastically deformed (see Fig. 6c), with a complex internal deformation structure, and they are dissolved into the ferrite matrix by heavy cold rolling at their sharp tips (i.e. thinnest section at both ends of the particles, see Fig.6c), as demonstrated by HRTEM, EDS and DSC analyses, as well as X-ray diffractometry. The aspect ratio of soft ε-Cu particles increases with strain but less than that predicted by geometry consideration alone.

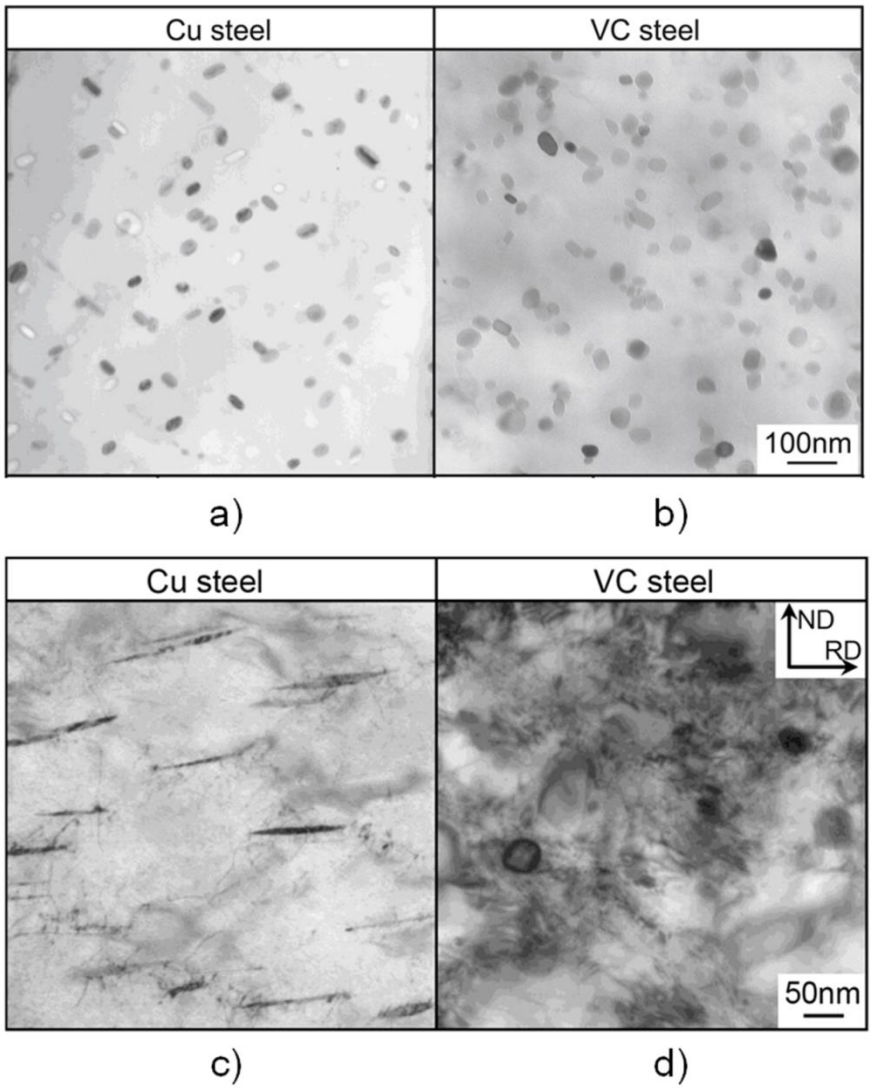

Fig. 6 TEM bright field images of particles

a) Undeformed Cu steel; b) undeformed VC steel; c) 70% cold-rolled Cu steel; d) 70% cold-rolled VC steel. Reprinted from [210], with permission from Elsevier.

The hardness of the Cu steel was nearly close to that of the VC steel at small strain levels (low dislocation density), but it gradually deviated towards the lower hardness side with increasing dislocation density, as illustrated in Fig.7. This indicates that the strengthening effect by the hard VC carbide particles was maintained, while that by the soft Cu particles diminished after heavy cold deformation. Two reasons were put forward to explain the decrease in the particle dispersion strengthening: i) the volume fraction of the Cu particles was decreased due to dissolution by cold working, and ii) the pinning force of Cu particles was decreased through the thinning of the Cu particles.

The dissolution of ~5nm Guinier-Preston (GP) zones during cold rolling to strains up to ~40% was reported by Hutchinson et al. [211] in an Al-3Cu-0.05Sn (wt.%) alloy. Murayama et al. [212] demonstrated that the θ' phase in an aged Al-1.7 at% Cu alloy first fragment into smaller segments which then eventually dissolve into the Al matrix to form supersaturated solid solution during ECAE at room temperature. However, this type of studies only focused on the evolution of particles, with no detailed discussion on its effect on dislocation density or stored energy variations and subsequent recrystallization behaviour. The deformation process can also change the precipitate spatial distribution and their coherency with the matrix [213].

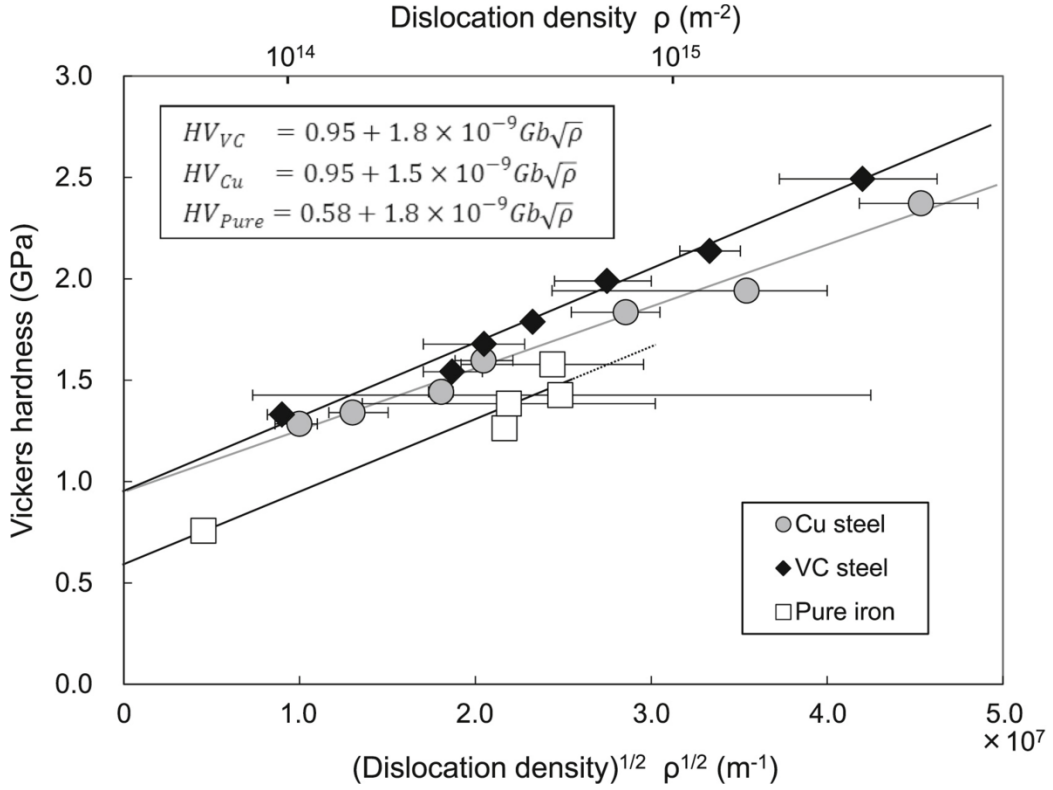

Fig.7 The correlation between the Vickers hardness and the dislocation density in the Cu steel, VC steels and pure iron. Reprinted from [210], with permission from Elsevier.

In terms of alloys containing larger particles, Gutierrez-Urrutia et al. [206] performed severe plastic deformation by ECAP of an Al-7 wt% Si alloy to study the evolution of large Si particles and its effect on microstructure and mechanical properties evolution. As shown in Fig. 8a, interdendritic networks of lamellar eutectic silicon are the main feature in the as-cast Al–7% Si. These Si particles continue to decrease in size at larger strains and reach ~1μm after 10 ECAP passes, see Fig. 8b.

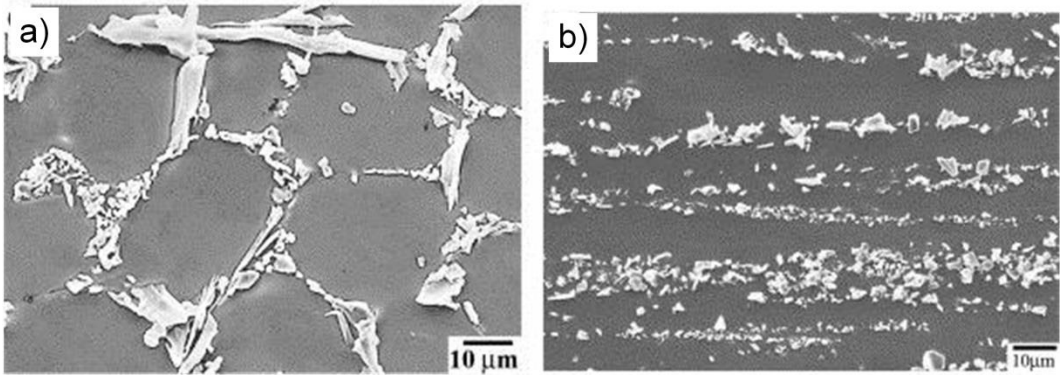

Fig.8 a) Si particle distribution in the as-cast state; b) after 10 ECAP passes. Reproduced from [206], with permission from Elsevier.

As compared to the Al-0.5%Si alloy under the same deformation conditions (see Fig.9a), it is clear that the grain size of the Al–7% Si alloy sample is much smaller, together with a much higher internal dislocation density (see Fig.9b).

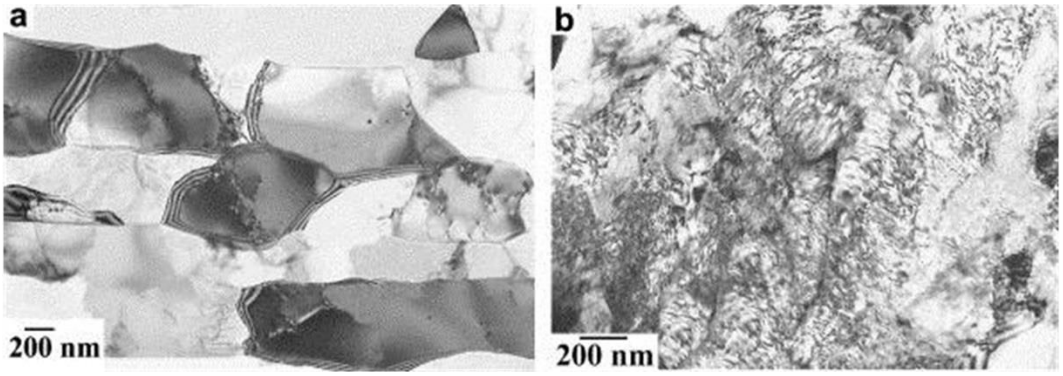

Fig. 9 Bright field TEM micrographs showing the different microstructures after deformation to 8 ECAP passes: (a) Al–0.5% Si, (b) Al–7% Si. Reproduced from [206], with permission from Elsevier.

When deformation and precipitation occur simultaneously, the interaction is dynamic and thus more complicated, as summarized by Deschamps et al. [214]. In general, several possible mechanisms can act together: i) acceleration of nucleation of precipitates due to more heterogeneous nucleation sites by the presence of dislocations; ii) increased growth or coarsening of precipitates due to pipe diffusion and solute transport by dislocation sweeping; iii) acceleration of nucleation, growth or coarsening of precipitates due to a non-equilibrium vacancy concentration related to the plastic deformation; and iv) deformation induced partial or complete dissolution or reprecipitation of precipitates. The net effect of plastic straining on precipitation

depends on the balance between these different mechanisms. It is observed that the distribution of dynamic precipitation is more heterogeneous than in the un-deformed metal, but less heterogeneous than in the pre-strained metal [215]. Dynamic precipitation is strongly affected by deformation temperature, exposure time [216] and plastic strain [214]. In severely deformed Al-Mg-Si, it was shown that dynamic precipitation could occur at room temperature [217]. Concurrent nucleation of precipitation in turn affects deformation, typically increasing the strength. For instance, dynamic precipitation of new particles on dislocations and subgrain boundaries during creep restricts the movement of dislocations and boundaries, increasing creep resistance [218,219]. When DRX occurs, the interaction is more complex. DRX can promote dynamic precipitation [220], and a new phase different from those in ordinary aging of un-deformed metal can appear [221], at the same time dynamic precipitation retards DRX due to the pinning effect of precipitates on nucleation of DRX and grain boundary migration [222].

3.5 Numerical modelling

The work hardening behaviour of FCC metallic materials has been reviewed by Nes [223] and Kocks and Mecking [224], but the effect of second-phase particles was mostly left unexploited. The shearable precipitates are usually considered not to affect the work hardening evidently, and modelling work hardening is then similar to single-phase materials. Non-deformable particles affect plastic deformation mainly in two ways: i) they increase the density of GNDs; ii) they increase the Orowan stress. Only the physically-based numerical models addressing these two aspects are discussed here, even though second-phase particles also affect deformation in other ways, such as the Bauschinger effect [225,226,227,227,228], i.e. reduction in the yield stress following pre-strain in the reverse direction. In the previous sections, focus was given on second-phase particles induced microstructure changes during deformation. However, microstructure evolution in the matrix without particles also needs to be considered when analysing the deformation structures for particle-containing materials.

In terms of the effects of second-phase particles on GNDs, the basics of theoretical models for work hardening of particle-containing materials is the accumulation of extra dislocations as a set of dislocation loops (Orowan or prismatic loops) around particles. The dislocation storage term is generally defined by a differential equation of the form:

$$\frac{d\rho^{+}}{d\gamma}=\frac{2}{bL} \tag{4}$$

where L is the average distance over which the mobile dislocations can migrate before being stored, while γ and b are the shear strain and Burgers vector, respectively. In pure metals, L is determined only by the interactions between the stored dislocations in the dislocation forest and the mobile dislocations. In alloys containing non-deformable second-phase particles, the effect of additional GNDs caused by particles can be accounted for by replacing the slip length L in Eq. (4) by a strain invariant term, i.e., a geometric slip distance, L_g, where $L_g = r/2f_V$ is derived from Eq. (3) by Ashby [175]. Of course, the dislocation storage due to interactions with forest dislocations (statistically stored dislocations (SSDs)) and GNDs around second-phase particles should be combined to give the total dislocation density in this type of alloys, this has been treated by Marthinsen and Nes [229]. Attempts have also been made to consider more complex situation of precipitate coarsening and concurrent precipitation [230]. Dynamic recovery is often considered by the following simple expression

$$\frac{d\rho^{-}}{d\gamma}=-k\rho \tag{5}$$

A high density of dislocation loops around dispersoids obviously accelerates recovery, and this enhanced local dynamic recovery was recently modelled by Zhao and Holmedal [231].

When it comes to their effect on work-hardening, the GNDs caused by second-phase particles also obstruct the motion of other moving dislocations, as do the SSDs. The mechanism of work hardening is proposed to be short-range dislocation interactions [175] or long-range elastic internal stress [232, 233] in the literature. The short-range interaction approach treats dislocation loops similarly to forest dislocations, and the stress is proportional to the square root of the total dislocation density, ρ_{tot}, i.e. the sum of SSDs and GNDs:

$$\tau=\tau_0+\alpha\mu b\sqrt{\rho_{tot}} \tag{6}$$

where τ is the shear stress, τ_0 is shear flow shear stress of the material in the absence of dislocation interactions, α is a dimensionless parameter, μ is the shear modulus, and b is the Burgers vector. If only GNDs are considered, combining Eq. (3) and Eq. (5) yields:

$$\tau=\tau_0+2\alpha\mu b\sqrt{\frac{f_V\gamma}{rb}} \tag{7}$$

Since f_V , r and b are all strain independent parameters, this equation predicts that materials dominated by GNDs should show a parabolic stress-strain behaviour. Early research on single-crystals containing oxides has demonstrated that dispersoids result in a parabolic hardening, as compared to a more linear initial hardening in single crystals without dispersoids [234]. In commercial aluminium alloys containing dispersoids, the initial work hardening rate is increased, but this is followed by a rapid decrease [231,235]. On the other hand, the long-range internal stress approach considers the elastic back stress caused by dislocation loops, and gives a similar stress contribution as the one formed with the short-range interaction approach. Since both approaches give similar work hardening behaviours, no further discussion is provided here, interested readers are referred to Refs [232, 233]. A review by Gerold [236] has given a good summary of experimental results and theoretical models before 1980. Recent modelling combines the two approaches together [225, 226,228, 231].

The above mentioned treatment on dislocation density and work hardening behaviour could also be applied to coarse particles, however, due to their typical small volume fractions and large sizes in conventional alloys, their contribution to overall dislocation density (Eq. (3)) and stress (Eq. (7)) is not expected to be strong. It is recalled that the volume fraction of fine dispersoids is usually smaller than that of coarse particles. However, the average size of dispersoids is usually about two orders of magnitude smaller than that of coarse particles, which yields much higher value of f_V / r that contribute to increase of dislocation density (Eq.(3)) and stress (Eq.(7)). The purpose of introducing coarse particles in conventional alloys is not to increase their strength, but mainly to change the deformation microstructures, which then modify the subsequent recrystallization behaviour and texture [e.g. 2, 36], a topic that will be detailed in the next section. In terms of the modelling of the individual deformation zone near coarse particles, simple models based on dislocations and crystal plasticity have been previously developed [e.g.237,238]. Finite element models (FEM) incorporating crystal plasticity (i.e. CPFEM) have been widely applied in the last decade to analyse the strain distribution and orientation evolution around coarse particles during deformation [191,239,240]. Modelling suggests that the strain distribution around coarse particles significantly deviates from the macroscopic strain mode [191, 240]. The aspect ratio and clustering of particles influence the heterogeneous strain field, compared to an isolated spherical particle. The modelling is consistent with the macroscopic strain field measured by high resolution digital image correlation [241]. The developed

deformation zones around coarse particles have significant influence on subsequent recrystallization behaviour, which will be detailed in Section 4.2.

4. The effect of second-phase particles on recrystallization

Besides affecting deformation structures during deformation before recrystallization (see **Section 3**), second-phase particles also play an important role during recrystallization, notably by pinning the rearrangement of dislocations and (sub)grain boundary migration, by modifying the nature of nucleation sites, and by changing recrystallization textures. This influence comes from pre-existing particles before deformation and annealing which are often uniformly distributed in the microstructure, precipitated fine particles after deformation during annealing before the onset of recrystallization, as well as concurrent precipitation. All these different types of particles can become unstable during annealing, due to particle coarsening, dissolution, re-precipitation and migration etc., which makes the analysis of their effects on recrystallization quite complex.

4.1 Effect of fine dispersoids on recrystallization

4.1.1 Zener pinning principle

Zener pinning [242] or Smith-Zener pinning refers to the retarding force or pressure on the moving (sub)grain boundaries by a dispersion of fine particles. Considering a moving flat boundary separating two grains (A and B) interacting with a single particle (C) of radius, r, three surface tensions are involved once the boundary meets the particle at D and E, i.e., the boundary tension γ_{AB} and two particle surface tensions γ_{AC} and γ_{BC}, as shown in Fig.10. If we assume, as Zener/Smith did, that the particle is incoherent, i.e., $\gamma_{AC} = \gamma_{BC}$, then these two surface tensions will balance, leading to α =90°. The pinning force that opposes the boundary pulling off the particle is given by Smith [242]:

$$F = 2\pi r \cos\theta \cdot \gamma_{AB} \cdot \sin\theta \tag{8}$$

where the interface between the grain boundary and the particle is a circle of radius $r\cos\theta$, and the $\sin\theta$ term is incorporated to consider only the pinning force along y direction. The force in the x direction is zero. The maximum value of the force, $F_{\max}$, occurs at $\theta = 45°$:

$$F_{\max} = \pi r \gamma_{AB} \tag{9}$$

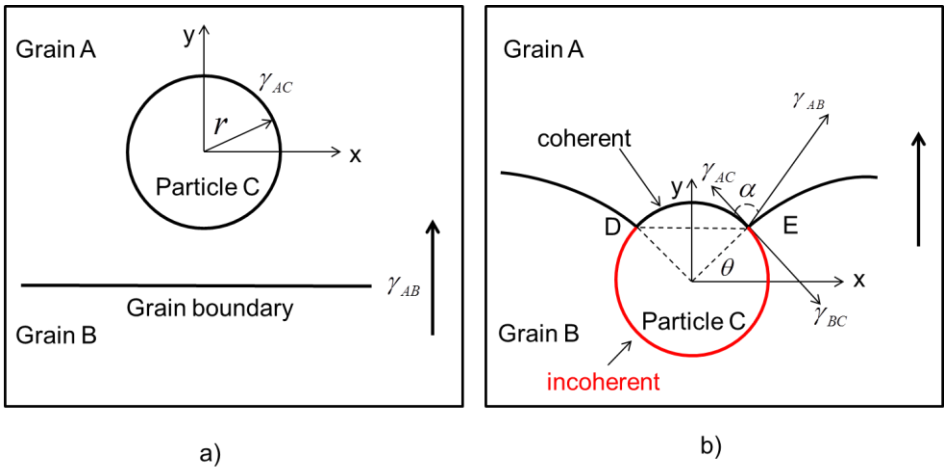

Fig.10 Schematic graph showing the interaction between a grain boundary and a spherical particle a) Before interaction; b) During interaction. Reproduced from [163], with permission from Elsevier.

Based on the Zener pinning analysis from a single particle on a grain boundary, one can now turn to the more complex situation, where the effect of all particles on a grain boundary is calculated. If the surface density of the particles is N_s, then the total pinning force acting on the grain boundary is $N_s \cdot \pi r \gamma_{AB}$ assuming that every particle acts on the grain boundary with the maximum pinning force. The surface density of the particles was approximated by Zener/Smith as $N_V \cdot r$, where N_V is the number of particles per unit volume. This latter term is actually equal to $f_V \Big/ \frac{4}{3}\pi r^3$, where f_V is the fraction of the total volume occupied by particles. This yields the classical Zener pressure expression according to Zener/Smith:

$$P_Z = \frac{3 f_V \gamma_{AB}}{4r} \tag{10}$$

It should be noted, however, that particles within a distance r on each side of the grain boundary will interact with it, which gives $N_s = N_V \cdot 2r$, and the following equation, which is the most commonly used form nowadays and also used for the subsequent analyses in this paper:

$$P_Z = \frac{3 f_V \gamma_{AB}}{2r} \tag{11}$$

When the Zener pressure (P_Z) is equal to the driving pressure due to boundary curvature (P_C), growth will stop and a limiting grain size will be obtained. The driving pressure for grain growth comes from the curvature of the grain boundaries:

$$P_C = \frac{\alpha \gamma_{AB}}{R} \tag{12}$$

where $1/R$ is the mean radius of curvature, and α =2 for spherical grains. The limiting grain size is thus:

$$D_{Lim} = 2R = \frac{4\alpha r}{3 f_V} \tag{13}$$

Or more generally:

$$D_{Lim} = K \frac{r}{f_v^m} \tag{14}$$

where m is a constant.

From the above analysis, it can be seen that Eq. (11) is obtained based on several simplifying assumptions: i) the particles have spherical shape and they are stable; ii) the surface tensions γ_{AC} = γ_{BC}, i.e., the particles are incoherent; iii) the particles are randomly distributed; iv) all particles are of equal size; v) each particle exerts the maximum force. These assumptions are rarely observed in reality, and modifications/improvements of various kinds have repeatedly been performed since 1948. When a coherent particle is considered, the maximum drag force is found to occur when $\theta = 0°$ and $\alpha = 180°$, which is twice ($2F_{\max}$) as effective in pinning a grain boundary as an incoherent particle of the same size (see Eq. (9)). The consideration of other more complex situations is generally even more challenging. However, it has been shown, based on a level set description of interfaces in a finite element context [243, 244], that it is possible to consider the morphology of real particles as measured by microscopy (without any assumption on particle structure) [245], and new algorithm which significantly improves the computational efficiency has been proposed [246]. The Zener pinning theory has been carefully reviewed several times, the interested readers can refer to Nes et al. [25], Manohar et al. [162] and Huang and Logé [163] for more details.

4.1.2 On grain boundary migration during recrystallization

The effect of fine second-phase particles on the boundary migration rate (V) is usually considered by applying a Zener pinning term using Eq. (11) or similar on the effective driving force:

$$V = MP_{Eff} = M_0 \exp(-\frac{Q}{RT})(\mathrm{P}_D^{Rex} - \mathrm{P}_Z - \mathrm{P}_C) \quad (15)$$

where Q is the apparent activation energy and M_0 is a constant of boundary mobility M, P_D^{Rex} is the driving force for recrystallization and can be approximated as a function of dislocation density (ρ), shear modulus (μ) and Burgers vector (b) as $\sim 0.5\rho \mathrm{Gb}^2$, P_Z and P_C are retarding pressures due to Zener pinning (Eq. (11)) and boundary curvature (Eq. (12)), respectively. It should be noted that the boundary curvature term can change from retarding pressure to driving pressure depending on concavity. The discussion here is focused on the migration of HAGBs during recrystallization, the effects of second-phase particles on LAGBs are treated in **Section 4.1.3**. Second-phase particles may also modify the driving force P_D^{Rex} as compared to particle-free materials, as already discussed in **Section 3**. Recent progresses on grain boundary migration during recrystallization of particle containing materials are mainly focused on how to more accurately calculate P_Z, since Eq. (11), as already stated, is based on some highly idealized assumptions that barely exist in conventional materials.

The first type of attempts involves the consideration of non-idealized particles, e.g., heterogeneous distribution of second-phase particles, non-spherical particles, coherent particles, and orientation of particles with respect to the deformed sample or moving boundary etc. These aspects are mainly investigated during grain growth where the large number of heterogeneity sites that existed during recrystallization are absent and grain boundary energy is the only driving force. Relevant studies on grain boundary migration during recrystallization are discussed below.

The spatial distribution of particles and shape effects on the moving boundary of recrystallizing grains were considered by Nes et al. [25] for a relatively simple but important case. During annealing of cold-rolled Al-Mn alloys, which are widely used in packaging, beverage cans, heat exchanger industries, heterogeneous precipitation preferentially takes place on (sub)grain boundaries which are aligned with the rolling direction (RD), as schematically

shown in Fig.11a. The precipitates are frequently not spherical but plate-shaped in this type of alloy, which has been treated as ellipsoidal shape with the longer axis along RD, see Fig.11b. Considering the pinning force from one single particle and assuming a grain boundary which meets the particle at 90° (grain boundary perpendicular to RD or parallel to it), it was demonstrated that the shape of the particle does affect the pinning force F , as shown in Fig.11c. However, the pinning effect is significantly larger than that of a spherical particle only in the case when a particle with a small aspect ratio (convex lens shape or penny-shape) meets the boundary with its shorter axis (b) perpendicular to it (Case 1 in Fig.11c), or a particle with large aspect ratio (needle-shape) encounters a boundary with its longer axis (b) parallel to it (Case 2 in Fig.11c). When a group of particles are considered, as seen in Fig.11a, it was shown that the shape of recrystallized grains is strongly dependent on the pressure ratio (q) of P_Z / P_D^{Rex}, particle distribution parameter δ of L/d (see Fig.11a), and particle shape parameter ($e = b/a$) represented by the eccentricity of the ellipsoidal particle, as shown in Fig.12. The importance of considering the spatial distribution of particles, whether they are located at rigid/flexible grain boundaries or subgrain boundaries, was also discussed by Kwon and DeArdo in microalloyed steels [100], this will be further discussed when dealing with precipitates in **Section 4.4.1**. The elongated grain structures observed after annealing of cold rolled or extruded particle-containing materials are usually explained from these spatial distributions of particles. In fact, the misorientation dependent Zener pinning as well as the effect of second-phase particles on retarding nucleation of recrystallization, which will be discussed later, can also contribute to an elongated grain structure along RD.

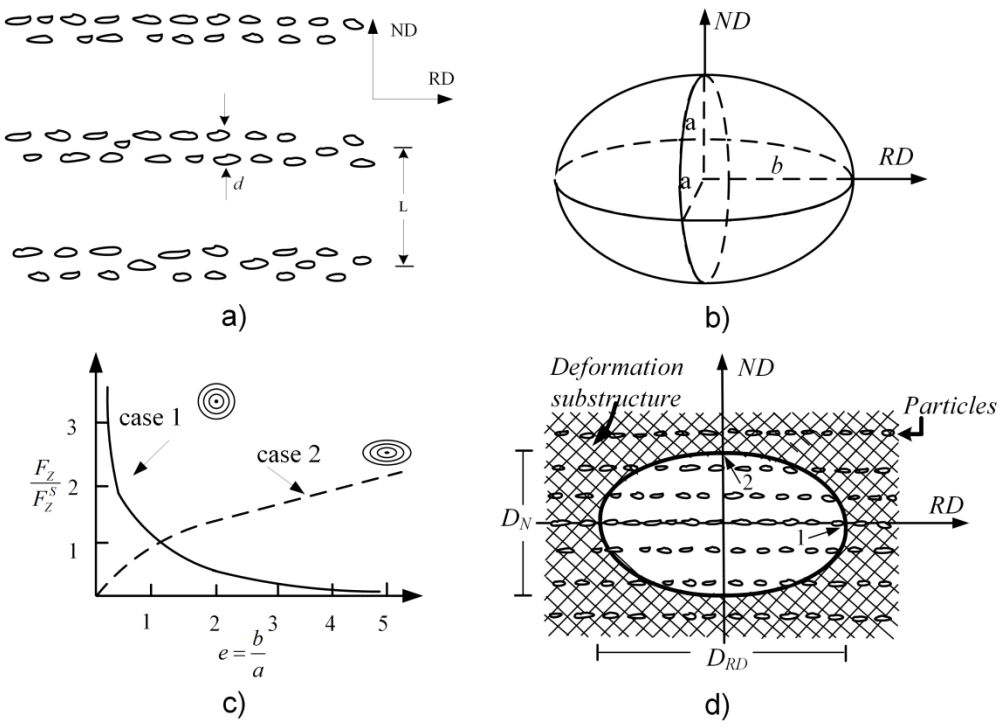

Fig.11 a) Schematic representation of the particles structure in sheet metals; b) The particles in a) have an ellipsoidal shape, rotational symmetry around the RD axis; c); The drag force as a function of particle aspect ratio for the two cases indicated; d) A short transverse-longitudinal section of a recrystallized grain. Reproduced from [25], with permission from Elsevier.

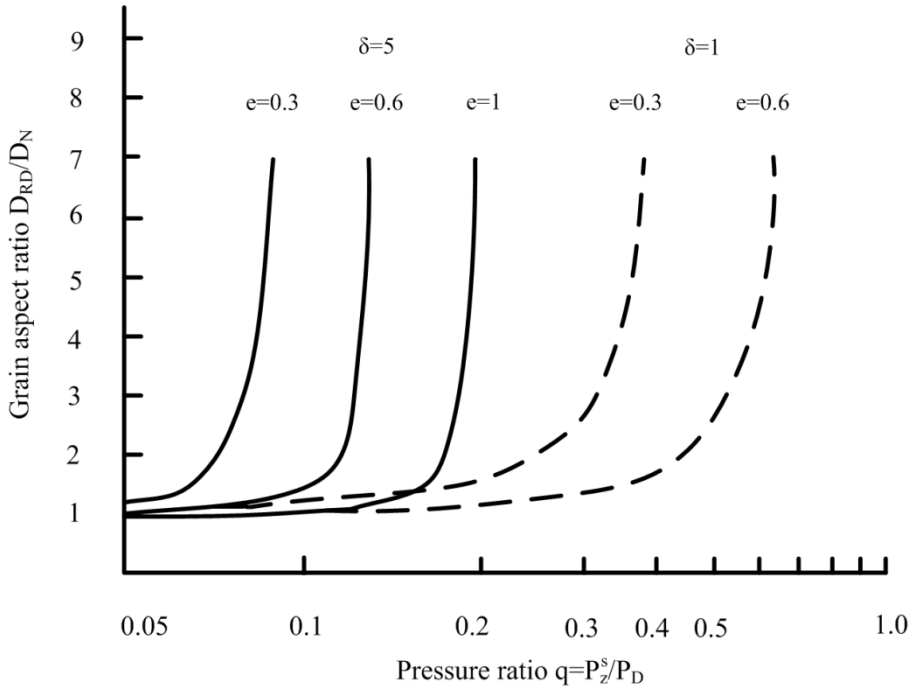

Fig.12 The recrystallized grain aspect ratio as a function of the pressure ratio q, considering different combinations of the distribution parameter δ and the particle shape parameter e. Reproduced from [25], with permission from Elsevier.

The heterogeneous spatial distribution of the Al_3Zr dispersoids within the grains in an AA7010 alloy with different Zr contents during recrystallization after hot deformation was studied by Driver et al. [247]. The local volume fraction f_V of the dispersoids varies significantly within the grain, and this has a pronounced effect on the recrystallization process, e.g., in regions of high local f_V values recrystallization is largely suppressed while substantial recrystallization does take place in regions with small local f_V. These authors calculated the local volume fractions with the help of a thermodynamic software, the results are shown in Fig.13, which are then used to calculate the local Zener pinning effect using Eq. (11).

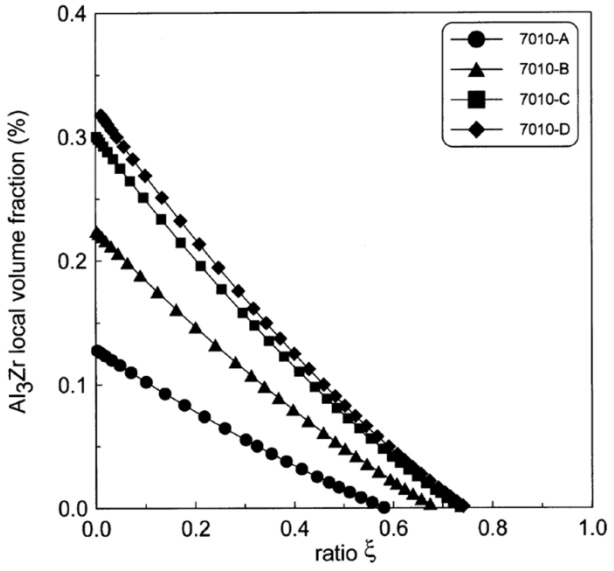

Fig.13 Thermodynamic software calculated local Al_3Zr volume fractions across a grain from the center (ξ=0) to the boundary (ξ=1) for four model alloys. Reproduced from [247], with permission of Springer.

Besides the consideration of non-ideal particle shape and spatial distribution, the effect of non-uniform particle size on recrystallization has also been analyzed. Eivani et al. [248] found that particles with different size distributions introduced by different homogenization processes, but with similar calculated Zener drag pressure according to Eq. (11), lead to different recrystallization microstructures, even though the same deformation condition was applied on an

AA7020 alloy. Based on this experimental observation, a "new relationship" for calculating the Zener drag pressure, which is actually similar to the treatment by Fullman [249], is proposed for taking into account the size distribution of particles. Instead of using the average particle size, r, and volume fraction, f_V, the particles are distributed into n different size classes described by their individual r_i and f_{Vi}, and the total Zener pinning pressure calculated as:

$$P_Z = \frac{3\gamma_{AB}}{2} \sum_{i=1}^{n} \frac{f_{Vi}}{r_i} \tag{16}$$

It was demonstrated experimentally, in two samples with identical parameters except the size distribution of particles, that when the different categories of particles have similar number densities (broad distribution), it gives rise to a larger Zener drag pressure as compared to the case where most of the particles are in the same size range (narrow distribution). The main problem with the experiment is that grain growth might have occurred (i.e., the result is not only due to particles-recrystallization interaction), since annealing was performed at 575°C for 10 min, and it is not clear whether there is particle dissolution and/or coarsening at such a high temperature. The same approach has been used in the static recrystallization model developed by Buken and Kozeschnik [250] where simultaneous precipitation and solute drag were both considered. However, the advantages of using the modified Zener pinning expression (i.e. Eq.(16)), instead of the original one (see Eq. (11)), were not discussed.

There is also considerable evidence showing that the Zener pinning effect can be ignored during annealing of heavily deformed materials where the driving force is very high: it is either reflected by the similar recrystallization temperature (i.e. a critical temperature for recrystallization to take place) or similar recrystallization kinetics at the same temperature with respect to particle-free counterparts [251]. This can be rationalized by a simple calculation of the driving pressure and pinning pressure in typical alloy systems. The driving force for recrystallization (P_D^{Rex}) can be estimated with respect to dislocation density as ~$0.5\rho\mu b^2$. Using typical values for the dislocation density, the shear modulus and the Burgers vector of heavily deformed copper, which are 10^{16} m^{-2}, 42 GPa, 0.26 nm, respectively, it yields a driving pressure of ~20MPa. For the grain boundary energy, a reasonable value would be 0.6 J/m^2, and assuming a precipitate volume fraction of 1 vol. % with an average particle radius of 50 nm, Eq. (11) gives P_Z ~0.18MPa. It can be easily seen that in heavily deformed metallic materials, the driving

pressure is generally much larger than the pinning pressure, which finally implies a negligible Zener pinning effect. This is even more so if the particle size increases or volume fraction decreases, however, it is also evident that higher volume fraction of finer particles could still lead to the full suppression of recrystallization in heavily deformed materials.

The third type of challenge in the classical Zener pinning theory during grain boundary migration involves the consideration of the possible temperature dependent effects. If only *stable* second-phase particles are concerned, a deformed microstructure can be stabilized by sufficiently small spaced fine particles up to the melting temperature of the matrix, a good example is the copper alloys [18] with densely distributed stable oxides particles inside. However, if the driving force of grain boundary migration P_D^{Rex} is not significantly larger than the Zener pinning pressure P_Z, a variation of P_Z with temperature, if existing, can be detected. The driving force for grain boundary migration P_D^{Rex} is supposed to decrease due to the decrease of dislocation density by recovery. The only other temperature dependent term in Eq. (11) is the grain boundary energy γ_{AB}, which actually increases with temperature for particle-containing alloys [252], i.e., a higher Zener pinning pressure should be the result. The mobility of a grain boundary will increase with temperature (cf. Eq.15), but grain boundary migration also requires $P_D^{Rex} > P_Z + P_C$. This implies that if a deformation structure is totally pinned by stable fine particles ($P_D^{Rex} < P_Z + P_C$), i.e., no dissolution or coarsening, recrystallization should not occur even by increasing the annealing temperature during which P_D^{Rex} tends to decrease while P_Z and P_C increase due to the increase of grain boundary energy [252]. Nevertheless, a recent study shown by Huang et al. [253], who studied recrystallization in a cold-rolled Al–Mn–Fe–Si alloy, demonstrated recrystallization of a pinned microstructure by an abrupt increase of annealing temperature. The results were interpreted by these authors as a possible indication of temperature dependent Zener pinning effect. However, with respect to this interpretation, the work described above was hampered by two complicating aspects: the deformation structure may not be totally pinned by fine particles and these particles may dissolve or grow. Even though the former was excluded by the absence of recrystallized grains even after long time annealing, while average particle size was found unchanged after the short time annealing (5s) at high temperature (500°C), local variations in deformation and particle structures are always possible. This type of studies can be ideally

carried out in alloy systems with a large amount of fine and stable oxides. Since the only temperature dependent term in Eq. (11) increases with temperature, it is difficult to understand why the Zener pinning pressure should decrease with temperature, unless dislocation-precipitate mechanisms at the atomic level are considered. In fact simulations by molecular dynamics technique have clearly shown that the critical stress for a dislocation to break away from a fine precipitate decreases and the dislocation line bows out less in the critical condition with increasing temperature [254]. This effect is more evident when the size of the incoherent precipitate increases, even though the considered precipitates sizes (<10nm) and temperatures (0-600K) are still much smaller than in the cases investigated by Huang et al. [253].

The structure of grain boundaries also plays a role in pinning the moving boundaries. This is because Zener pinning (Eq. (11)) is proportional to the grain boundary energy (γ_{AB}). Grain boundaries of low energy, such as special grain boundaries (e.g. coincident site lattice (CSL) boundaries [2]), should be less affected by second-phase particles. Humphreys and Ardakani [255], who have carefully performed annealing experiments on copper single crystals (constant driving force in the matrix) with small Al_2O_3 particles, showed that grains with close to 40°<111> ($\Sigma 7$) boundaries experience ~5-10% less pinning pressure than that of other HAGBs. The same reasoning was used to explain the formation of the strong P-texture during annealing of cold deformed particle-containing aluminium alloys, where P-grains also have close to 40°<111> orientation relationship with some deformation texture components [256,257,258, 259,260, 261, 262]. Molecular dynamic simulations by Zhou et al. [263] on the interactions between migrating grain boundaries and particles also showed that grain boundaries close to 40°<111> relationship were the fastest to overcome second-phase particles. Similar effects have also been reported for other low energy boundaries. For example, the formation of Goss texture in silicon-iron was explained by Homma and Hutchinson [264] as a result of the 39°<110> ($\Sigma 9$) boundaries between Goss-grains and matrix grains, which have lower energy than general grain boundaries and therefore are less inhibited by Zener pinning. Another example was reported by Raabe and Lücke [265], where it was found that 27°<110> ($\Sigma 19a$) boundaries in particle-containing Fe-Cr alloys were less affected by Zener pinning, even though the argument is weakened by the large deviation of 7° from the ideal orientation relationship. The result of a misorientation-dependent Zener pinning pressure is the preferential growth of grains with particular orientation relationship to the deformed matrix, which finally leads to a coarse grain

structure and strong texture components. Since the effect of misorientation-dependent Zener pinning pressure is usually not significant (~5-10% less for grain boundaries with 40°<111> orientation relationship to deformation matrix than other HAGBs according to [255]), a remarkable effect is usually only expected when the driving pressure and retarding pressure of recrystallization is of similar magnitude. If the simple case shown in Fig.11a is considered here, the recrystallized grain aspect ratio could further increase due to the preferential growth of grains which consume the elongated deformed grains after rolling or extrusion. An example of coarse elongated grain structure obtained duirng low temperature annealing of cold-rolled Al-Mn alloy can be found in a recent work by Huang et al. [262].

The Zener pinning theory is derived from energy considerations alone, it does not involve any indication of the kinetics of boundary migration. If the grain boundaries are assumed to migrate by the movement of kinked steps or ledges, as suggested by Gleiter [266], the interaction of particles with the moving boundary was calculated by Chan and Humphreys [267]. As shown in Fig.14, the considered ledge has a width of h and is assumed to have the same energy as the grain boundary energy (γ_{AB}). If a second-phase particle (with radius r) intersects with the ledge, the total area and energy of the ledge will be reduced, meaning that the ledge will experience an additional dragging force to move past the particle. The authors worked out an equation to describe the pinning force on the boundary (F_B)

$$F_B = (\frac{6}{\pi})^{1/2} \frac{f_V^{1/2} \gamma_{AB}}{r} \tag{17}$$

which predicts much higher boundary pinning force than the original Zener pinning expression (Eq. (11)) at typical volume fractions of second-phase particles (f_V <0.05).

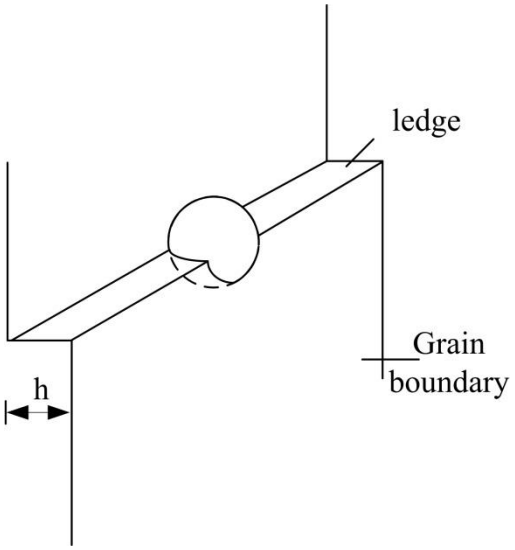

Fig.14 Schematic graph showing second-phase particle intersected by a grain boundary ledge. Reproduced from [267], with permission from Elsevier.

In contrast to the pinning effect of fine particles, it has been documented that the velocity of a recrystallization front can be enhanced by discontinuous precipitation [268]. This phenomena refers to the formation of a solute-depleted matrix and a precipitate phase, usually lamellar, when the grain boundary advances into a supersaturated matrix [269], as schematically shown in Fig. 15b. The difference in free energy of the supersaturated crystal and the crystal in which decomposition has occurred provides the driving force for discontinuous precipitation, i.e., recrystallization is by no means a prerequisite for its occurrence. If discontinuous precipitation does take place in a deformed and supersaturated solid solution [e.g., 270], its driving force further adds to the stored energy due to dislocations (see Fig.15c) and thus accelerates grain boundary migration. Of high interest to notice is that this reaction generally deteriorates the mechanical, physical, and chemical properties of many commercial alloys. This reaction is different from heterogeneous and homogeneous precipitation reactions which usually give a morphologically similar product (see Fig.15d). The product after discontinuous precipitation is actually a duplex phase material, further discussion on this topic is thus out of the scope of this review. The effect of unstable particles, e.g., particles that change their size (coarsening or dissolution) and/or their coherency with the matrix, on grain boundary migration during recrystallization will be dealt with in a separate section (**Section 4.4**). Great effort has been made

on Zener pinning during grain growth after recrystallization (see e.g. [271]), further discussion is, however, out of the scope of this review.

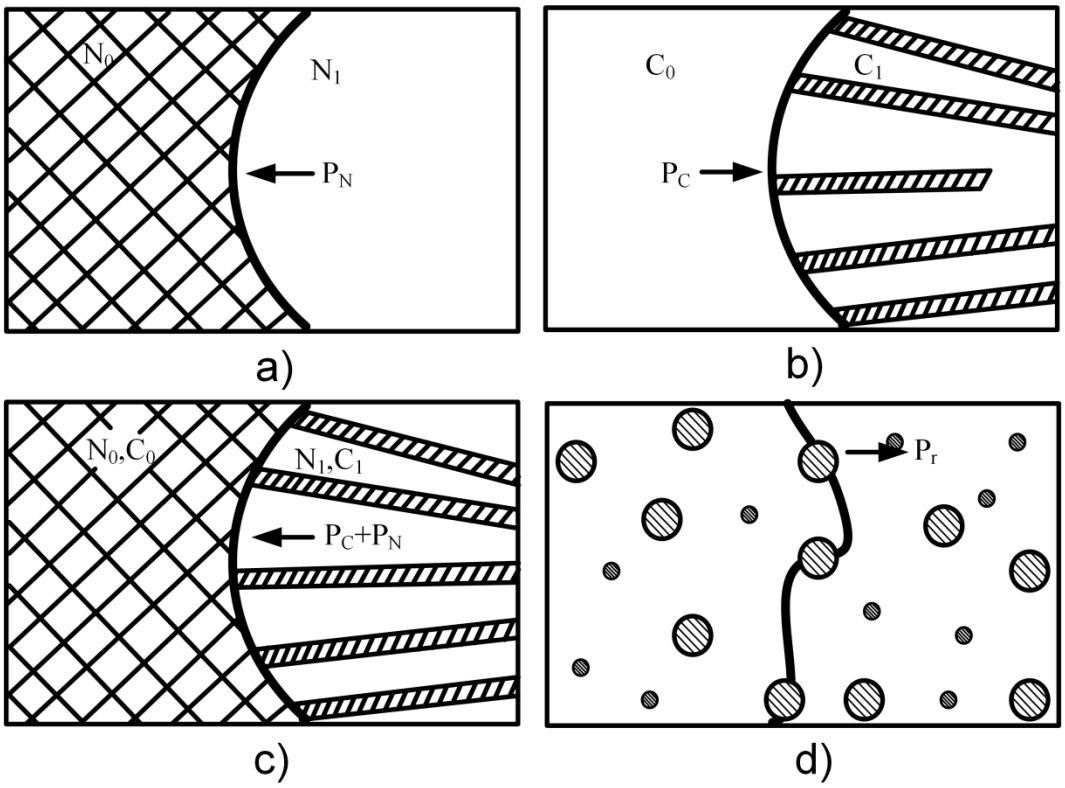

Fig. 15 Schematic micrograph of discontinuous precipitation and its connection with recrystallization. a) A moving grain boundary with driving pressure P_N reduces the dislocation density from N_0 to N_1; b) Discontinuous precipitation driven by P_C due to the difference in free energy of the supersaturated crystal with concentration C_0 and the crystal in which decomposition has occurred and solute level has decreased to C_1; c) Combined recrystallization and discontinuous precipitation reactions; d) Dispersed particles exert a retarding force P_r. Reproduced from [268], with permission from Taylor & Francis Ltd.

4.1.3 On nucleation of recrystallization

While most investigations on recrystallization of particle-containing materials consider the Zener pinning effect on boundary migration, i.e. growth rate (see **section 4.1.2**), much less work has focused on the influence of fine particles on nucleation behaviour. It is now widely accepted that precipitation can affect both the nucleation and growth stage of recrystallization [2,272]. In fact, the effect of fine particles on the nucleation of recrystallization has been claimed as more

important than that on the growth of these nuclei [273], this effect was even suggested as the only mechanism for retardation of recrystallization [251]. The fact that the final grain size of an alloy exhibiting retarded recrystallization by fine particles is usually much larger than that of its particle free counterpart also favours the argument that the rate of nucleation is more affected by fine particles than the rate of growth is. The important effect of second-phase particles on nucleation of recrystallization is unfortunately often accompanied with an over-simplification in numerical modelling [e.g.274, 275, 276] and thermomechanical process design. For this reason a detailed discussion on this point is provided in this section.

The nucleation of recrystallization involving fine second-phase particles was carefully reviewed in 2004 by Humphreys and Hatherly [2]. They concluded that, due to the lack of quantitative information, "it is still difficult at present to develop a satisfactory model for the effect of particles on recrystallization nucleation in alloys containing only small particles" [2]. While this argument still is true in many ways, important attempts have been made in recent years in this direction. It is pointed out here that nucleation of recrystallization may take place at prior grain boundaries, by discontinuous subgrain coarsening, as well as at other deformation heterogeneities such as shear bands.

Eq. (15) can also be used to analyse nucleation of recrystallization by strain induced boundary migration (SIBM) at prior grain boundaries in particle containing materials. Nucleation can only occur once the radius of the bulging boundary (R) keeps growing and becomes large enough to reach the critical value (R_{crit}) such that $\mathrm{P}_D^{Rex} = \mathrm{P}_Z + \mathrm{P}_C$. As compared to particle free materials ($P_Z = 0$), the additional pinning pressure from fine particles increases the critical size for nucleation:

$$R_{crit} = \frac{\alpha \gamma_{AB}}{P_D^{Rex} - P_Z} \tag{18}$$

It is worth noting that, in Eq. (18), P_D^{Rex} can be different from that of particle free counterparts and the critical size for nucleation will increase if multiple subgrain SIBM is considered [2]. It appears that it is relatively easy to implement the effect of fine particles on recrystallization at prior grain boundaries, as long as only stable particles are concerned. The interaction between precipitation (Nb(CN)) and recrystallization was investigated in Niobium steels by Luton et al.

[277], it was quantified that increasing volume fraction of precipitates leads to the transition from retardation of recrystallization to the full suppression of recrystallization.

The effect of fine particles on recrystallization by discontinuous or abnormal subgrain growth (not necessarily near original grain boundaries as SIBM) has also been extensively studied. This nucleation mechanism requires the migration of LAGBs to increase subgrain size and also their misorientation angle (due to the existing orientation gradient). Large subgrain size provides the driving force for subgrain growth and a higher misorientation angle increases the mobility of the boundary, both of which are necessary for the onset of nucleation. The mobilities of LAGBs are more complicated than HAGBs since they also depend on their misorientation angles which increase with the migration of LAGBs in the deformed matrix with an orientation gradient [2]. However, just like nucleation by SIBM, nucleation only occurs once a critical subgrain size (R_{crit}^{LAGB}) is reached:

$$R_{crit}^{LAGB} = \frac{\alpha \gamma_{AB}^{LAGB}}{P_D^{LAGB} - P_Z^{LAGB}} \tag{19}$$

where P_D^{LAGB} is the stored energy in the cellular microstructure, P_Z^{LAGB} can be calculated by replacing γ_{AB} in Eq. (11) by γ_{AB}^{LAGB}. It has also been realized that the rapidly growing subgrains usually are those which are slightly larger and more misoriented than the average [2]. Subgrain growth in an orientation gradient thus helps the nucleation of recrystallization. Humphreys derived an equation for the growth of subgrains in this situation:

$$\frac{dR^{LAGB}}{dt} = \frac{\alpha M \gamma_{AB}}{\theta R^{LAGB}} [\theta_0 + \Omega (R^{LAGB} - R_0^{LAGB})] \tag{20}$$

where γ_{AB} is the misorientation dependent boundary energy predicted by the Read-Shockley equation when the misorientation reaches θ, Ω is the orientation gradient, θ_0 and R_0^{LAGB} are initial values of subgrain misorientation and size, respectively. The Read-Shockley equation is often written in the form:

$$\gamma_{AB} = \gamma_m \frac{\theta}{\theta_m} (1 - \ln \frac{\theta}{\theta_m}) \tag{21}$$

where γ_m and θ_m are boundary energy and misorientation for transition angle from LAGB to HAGB, e.g. 15°.

Pinning of subgrain boundaries as a cause of retarded nucleation, which was originally proposed by Doherty and Martin [278], was observed in Al-Cu alloys after recovery where sub-boundaries were held up at θ-$CuAl_2$ particles. The pinned subgrain size was of the same order as the particle spacing, approximately 1 to 2 μm. It was further suggested that nucleation would be very difficult unless the nuclei had become mobile before being pinned by particles. If not, the formation of viable nuclei then becomes extremely difficult since the spacing of second-phase particles is so small that each developing subgrain is affected by a particle before it can grow to become a potential nucleus. A well-known example of this is sintered aluminium powder (SAP), where very stable, closely spaced oxide particles are present. These particles act to prevent the rearrangement of dislocations into cell walls or LAGBs, as well as the movement of LAGBs to form HAGBs. Samples produced by SAP must be heated to a very high temperature, usually close to the melting point, before recrystallization starts. In other words, LAGBs in these cases are not able to migrate to form critical subgrains that are large enough to overcome the Zener pinning and capillarity terms shown in Eq. (15).

Fine particles were also suggested to affect nucleation by homogenizing the deformation substructure [182, 279, 280]. Homogenization of slip by a fine dispersion of particles eliminates regions of high lattice misorientation, which are considered as preferential sites for nucleation of recrystallization. In a set of carefully designed experiments on copper single crystals with different types of stable dispersion of Al_2O_3 particles (average particle size ranging 28 - 41μm), Baker and Martin [273] demonstrated that variants exhibiting retarded recrystallization cannot be due to (sub)grain boundary pinning by the dispersed phase since calculation gave negligible pinning pressure (~1 MPa) as compared to the driving pressure (~100MPa). It was concluded that the retarding effect is due to the homogenization of dislocation distribution by the fine particles, which decreases the orientation gradient necessary for nucleation and thereby suppresses nucleation. However, this homogenization of the deformed microstructure is only significant when the interparticle spacing is similar to the cell/subgrain size [2]. In cases of larger interparticle spacing, similar misorientations were found in Cu- Al_2O_3 [178] and Al-Al_2O_3 [251] as compared to those of single-phase alloys, i.e., there was no particle-enhanced homogenization of dislocation structures during deformation in such cases.

Another important issue that should be emphasized here is that fine particles were found to not only retard but also accelerate recrystallization even though their sizes are clearly smaller

than the critical size for PSN. It has been shown, using Al-Cu alloys with the same solute content of Cu but with different *unstable* θ phase particles (volume fraction and particle size may change during annealing), that dispersed particles (<0.8μm) can lead to either acceleration or retardation of recrystallization by changing the inter-particle spacing [278]. Martin and his co-workers [273, 281] further confirmed this phenomenon in a single crystal copper-silica alloy containing only stable particles and single copper crystals with stable Al_2O_3 particles. Acceleration and retardation of recrystallization were observed in both cases when compared to their particle free counterparts. It is actually very difficult to separate the individual effect of particle size and interparticle spacing since they are often interconnected. Careful analysis of more investigations shows that the transition from accelerated to retarded recrystallization can be rationalized by considering the volume fraction (f_V) and particle radius (r). Humphreys [282] showed that acceleration of recrystallization could take place if $f_V / r < 0.2\mu m^{-1}$, even when the particles are not coarse enough to trigger PSN, which will be discussed in the **Section 4.2**. The degree of cold deformation and the annealing temperature, amongst others, also play important roles in determining whether retarded or accelerated recrystallization takes place [251, 283].

While it is straightforward to understand the retarding effect of fine particles on recrystallization, the considerable literature on particles (with size smaller than critical size for PSN) accelerating recrystallization [278, 281, 283] deserves more discussion. It could be rationalized by considering the following aspects: i) these particles introduce more geometrically necessary dislocations during deformation while they can also serve as pinning source during annealing, what matters is their net effect; ii) clustering of medium size particles or ultra-high deformation strains are enough to cause PSN since the critical size of the recrystallization nuclei is reduced at large cold deformation.

Besides their effect on recrystallization kinetics, fine particles are also reported to play an important role on recrystallization texture, or even the recrystallization mechanisms. It is now widely accepted that the orientation of the nucleus is present in the deformed structure. To the best knowledge of the present authors, there is no convincing evidence that new orientations can be formed during nucleation of recrystallization, with the only exception of nucleation by twinning. Nuclei with new orientations were reported during annealing by 3DXRD experiments with low spatial resolution (≥4μm) [e.g. 157], but more careful experiments with higher spatial and angular resolution using differential aperture X-ray microscopy (DAXM) with

polychromatic synchrotron X-ray microbeams demonstrated that "nuclei form with orientations already present in the matrix" [160]. However, this does not mean that recrystallization texture is independent of nucleation. For example, there is evidence that the pinning pressure from fine particles favours the recrystallization of cube oriented grains during annealing at low temperatures in cold rolled AlFeSi alloy, the reason being that cube oriented subgrains have a size advantage over that of other orientations [284]. The reason of fine particles affecting the recrystallization texture is also often ascribed to the preferential growth of crystals (subgrains or grains) with certain orientation relationships to their surroundings, as already discussed in **Section 4.1.2**. In terms of their effect (also effect from solutes) on determining recrystallization mechanisms, good examples include the change from CDRX to DDRX for aluminium during hot deformation when its purity is improved [285, 286,287] or for aluminium alloys when high solute addition (e.g. Mg) raises the overall dislocation density in the deformed matrix and large particles stimulate nucleation [288,289]. A transition from discontinuous to continuous static recrystallization was also found for aluminium alloys with different second-phase particles [110].

4.2 Effect of coarse particles on recrystallization

4.2.1 Mechanism of Particle Stimulated Nucleation (PSN)

It was mentioned in **Section 3** that coarse second-phase particles could promote PSN by forming deformation zones, we will address it in detail now. PSN has been extensively studied during static recrystallization following cold deformation. However, there are also ample examples showing PSN during or after hot deformation.

It is helpful to first examine the deformation zones around coarse second-phase particles. Such zones are often associated with local lattice rotations close to the particle, an example of a ferritic stainless steel cold-rolled to 80% reduction [290] was characterized by EBSD and shown in Figs.16a-e, and another example of an Al-Mn alloy cold-rolled to 95% reduction [258] is illustrated in Fig.16f by SEM BSE micrographs. The deformation zones around coarse particles with different shapes can be found in Ref [290]. The texture evolution during deformation in the deformation zone of coarse second-phase particles has been simulated by means of the finite element method [191, 240], which confirms experimental results in that texture within the deformation zone is not completely random [2, 259, 290].

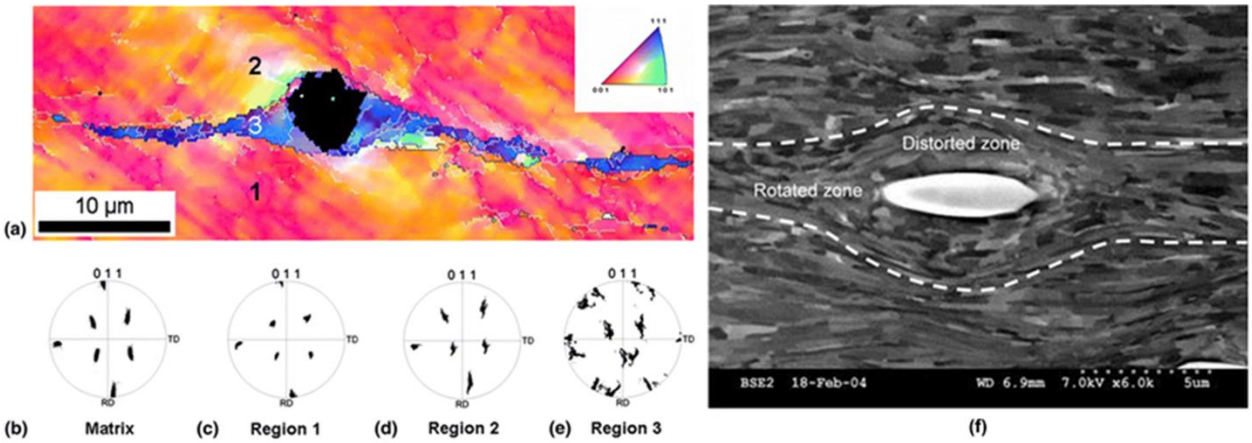

Fig.16 EBSD results showing the deformation zone around a spherical particle (black in the map) in a ferritic stainless steel cold-rolled to 80% reduction: (a) EBSD inverse pole figure (IPF) map; (b) {011} pole figure of the large grain; (c) through (e) {011} pole figures corresponding to the regions 1, 2, and 3, respectively. Reproduced from [290], with permission from Elsevier; and f) BSE micrograph showing a deformation zone around a large particle formed during cold rolling of an Al-Mn alloy to a strain of 3.0. The white broken lines envelope the typical deformation zone. Reproduced from [258], with permission of Springer.

Much of the analyses on the crystallographic misorientations and dislocation density around coarse second-phase particles are still using the empirical equation proposed by Humphreys [183] based on experiments conducted on single crystals of aluminium and copper, oriented for single slip in tension:

$$\tan\theta = \tan\theta_{max}\exp(-\frac{c_1 x}{2r}) \tag{22}$$

where c_1 is a dimensionless constant, r is the particle radius and x is the distance from the particle (r and x have the same unit). The maximum misorientation is independent of particle size once $2r > 2.5$ μm, and it is only a function of the shear strain (γ):

$$\theta_{max} = c_2 \tan^{-1}\gamma \tag{23}$$

For smaller particles with diameters in the range from 0.1 to ~2.5μm, the maximum misorientation $\theta'_{\max}$ is best fitted by:

$$\theta'_{\max} = 0.8\theta_{max}(2\,\mathrm{r} - 0.1)^{0.2} \tag{24}$$

where c_2 is a constant of the order of unity and γ is the shear strain. The shape of the deformation zone, however, was not specified. Even though the empirical Eqs (22-24) were developed based on simplified conditions (single crystal with single slip), later experimental

work seem to justify their validity in both single crystal [37] and polycrystalline alloys [291], see Fig.17. The dislocation density variation with the distance from the particle (x) can also be estimated with respect to the misorientation angle (θ):

$$\rho = \frac{K}{b}\frac{\theta}{x} \tag{25}$$

where K depends on the dislocation structure, a value of 2 is chosen assuming that low angle boundaries with misorientation (θ) consist of square networks of dislocations [2, 292]. With the absolute orientation gradient, $\left|\mathrm{d}\theta / \mathrm{dx}\right|$, calculated from Eq. (22), the dislocation density is

$$\rho = \frac{c_1 \tan\theta_{max} \cos^2\theta}{br} \exp(-\frac{c_1 x}{2r}) \tag{26}$$

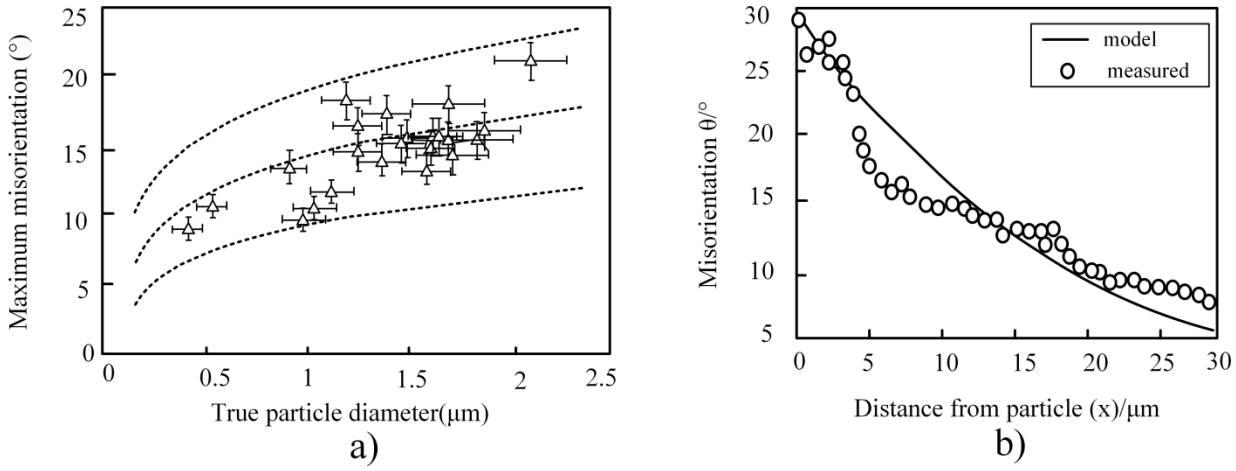

Fig. 17 a) Maximum misorientation (θ_{max}) as a function of particle diameter with trends (dashed lines) expected from Eq. (24) for θ_{max} = 15–25°. Reproduced from [37], with permission from Elsevier; b) The measured misorientation profile away from a particle cluster in Mg alloy deformed to 1.2 compared with the empirical Eq. (22). Reproduced from [291], with permission from Elsevier.

With a better image of the deformation zones around coarse second-phase particles in mind, we are now able to treat nucleation of recrystallization in and near these zones, a topic that has been systematically studied by Humphreys [2, 293] in Al alloys. Like most of the other nucleation mechanisms, two necessary criteria for the formation of a nucleus must be met. The first one is a HAGB (θ_{max} > 10–15°) with the surrounding matrix substructure which possesses

high mobility. It can be seen from Fig. 17 that misorientations of this magnitude may already exist after deformation around particles greater than 1.5–2.0 μm, it can also be easily accumulated by the migration of LAGBs (subgrain growth according to Eq. (20)) since a misorientation gradient is already present around coarse particles, i.e. nucleation not always takes place near the particle. The second critical condition for PSN is that a critical *nucleus* size must be reached to give a driving force advantage, which can be calculated according to Eq. (18). The critical *particle* size ($d_{crit} = 2r_{crit}$) to trigger PSN is estimated by assuming that when the nucleus has consumed the deformation zone, it has a radius of curvature equal to the size of the particle, i.e. Eq. (18).

$$r_{crit} = \frac{\alpha\gamma_{AB}}{P_D^{Rex} - P_Z} \tag{27}$$

Since the driving pressure is a function of dislocation density ($\sim 0.5\mu\rho b^2$), which can actually be estimated with Eq. (3) or Eq. (26), both of which are dependent on shear strain (noting that θ_{max} in the latter equation is dependent on shear strain), it follows that the critical size for PSN decreases with increasing strain, i.e. the critical particle size is not a constant value. This dependence has been confirmed by experiments [293]. Typically, PSN occurs at particles greater than ~1 μm [2]. However, a smaller critical particle size of 0.68 μm (close to the subgrain diameter) was indicated for cold-rolled (65% reduction) and then annealed (480°C for 0.5 min) Fe-0.4% C alloy [294]. Moreover, particles in close proximity also enhance the recrystallization tendency [39, 294], an example of a deformation zone induced by a cluster of relatively small particles is shown in Fig.18.

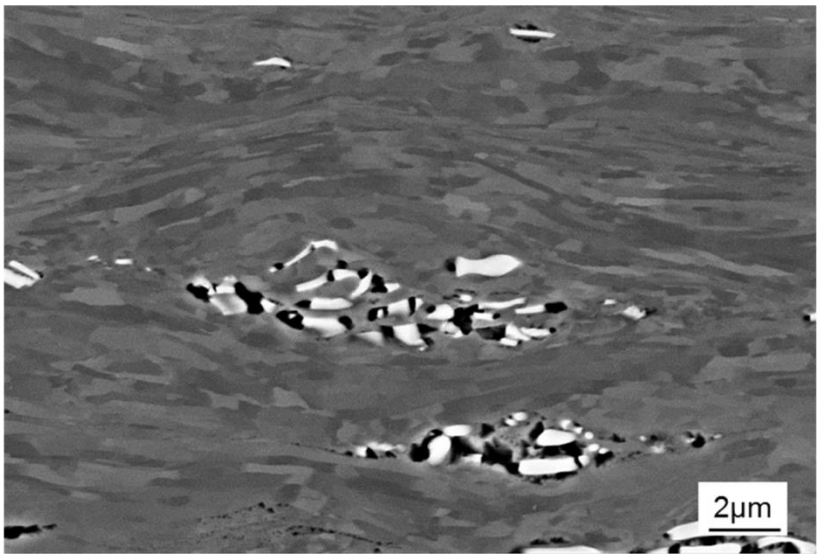

Fig. 18 BSE micrograph showing a deformation zone around a cluster of relatively small particles in Al-Mn alloy cold-rolled to 95% reduction.

An example of early stage PSN illustrated by EBSD mapping is shown below in Fig.19 for a Fe_3Al-based alloy that has been warm rolled at 630°C to thickness reduction of 82%. The disturbance of microstructure around the coarse particle is obvious, noting that the particle was embedded in one grain with reference colour shown at (a), and the distinctly different grain orientation near position (b).

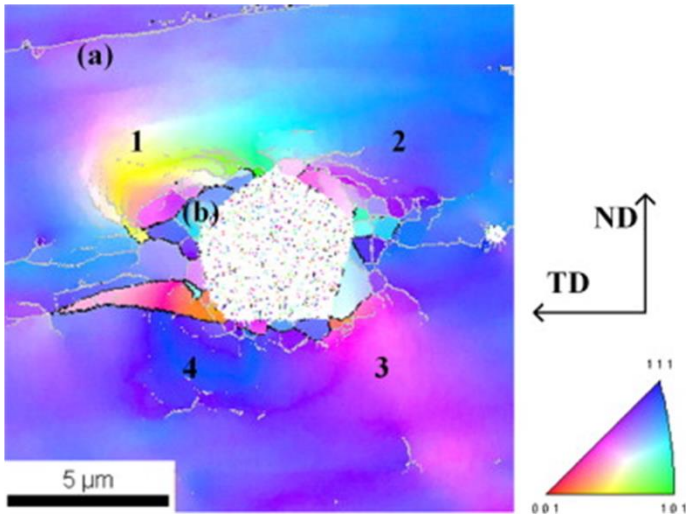

Fig. 19 Inverse pole figure EBSD map showing the deformation zone around a $(Fe,Al)_2Zr$ Laves phase particle after warm rolling at 630°C to true logarithmic strain of 1.7. Reproduced from [36], with permission from Elsevier.

The 3D-EBSD technique, i.e. sequentially removing sections of a material by FIB and mapping the microstructures of each created surface by EBSD, also sheds light on PSN that is not clearly evident in 2D-EBSD [36, 37]. Using this technique, the deformation and recrystallization behaviour of a cold-rolled Ni-0.03 wt.% Si containing 0.4–2.2 μm silica particles was investigated [37]. It was confirmed that PSN occurred at particles greater than 1.5–2 μm, and also observed was the formation of interfacial voids at all particles. More interestingly, PSN was found to generate contiguous grains separated by both coherent and incoherent twin boundaries. Coherent boundaries dominate and remain parallel to the primary growth direction of the grains on further growth of these grains into the matrix, as schematically shown in Fig.20.

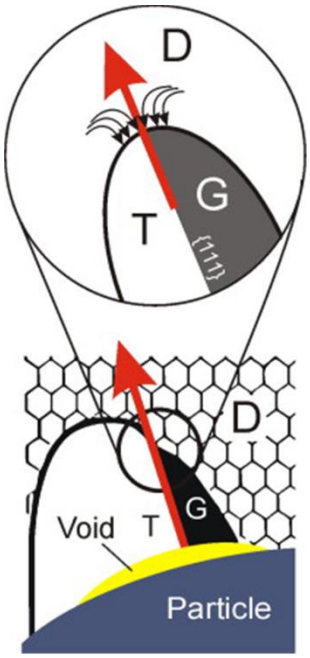

Fig. 20 Schematic diagram showing the primary growth direction (indicated by the red arrow) of a twinned grain during PSN and the grain/twin/substructure triple junction. Reproduced from [37], with permission from Elsevier.

Even though PSN has been extensively studied in FCC materials, in particular Al alloys, examples in BCC material [36, 290, 294] and HCP materials [291] also exist in the literature. Besides PSN during SRX, this nucleation mechanism is also found in DRX and MDRX experiments [291, 295, 296, 297]. However, it was concluded that PSN will not be as effective during DRX and/or MDRX than during SRX due to the fact that dislocations may bypass particles without forming a deformation zone [298], or due to the development of a dislocation

structure within the newly formed grains as a result of the concurrent deformation [299], or to the activation of other nucleation mechanisms such as nucleation at original grain boundaries [300]. Quite differently from PSN during hot deformation, coarse primary γ'particles in a Ni-based superalloy with γ matrix were ascribed to induce heteroepitaxial recrystallization [301], i.e., nucleation of coherent γ grains around γ'particles prior to deformation and then growth of these γ grains during deformation driven by the stored energy difference with the surrounding γ matrix.

4.2.2 Acceleration of recrystallization and grain refinement by PSN

PSN is generally regarded as an effective approach to accelerate recrystallization and to obtain a fine-grained microstructure. An essential question regarding PSN is how many nuclei can each particle that is larger than the critical size create? Also of interest is how different factors such as the particle sizes and their spacial distribution affect PSN.

After the deformation zone with large misorientation gradient is consumed, nucleated grains with HAGBs and a large enough nucleus/grain size might grow out of the deformation zone under the driving force of the matrix stored energy, however, this is not always the case. The determining factors which affect their further growth will be the same as other nucleated grains as discussed in **Section 4.1.2.** If an efficiency (number of nuclei per particle) of 1 is assumed, such as in alloys with large and widely spaced particles, the final recrystallized grain size (R) based on PSN can be related to the particle volume fraction (f_V) and size (r) as [2]:

$$R = r / f_V^{1/3} \tag{28}$$

Experimental work has clearly shown that the efficiency of PSN near coarse particles (with size over critical size) is often significantly less than 1. An efficiency <1% (with respect to those with diameter>1μm, noting that 1 μm is not necessarily the critical size for PSN for this case) was reported during annealing at 400°C of a hot compressed Mg-Mn alloy systems, deformed at 300°C, strain rate of $10^{-3}s^{-1}$, strain of 1.2, where no significant solute elements or fine dispersoids were involved [291]. Vatne et al. [302] developed a model to describe recrystallization (including PSN) after hot deformation of Al alloys, the efficiency of PSN was tuned to fit the experimental results, the values of 0.18 and 0.1 were found for AA3004 alloy and AA1050 alloy, respectively. While this low PSN efficiency after hot deformation could be

explained by the recovery activities which reduce the turbulent microstructure near coarse particles, similar low efficiency levels were also reported by Hansen and Bay [303] during annealing of 90% cold-rolled Al containing large $FeAl_3$ particles (>1.5-2.0 μm). The difficulty in experimentally determining PSN grains should not be ignored, it lies in the 2D nature of the observed surface sections, i.e., some isolated grains in the observed surface section might be in contact with a coarse particle in the bulk, and a grain in contact with a coarse particle in the observed surface might be nucleated from other sites but subsequently grow to touch or even encircle the particle, see e.g. Ref [294]. Experiments using 3D-EBSD and the electron channelling contrast technique can be used to resolve this problem, an example is given in Fig.21 where it was found only 74.3% of the PSN nuclei in 3-D would have been classified as near large particle clusters in 2-D [39]. These authors reported that *all* single big particles (>3 μm) and clusters of big particles have stimulated nuclei in a 80% cold-rolled AA3104 Al alloy, even though it might be possible that an isolated recrystallized grain could further grow to touch large particles. The fact that coarse particles are usually preferentially located at HAGBs after deformation further complicates this problem. The PSN efficiency was also found to change with annealing temperature, more than one nucleus per large particle (5.95±2.68 μm) can be formed during high temperature annealing (over 400°C) of 75% cold-rolled Al-1.6wt %Si, as reported by Chan and Humphreys [267]. It should be noted that the PSN efficiency results reported above are not strictly based on the number of particles with calculated critical size (cf Eq. (27)), i.e., fine dispersoids are involved, except for the first example. Actually, the PSN efficiency from particles over the critical size still depends on whether their sizes are close to or far bigger than the critical size [2]. The efficiency of PSN can be affected by a number of factors through their influence on grain boundary mobility, driving force and retarding force for nucleation, such as the annealing temperature, applied strain, deformation temperature and stacking fault energy of the material, which influences the recovery rate. As stated already, it is also strongly affected by other competing nucleation mechanisms such as nucleation at original grain boundaries or shear bands [291].

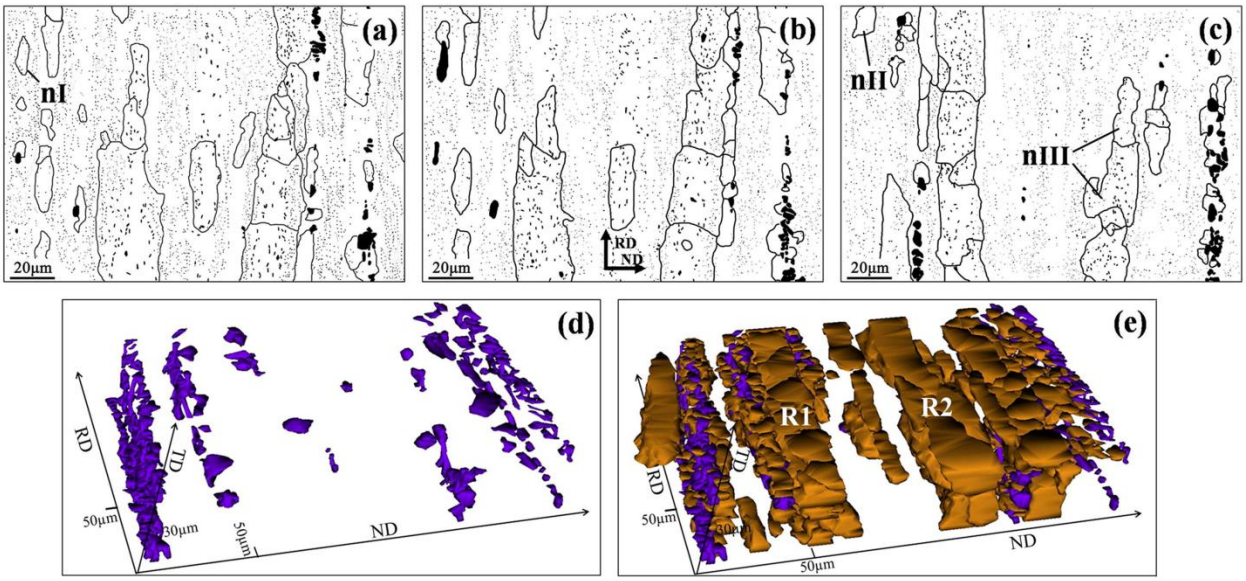

Fig. 21 Recrystallization of cold-rolled (80% reduction) AA3104 alloy after annealing at 300°C for 1h (a–c) Sketches of the same area after different steps of serial sectioning. Big intermetallic particles are represented by the solid black areas and areas surrounded by black lines represent the nuclei/recrystallized grains. Nuclei nI, nII and nuclei cluster nIII are pointed out since they would have been wrongly classified as nuclei away from big particles if only one section was characterized. (d) 3-D reconstruction of all big intermetallic particles within the area of (a–c). (e) 3-D reconstruction of both big intermetallic particles and nuclei. Reproduced from [39], with permission from Elsevier.

To summarize, we conclude that PSN does not necessarily occur at each overcritical particle, a lower efficiency is instead often observed. Therefore, the acceleration of recrystallization and grain refinement could only be reached when the affecting factors are in favour of PSN, e.g. large number of coarse particles, high strain levels, high annealing temperatures etc.

4.2.3 Orientation of PSN nucleated grains

Besides their effect on acceleration of recrystallization and producing finer grain structure, large second phase particles have also been frequently reported to modify the recrystallization texture. Even though PSN is often reported to randomise or at least weaken the recrystallization texture [187], the opposite effect, i.e., strengthening of recrystallization texture, has also been documented [e.g. 258]. For a detailed survey of literature before 2004, the reader is referred to the textbook of Humphreys and Hatherly [2]. The main conclusions from Ref [2] and literature

before 2004 can be summarized as follows: i) PSN nuclei near single coarse particles are not randomly oriented [304]; ii) the spread of total PSN nuclei over all the coarse particles may still lead to an almost random distribution of nuclei orientation, particularly in heavily deformed polycrystalline materials [2]; iii) the recrystallization texture from PSN is temperature dependent [305,306], i.e., similar to the deformed matrix orientations at low annealing temperature but nearly random at high recrystallization temperature. This latter result was ascribed to the fact that PSN nuclei are initiated at different places in the deformation zone, PSN from subgrains were found to locate in the outer periphery of the deformation zone at low annealing temperatures but close to the particle at high annealing temperatures; iv) a strong recrystallization texture can still result when the volume fractions of particles are low [2], or if deformation strain is small [307], or if there is a pinning effect from small particles [255] and/or there is oriented growth [308] (grains with a special orientation relationship to the deformed matrix will have a higher growth rate). Most of the recent works on this topic agree well with these conclusions. We are mainly concerned here with new information obtained after 2004.

Recent advance in characterization techniques, especially the use of 3D-EBSD, shed new light on our understanding of the orientations of PSN grains. The early recrystallization (see also Fig.21) of a particle-containing AA3104 alloy cold rolled to reduction of 80% was examined using 3D-EBSD [39]. A total of 2423 nuclei were inspected, and 90% of the nuclei were found at clusters/bands of big particles, the orientations of all the nuclei are shown in the ODF map in Fig.22. The resulting texture is clearly not random, even though the intensity of the texture is not very high. Statistical measurements show that 2.6%, 52.9% and 44.5% of the nuclei belong to the cube, rolling and random orientations, respectively. The texture after full recrystallization was not provided in Ref [39], which inevitably will contain nucleation from other sites such as grain boundaries and shear bands, and may also include orientation dependent growth rate differences, i.e. conditions not considered as ideal to study orientations of PSN grains. The fact that PSN does not lead to a random texture but also consists of retained rolling orientations was also discussed with respect to 3D-EBSD experiments [36]. Twin formation during PSN, which obviously will change the orientation of growing grains, was also reported using 3D-EBSD experiments [37].

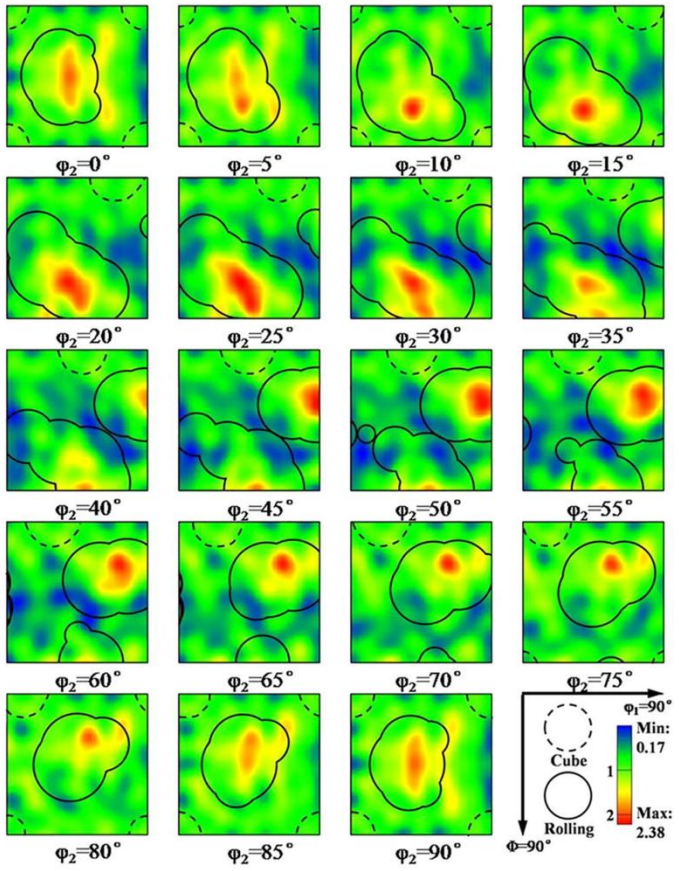

Fig. 22 Recrystallization of a cold-rolled (80% reduction) AA3104 alloy after annealing at 300°C for 1h. The ODF map showing the orientations of all nuclei within the entire examined volume; black broken line areas show cube and full line areas show rolling orientations. Reproduced from [39], with permission from Elsevier.

Recrystallization textures can still develop even if close to randomly distributed orientations are nucleated. They are usually explained by the preferential growth of certain orientations (oriented growth) or nucleation by mechanisms other than PSN, i.e. it is a problem related to the growth of the nuclei instead of the nucleus orientations. The growth of nucleated grains can be affected by different factors, such as fine dispersoids as discussed in **Section 4.1.2,** the deformed microstructure (hot or cold deformation), and the annealing temperature. Unfortunately, except few investigations on single crystals [e.g. 307], none of these existing studies made an effort to distinguish orientations nucleated from PSN from those of other sites (as was done in Fig.21), so care should be taken in interpretation of these results. The oriented growth theory relies on the growth advantage of certain PSN orientations (e.g. P or ND rotated cube orientations) mostly due to their close to 40°<111> orientation relationship (or other ones such as 24°<150> [307]) with

the deformed matrix [e.g. 309] or to misorientation dependent Zener pinning effect [256]. Nucleation mechanisms other than PSN include nucleation at original (HAGB) grain boundaries, shear bands, transition bands (boundaries separating highly misoriented blocks within a single grain) [310] or retained deformed cube bands etc. Nucleation at original grain boundaries by SIBM usually leads to a near retained deformation texture since that is where they originate from [311]. Shear bands are also preferred sites for nucleation, which typically leads to P-, Q- and Goss-components [309]. Recrystallization of hot rolled Al alloys often results in a strong cube texture, the nuclei of which come from retained cube bands having both number and size advantage over the others [256]. On the other hand, annealing of cold-rolled Cu also leads to the formation of cube orientations at transitions bands due to their fast recovery [185]. The annealing temperature affects the recrystallization texture not only because of the change of nucleation mechanisms, but also because concurrent precipitation is strongly temperature dependent, a topic which will be further discussed in the next sections.

4.3 Bimodal second-phase particles structure

Many conventional alloys exhibit a bimodal second-phase particle structure, typical examples are aluminium alloys, which make the analysis of their effect on recrystallization more complex. The relatively simple cases with stable coarse particles and fine dispersoids present prior to annealing are first considered here, a special case with two different types of fine dispersoids is also included, and more complex cases with unstable particles such as those with concurrent precipitation will be addressed in later sections.

4.3.1 On grain size

Recrystallization of alloys containing bimodal second-phase particles has been analysed by Nes and co-workers [312,313, 314] on Al-Mn alloys. In alloy systems with both coarse particles and fine dispersoids prior to recrystallization, it can be assumed that nucleation of recrystallization is restricted to the deformation zones surrounding large particles by PSN [267,314]. Only particles exceeding a critical size ($d_c = 2r_c$, which could be calculated from Eq. (27)) can potentially lead to PSN (with nucleation efficiency k). The total number of potential

nucleation sites per unit volume, $N(r_c)$, can be calculated if the distribution of particle size ($f(\mathrm{r})$) is available.

$$N(r_c) = \int_{r_c}^{\infty} f(\mathrm{r}) dr \tag{29}$$

Since the PSN near coarse particles is more or less randomly distributed in space, the Johnson-Mehl, Avrami and Kolmogorov (JMAK) approach [315,316,317,318,319] should apply. During recrystallization, some potential sites are consumed by nucleating a recrystallized grain and the remaining sites after recrystallization time t is:

$$N = N(r_c)\exp(-k\,\mathrm{t}) \tag{30}$$

which leads to the rate of disappearance of the remaining nucleation sites:

$$\dot{N} = -N(r_c)k\exp(-k\,\mathrm{t}) \tag{31}$$

If site saturated nucleation is considered, i.e. $kt_f >> 0$ (t_f is the time needed to complete recrystallization), the average grain size (D) is given by:

$$D = (\frac{6}{\pi} N(\mathrm{r}_c))^{-1/3} \approx (N(\mathrm{r}_c))^{-1/3} \tag{32}$$

In another extreme case when $kt_f \to 0$, nucleation rate is $N(r_c)k$ according to Eq. (31) (nucleation rate is the opposite of the rate of disappearance of the remaining nucleaiton site) and the average recrystallized grain size will be:

$$D = (\frac{M(P_D - \mathrm{P}_Z)}{kN(r_c)})^{1/4} \tag{33}$$

where the effect of fine dispersoids are considered during nucleation by Eq. (27) and grain boundary migration by Eq. (15). This means the recrystallized grain size can be controlled by the following parameters: i) size distribution of coarse particles with radius larger than r_c (i.e. $N(r_c)$); ii) the stored energy P_D; and ii) Zener pinning from fine dispersoids P_Z, which is a function of the size and volume fraction of dispersoids. This is of course an over-simplified analysis, where the more complex effects of fine dispersoids on nucleation and grain boundary migration as discussed in **Section 4.1** are not considered, neither are the turbulent microstructures around the coarse particles presented in **Section 4.2**. Moreover, assuming nucleation is totally coming from PSN near a large number of coarse particles would in general imply a close to random recrystallization texture, with some dependence on annealing temperature [305, 306].

Recrystallization of alloy systems with more stable bimodal second-phase particles than the Al-Mn alloys considered by Nes and co-workers have also been reported. Hansen and Bay [303] investigated the recrystallization behaviour of 90% cold-rolled Al with fine Al_2O_3 (0.047 μm) and coarse $FeAl_3$ particles (average size of 0.48 μm, ranging 0.2-4 μm). They found that the recrystallization nuclei were mainly formed at the initial grain boundaries and at deformation bands, and nucleation at these sites was enhanced with the presence of $FeAl_3$. Even though the average size of $FeAl_3$ particles was smaller than the typical size for PSN, these authors measured a very low PSN efficiency on isolated large $FeAl_3$ particles (>1.5-2 μm). They concluded that nucleation was delayed by fine alumina particles and both coarse and fine grain structures (or accelerated and retarded recrystallization) can be achieved by appropriate control of the bimodal particle structure. It is also possible that the net effect from coarse and fine particles is very small. The fraction of large $FeAl_3$ particles (>1.5-2 μm) was not given in this study, however, it is very likely to be very low considering the small average particle size (0.48 μm). Even for the small fraction of large particles, their size was close to the critical particle size for PSN, the retardation of nucleation by fine dispersoids is therefore reasonable. In an Al-Si alloy with stable bimodal particles, 0.35 vol % of coarse particles (5.95±2.68 μm) and 1.36 vol % of small particles (0.12±0.07 μm), recrystallization kinetics was delayed and similar to an alloy containing only small particles [267]. This demonstrated that even when the size and volume fraction of coarse particles are enough to trigger substantial PSN as compared to a particle-free counterpart, a large number density of fine dispersoids could still act to compensate the PSN acceleration effect through a strong Zener pinning during the growth of the nuclei. However, the large particles were observed to stimulate nucleation, the retardation of recrystallization was ascribed to the retarding influence of fine dispersoids during early stage growth of recrystallized grains [267]. Generally speaking, the fact that nucleation at coarse particles could still take place in alloys containing fine dispersoids is not surprising. It is likely that there exist particle free zones (PFZs), which arise due to the local depletion of dispersoids-forming alloying elements in supersaturated solid solution around coarse particles. This is of course dependent on the investigated materials, examples of PFZs in an Al-Mn alloy are shown in Fig.23 [258]. Even if nucleation was still affected by fine dispersoids, the large dislocation density and orientation gradient around such coarse particles (see **Section 4.2.1**) may be high enough to overcome the pinning effect from fine dispersoids to form PSN nuclei. Another possibility (not necessarily in

this case) would be that PSN nuclei are too small to be affected by fine dispersoids, i.e., the size of PSN nuclei is smaller than the spacing of fine dispersoids. There is also evidence that some orientations may have growth advantage and/or are less affected by the fine particles, as already discussed in **Section 4.1.2**.

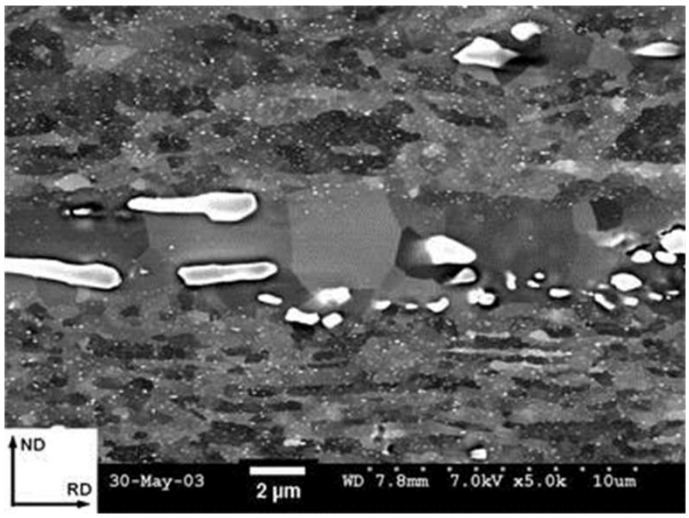

Fig. 23 Micrograph showing nucleation at constituent particles in Al-Mn alloy. The bimodal particles were produced by homogenization (i.e., they can be considered as stable particles), the sample was 95% cold-rolled and then annealed at 300 °C for 10^4 s. Reproduced from [258], with permission of Springer.

Significant grain refinement of an AZ91 Mg alloy matrix was achieved during hot deformation with 1 vol.% of small SiC particles (0.2µm) and 9 vol.% of coarse SiC particles (10 µm) as compared to its two counterparts with only one type of particles deformed under identical conditions [320]. This was ascribed to the combined effect of stimulated nucleation by coarse particles (i.e. higher nucleation number density) and a pinning effect on grain boundary migration from small particles during hot deformation (i.e. slower grain boundary migration). A careful study on recrystallization behaviour of a Cu-Cr-Zr a**l**loy with a bimodal distribution of particles was reported by Morris et al. [321]. These authors compared the recrystallization behaviour of different variants with different particle structure combinations, taking into account the effects of cold deformation strains and annealing temperatures. However, a major drawback of this work in interpreting the effect of bimodal particle structure on recrystallization is that the average size of the coarse particles was only 1.2µm and the maximum diameter never exceeded 2µm, i.e., most probably a very weak PSN effect was involved. The early stages of

recrystallization in severely deformed AA3104 alloy containing bimodal second-phase particles were investigated by Paul et al. [322], nucleation was clearly observed both at and far away from coarse particles. However, no detailed information was given on the average sizes and volume fractions of coarse and fine particles, nor did they provide a comparison of recrystallization behaviour with particle-free counterparts. In cases where the size of coarse particles is smaller or close to the critical size for PSN or their volume fraction is very small, the acceleration of recrystallization or grain refinement is expected to be small. It appears that all these examples are in qualitative agreement with the simple analysis provided by Nes and co-workers [312, 314], however, further improvements are still needed to aim for better quantitative prediction against experimental data.

Besides coarse and fine bimodal particle structures, it is also possible to tailor microstructure and texture with different types of fine dispersoids. This is important in that a large volume fraction of coarse second-phase particles is usually detrimental to material properties such as fatigue life, as will be further discussed in **Section 5**. In Al-Cu-Li alloys, the addition of Zr leads to the precipitation of fine spherical Al_3Zr dispersoids that are coherent with the Al matrix, while Mn additions result in larger lath-shaped semi-coherent $Al_{20}Cu_2Mn_3$ dispersoids. The opposite microsegregation patterns of these two elements should intuitively give a more even distribution of dispersoids in the rolled products, which in principle should increase recrystallization resistance. An excellent example with very detailed characterization of particle size, volume fraction for each of the two types of dispersoids, as well as the stored energy before recrystallization, was given by Tsivoulas and Prangnell [62]. In their study, the influence of individual and joint Zr and Mn additions on the recrystallization behaviour of a hot-rolled AA2198-base (Al-Cu-Li) alloy was analysed during annealing at 535 °C. It was shown that the recrystallization resistance effect from Zr decreases with the addition of Mn. This is because the formation of additional $Al_{20}Cu_2Mn_3$ dispersoids by adding Mn into AA2198 also leads to the expansion in width of the Al_3Zr-free bands, and their own pinning pressure are not enough to adequately compensate for this, even with the same Zr content (i.e. more total number of dispersoids). The pinning pressure of $Al_{20}Cu_2Mn_3$ dispersoids in retarding recrystallization is about a factor of four lower to that of the Al_3Zr phase, due to their poorer coherency with the matrix, as well as the higher aspect ratio. Moreover, the coarser $Al_{20}Cu_2Mn_3$ dispersoids also increase the stored energy during hot rolling before recrystallization. The addition of Zr and Mn

also to a large extent determines the recrystallization mechanisms. The alloys with effective Al_3Zr dispersoids nucleate by broad front SIBM whereas the addition of Mn favours PSN, leading to the growth of recrystallized grains with orientations inherited from rolling orientations in the former case and randomly oriented grains during recrystallization in the latter case. It is noted that PSN was not directly due to the presence of $Al_{20}Cu_2Mn_3$ dispersoids since they were far below the critical size, instead it was from the small fraction of coarse constituent particles inherited from casting. The addition of Mn increased the volume fraction of constituent particles, i.e., led to more PSN sites, and also formed less effective dispersoids in pinning grain boundary migration.

4.3.2 On recrystallization kinetics

Now that the effects of bimodal second-phase particle structures on recrystallized grain size have been illustrated, it is also of high interest to further elaborate their influence on recrystallization kinetics. Recrystallization kinetics in terms of transformation time t_f is a function of growth rate of individual grains (cf. Eq. 15) and the number of remaining nucleation sites (i.e. N, including all potential nucleation sites (cf. eq. 30)), where an increase of both leads to faster kinetics. i.e. shorter time t_f to complete recrystallization. This means that, qualitatively, more PSN (from large particles) will lead to faster kinetics as well as smaller grain size. On the other hand, a strong Zener drag (from finely dispersed dispersoids) will slow down/retard kinetics both through a direct effect on the growth rate (Eq. 15) and indirectly through possible suppression of nucleation (fewer viable nucleation sites). Consequently, a coarser recrystallized grain size is usually obtained when finely dispersed dispersoids are involved. In alloys with a bi-modal particle size distribution, the net effect may be limited.

Quantitatively, the transformation kinetics can be conveniently and accurately described in most cases by the classical JMAK equation [315, 316, 317, 318,319]: $X_V(t) = 1 - \exp(-kt^n)$, where $X_V(t)$ is the volume fraction of transformed material at the annealing time t, k is a function of growth rate and nucleation rate/density of viable recrystallization nuclei and n the so called Avrami exponent. In the ideal case of constant growth rate and a random spatial distribution of nucleation sites, the JMAK equation is valid with n equal to 4 when the nucleation rate is also constant (Johnson-Mehl nucleation kinetics). If the nucleation rate decreases so rapidly that all

nucleation events effectively occur at the start of recrystallization (site saturated nucleation), *n* then equals to 3. However, Avrami exponents of 3 or 4 are seldom observed, in general the Avrami exponent varies with time (fraction recrystallized) and is in most cases found to be much less than 3 and often below 2 [2].

As mentioned several times in previous sections, nucleation of recrystallization is a highly heterogeneous process which typically takes place at deformation heterogeneities like grain boundaries, shear bands, and in deformation zones around large particles. Nevertheless, the assumption of a random spatial distribution of nucleation sites (a prerequisite for the JMAK-equation) can still be a good assumption in some cases. For instance, in heavily deformed commercial aluminium alloys containing coarse second phase particles, PSN is often the most important and dominating nucleation mechanism [293], and the spatial distribution of the large constituent particles is therefore important for the recrystallization behaviour. It has actually been confirmed experimentally that random distribution of coarse particles is an adequate assumption for an Al-Mg-Mn alloy (AA3004) deformed to large strains (>3.0) [256]. The assumption of a near random distribution of particles is fulfilled at large strains [323], however, at lower strains a rather non-uniform spatial distribution was documented by Marthinsen et al. [324] in Al alloys, with a transition to a more or less random distribution at high rolling strains. The spatial distribution of coarse particles with respect to rolling strain can be easily understood by changing *L* in Fig.11a, and the non-uniform spatial distribution of large particles after 80% cold rolling (~strain of 1.6) in 3D can be clearly seen in Fig.21d. Other notable examples showing non-random spatial distribution of nuclei include recrystallization in single crystals [325, 326] or in materials with PFZs (see e.g. Fig.23).

Results from numerical modelling have indicated that both the spatial distribution of nucleation sites and the nucleation rate may influence the recrystallization kinetics and the recrystallized grain structure in a significant way [293, 323, 327,328, 329]. Notably using a 3D computer simulation procedure [330, 331] it has been documented that that spatial clustering of nucleation sites may have a profound effect on both the Avrami exponent *n* and on the resulting sectioned grain size distributions [323]. Assuming site-saturation nucleation kinetics, an Avrami exponent *n* of less than 1.5, instead of the expected value of 3, was obtained with strongly clustered nucleation sites. This is consistent with the fact that *n* describes the dimensions along which the nucleus grows.

An important consequence in this connection is that the non-random distribution of nucleation sites, one of the basic assumptions of the JMAK approach [315, 316, 317, 318,319], is no longer valid. Recently, sophisticated extensions on the JMAK approach of recrystallization have been done and can be of help for relatively simple cases, see e.g. Refs [332,333,334]. For more complex conditions (e.g. considering different nucleation mechanisms), one has to rely on physically based computer simulations, which will be detailed in Section **4.6**.

4.4 Interaction between recrystallization and precipitation

In the previous three sections (i.e., Sections 4.1, 4.2 and 4.3), focus was mainly placed on the interaction between recrystallization and particles formed before deformation. However, particles could also be formed by precipitation during annealing after deformation. These particles also show strong interaction with recrystallization, but in a way that is different from the previously mentioned particles, as will be detailed in this section.

Precipitation is strongly dependent on the deformed microstructure, which affects its nature and its kinetics. The deformation structure introduced by plastic deformation may even introduce new types of precipitates that normally do not appear in the non-deformed material subjected to the same thermo-mechanical processing [221]. Precipitates could precede, follow or occur concurrently with recrystallization, the precipitated particles also reduce the solute levels in the matrix, all of these aspects make the analysis of the interaction between precipitation and recrystallization complex. While there is considerable work in the literature covering many inter-connected phenomena, e.g., [335], we here take the philosophy to simplify the problem by separating them and only highlight studies where micrographs are present to show the interaction between precipitation and recrystallization. To be more specific, we are mainly concerned with precipitation before recrystallization, simultaneous precipitation with recrystallization, and precipitation after recrystallization. The dissolution and coarsening of particles, as well as change of particle structures during recrystallization will be covered in **Section 4.5.**

4.4.1 Precipitation prior to recrystallization

We start with the simplest case where precipitation takes place during annealing after deformation, but still before the onset of recrystallization. Even though this category of precipitation exists, to different extent, during almost all annealing processes, it can be best studied during low heating rate annealing or step annealing where recrystallization is absent. It should be mentioned that even though the precipitation potential increases at lower annealing temperatures, the slow diffusion rate at lower temperatures also opposes fast precipitation, i.e. precipitation rate and extent is not necessarily monotonically temperature dependent (a maximum is obtained at an intermediate temperature with an optimum combination of precipitation potential (undercooling) and diffusion rate). For simplicity purpose, the following discussion is based mainly on conditions where low temperature annealing (or low temperature annealing step) is used. The readers are referred to Refs [e.g. 259,260, 336] for more details regarding precipitation during slow heating experiments.

The precipitation during annealing of 90% cold-rolled Al-1.3 wt.% Mn was investigated by Somerday and Humphreys [336] where recrystallization did not occur even after 24h annealing at 350°C. Even though not reported in this study, recrystallization could actually complete in a much shorter time for samples without precipitation and deformed to identical conditions, see e.g. Ref [337]. These authors demonstrated that precipitation first took place at HAGBs, but precipitates were also found at medium angle grain boundaries (MAGBs) and LAGBs after longer annealing time. This boundary misorientation dependent precipitation behaviour was further confirmed by Tangen et al. [258], who also concluded that dispersoids present prior to annealing, i.e., randomly distributed dispersoids formed during homogenization, have a less significant effect on the recrystallized grain size and texture than concurrent precipitation. The low temperature annealing (15 min at both 180°C and 290°C) of 70% cold-rolled Al-1 wt.% Mn alloy was investigated by Schäfer and Gottstein [259], but no significant precipitation was found from BSE micrographs after these annealing treatments. A more recent set of studies was conducted by Huang et al. [253,260,262,338,339] who systematically examined the interaction between second-phase particles and recrystallization during annealing of cold-rolled Al-Mn alloys and precipitation before the onset of recrystallization was involved in all of these studies, see e.g. Fig.24. Putting aside the dispersoids produced by homogenization before cold

deformation and subsequent annealing, an effort was made to distinguish the effect of precipitates formed before recrystallization from that of concurrent precipitation, both of which usually take place preferentially at (sub)grain boundaries during annealing after deformation. The former type of precipitation does affect the grain structure and texture, but it was found that the precipitation of these particles lowers the potential of concurrent precipitation, the effect of which is more significant than the introduction of precipitated particles themselves [339]. Homogeneous precipitation could also take place in some alloy systems during annealing, where precipitates (usually of small size) are more or less randomly distributed in the matrix, the kinetics of which seems to be less affected by deformation [60, 340] as compared to the heterogeneous ones. In what follows, we are mainly concerned with heterogeneous precipitation, since the effect of homogeneous precipitation on recrystallization is relatively easier to treat using the original Zener pinning theory. The large amount of literature concerning the precipitation behaviour in steels, particularly the HSLA steels [e.g., 100,335,341], will not be further discussed here. The reason is that the phase transformation from austenite to martensite during cooling removes the prior dislocation structure and therefore complicates the analysis, as the dislocation structure plays an important role on precipitation location and kinetics. For instance, it was recently found that precipitation occurs entirely on dislocations in the form of microband walls or cell structure in Fe-30wt.% Ni austenitic steel [24].

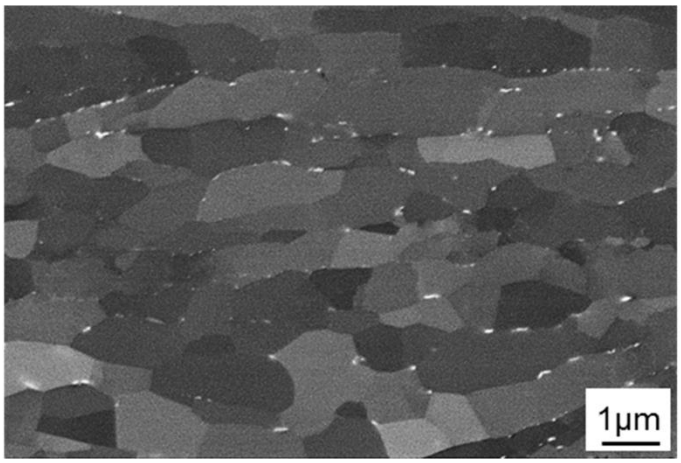

Fig.24 BSE images showing the dispersoids at subgrain boundaries of 95% cold-rolled as-cast Al-Mn alloy after isothermal annealing at 300°C for 10^4s, all the dispersoids come from precipitation. Reproduced from [339], with permission from Elsevier.

Now that heterogeneous precipitation on boundaries is discussed, we can consider Zener pinning in cases where precipitation takes place on subgrain boundaries prior to recrystallization, noting that the fraction of LAGBs is usually much larger than that of HAGBs after deformation. Instead of considering the pinning force from a single particle derived by Zener ($\pi r\gamma_{AB}$), Hansen et al. [335] adopted the expression ($4r\gamma_{AB}$) refined by Gladman [342] and calculated the retarding force (F_p) due to precipitated particles as:

$$F_p = 4r\gamma_{AB}N_S \tag{34}$$

where N_S is the number of particles per unit area of boundary. If precipitation is mainly on LAGBs, e.g., after hot deformation or low temperature annealing following cold deformation, the number of particles per unit subboundaries (N_{SB}) will be very different from N_S . Assuming the average LAGB intercept length is $\bar{l}$, the surface area per unit volume for such LAGB area is $2/\bar{l}$, and the number of particles per unit LAGB area is given by:

$$N_{SB} = \frac{N_V}{2/\bar{l}} \tag{35}$$

where N_V is the number of particles per unit volume, which is expressed as:

$$N_V = f_V \Big/ \frac{4}{3}\pi r^3 \tag{36}$$

Combining Eqs. (34-36) gives the retarding force from precipitates on subgrain boundaries:

$$F_p = \frac{3\gamma_{AB} f_V \bar{l}}{4\pi r^2} \tag{37}$$

This gives a larger pinning force as compared to Zener pinning shown in Eq. (11) as long as $\bar{l} > 2\pi r$, which is often the case considering a typical value for $\bar{l}$ is around 0.5μm, and radius of precipitates are usually smaller than 50nm. A similar analysis with also the same result was carried out by Nes and co-workers [256,343]. The increased pinning force is more evident for smaller precipitate sizes in Eq. (37), e.g. see calculated values for HSLA steel with an average Nb(C,N) particle radius of ~2nm [335]. This approach has been extensively used to analyse the pinning effect of fine precipitates on subgrain boundaries, e.g., for the same type of fine particles by Kwon and DeArdo [100], as well as more recently on fine NbC precipitates in a model austenitic steel by Rainforth et al. [24]. Other types of boundary-particle correlations can also be found in the textbook of Humphreys and Hatherly [2].

It can be intuitively understood that precipitation during annealing before the onset of recrystallization retards nucleation by pinning the movement of high and low angle boundaries. However, this annealing step can at the same time induce subgrain growth and promote recrystallization, which has been theoretically analysed [344] and was documented for different materials [345,346,347]. In particle-containing materials, subgrain growth can take place in regions with less precipitates such as PFZs [346] or when the spacing of the precipitates is larger than the subgrain size, the larger subgrains then serve as potential nuclei during subsequent annealing procedures and do promote recrystallization.

4.4.2 Concurrent precipitation

Of even more interest to recrystallization is the precipitation occurring simultaneously with recrystallization, i.e., concurrent precipitation. In many alloy systems, both recrystallization and precipitation take place at the prior grain boundaries, e.g., in Al alloys [336] and microalloyed steels [100]. As we did for other analyses, an effort is made here to highlight published work where either there is no other type of fine dispersoids or it is possible to distinguish the contribution from concurrent precipitation. In non-heat treatable Al alloys such as AA1xxx, AA3xxx and AA5xxx, annealing of cold-rolled as-cast samples with high supersaturation level of solute elements satisfies the criterion, for which recrystallization and precipitation (usually of size>30nm) starts simultaneously during high temperature annealing. A very short review on the influence of concurrent precipitation on recrystallization of Al alloys was given by Morris and Liu in 2005 [348], in which it can be seen that most of the studies were focused on AA3xxx (Al-Mn) alloys. Another material of interest is HSLA steel [349], where all particles can be dissolved after high temperature solution treatment for a long time before deformation, and fine precipitates (<~10 nm) are formed during annealing together with recrystallization. Other less frequently studied materials where concurrent precipitation interact with recrystallization by involving only a single type of fine particles include binary Al-Zr [350], Al-Sc [60], Al-Fe-Si-Ti [351], Mg alloys [352], Fe-Mn-C-Pd alloys [353], ODS alloys [51]. In this section, only examples with relatively large precipitate sizes (~30 - 100 nm) are considered. Precipitates within this size range are easily detected by conventional characterization methods, they are usually incoherent and can be approximated as stable particles, especially when the annealing

temperature is not too high. Recrystallization in alloy systems where precipitates may undergo further evolution during annealing will be considered in **Section 4.5**.

A systematic set of studies on this topic were conducted by Morris and co-workers on AA3xxx and AA5xxx [e.g. 354,355,356] alloys covering different affecting factors. However, direct evidence on the interaction between precipitates and recrystallization was not provided since the considered optical micrographs usually did not show a sufficient resolution to resolve fine precipitates. Even though disputes still exist, concurrent precipitation is generally accepted to affect the recrystallized grain structure, texture and material properties.

In most of the studies, the precipitation before the onset of recrystallization is usually not strictly distinguished from concurrent precipitation in the literature, see e.g. the work by Nes et al. [258], Zhao et al. [357] and Somerday and Humphreys [336]. Since both of them take place at (sub)grain boundaries for heterogeneous precipitation materials, their individual effect on recrystallization is not easily identified. The estimation of precipitation and recrystallization by electrical conductivity and hardness measurements, respectively, cannot be precisely used to analyse the very beginning of these two processes. This does not mean that these studies are not suited to analyse concurrent precipitation, since in many cases the precipitation before the onset of recrystallization is negligible, especially at high annealing temperatures. In a set of extensive experiments on the softening behaviour of Al-Mn alloys, Huang et al. [260, 262,339] were able to separate these two types of dispersoids using either slow heating rate annealing or step annealing tests, where the recrystallization starting time was also examined directly from micrographs to study the effect of genuine concurrent precipitation. The main effect of concurrently precipitated particles on recrystallization is still their pinning effect on (sub)grain boundaries migration. With pre-existing dispersoids, either randomly distributed or preferentially located on (sub)grain boundaries, migrating boundaries do not suffer from the large pinning effect as predicted by Eq. (37) once they break away from the particles attached to them, and a smaller Zener pinning pressure described by Eq. (11) is instead applied to account for the pinning effect from particles ahead of the moving boundary. During concurrent precipitation, which is also preferentially located along (sub)grain boundaries, the larger pinning force predicted from Eq. (37) is always valid, leading to higher recrystallization resistance. This recrystallization resistance comes from two aspects: i) the critical nucleus size increases (see Eq. (18)), i.e., resistance on nucleation of recrystallization; ii) a larger Zener pinning pressure during

growth of recrystallized grains. If non-isothermal annealing with slow heating rate is used, the temperature at which recrystallization starts will also increase due to concurrent precipitation. The size of concurrently precipitated dispersoids is usually smaller than that of pre-existing ones formed during homogenization or annealing before recrystallization, since there is less time for particle coarsening, which thus further increases the Zener pinning pressure. Moreover, the moving recrystallization front will actually encounter deformed grains of different orientations, with the possibility of creating special low energy boundaries which can be formed during recrystallization with respect to certain orientations, an example can be found in the recent study by Huang et al. [262]. The concept of misorientation dependent Zener pinning due to smaller grain boundary energy (see Eq.(11)), which is similar to that discussed in **Section 4.1.2**, then sets in. Moreover, the low energy of these boundaries makes them less likely as potential sites for concurrent precipitation [256,258,336]. The low volume fraction of dispersoids on special grain boundaries, which is unique when concurrent precipitation is involved, will further contribute to a smaller Zener pinning pressure (see Eq. (11)). This may explain the unusual microstructural features such as growth of faceted grains [60] or elongated coarse grain structures (see Fig. 25) and sharp textures during recrystallization with concurrent precipitation. Accompanying the concurrent precipitation is the decrease of solute drag, which is not involved in alloy systems when only pre-existing particles are involved, the analysis of which often requires the help from numerical models, as will be shown in **Section 4.6**. During SRX with concurrent precipitation, a larger recrystallized grain size is always obtained as compared to precipitation-free counterparts, reflecting their dominating influence on nucleation rate over growth rate.

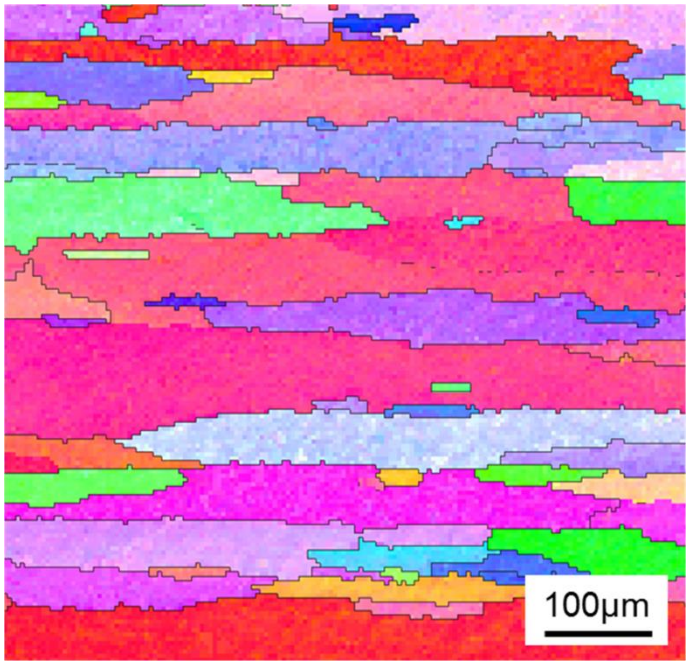

Fig.25 Elongated grain structure obtained after isothermal annealing at 400°C for 10^5s for an as-cast Al-Mn alloy cold deformed to ε=3.0 (where recrystallization starts immediately during annealing such that precipitation before recrystallization can be neglected). Reproduced from [337], with permission from Elsevier.

4.4.3 Precipitation after recrystallization

The direct consequence of recrystallization on precipitation is related to the fact that recrystallization removes deformation structures that are preferential sites for precipitation, it is thus expected that the precipitation kinetics will be much slower. This was illustrated in the work by Lok et al. [358] who investigated the microchemistry (i.e. solute and second phase) evolution during industrial processing of an Al-Mn alloy. The work by Jonas and Weiss [359] clearly demonstrated that precipitation in undeformed austenite in a microalloyed steel is at least one order of magnitude slower than precipitation in deformed austenite with 5% prestrain. The removal of deformation structure during recrystallization also modifies the distribution of subsequent precipitates, as well as their morphology, crystallography and coarsening behaviour of precipitates [360].

If recrystallization precedes precipitation, recrystallization is mainly affected by solute elements which may have a much weaker retarding effect than precipitates [100], the resultant microstructure is thus similar to that for a single-phase alloy, and an example is shown in Fig.26.

If precipitation interacts with recrystallization of a cold-rolled supersaturated Al-Mn alloy, a more elongated grain structure is usually observed, as shown above in Fig.25.

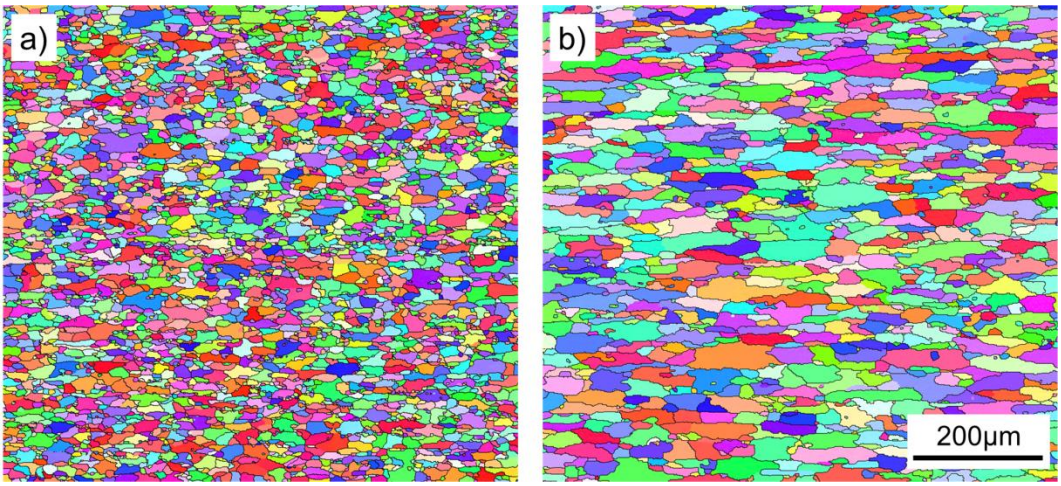

Fig. 26 EBSD maps showing the microstructure of 95% cold-rolled as-cast Al-0.4 wt.% Mn alloy after annealing. a) 500°C for 5s, precipitation is negligible due to the short time, b) step annealing at 300°C for 10^4s to introduce some precipitates, and then at 500°C for 5s. Reproduced from [339], with permission from Elsevier.

Even though not involved in recrystallization, dispersoids precipitated after recrystallization are frequently used to stabilize grain size by pinning grain boundary migration and notable examples include the ODS alloys, superplastic materials, as will be further discussed in **Section 6**. A large number of fine dispersoids could also significantly contribute to precipitation hardening. They also find their application in promoting abnormal grain growth for Goss-{110}<001> oriented grains in the transformer steel of Fe-3Si. More details on this topic will be given in **Section 6**.

4.5 Effect of unstable second-phase particles

Discussion on the recrystallization of particle-containing materials is mainly focused on stable particles which do not evolve after their appearance. The theories obtained in analysing these simple cases allow us to consider more complex situations with unstable particles. To this end, we are mainly concerned with the dissolution and coarsening of particles during recrystallization, changes of particle structures during recrystallization are also covered in this section. More details on the shape change of second-phase particles are given by Doherty [361].

4.5.1 Dissolution and coarsening of second-phase particles

The dissolution and coarsening of particles during recrystallization have not been equally addressed in the literature. In many age-hardenable alloys, particularly Al alloys, the fine particles precipitated during natural and/or artificial aging may either dissolve or rapidly grow before reaching the typical recrystallization temperature, so no significant interaction between these particles with recrystallization is expected for these alloys and conditions. The effects of recrystallization on the γ' distributions in Ni-based superalloy have been investigated, e.g. by [362,363], where both coarsening and dissolution of γ' precipitates were observed during recrystallization, more details will be given in **Section 6.1** when dealing with high temperature alloys. The coarsening and dissolution of particles by grain boundary migration during recrystallization is not a phenomenon restricted to Ni-based superalloys. For instance, it was found that niobium carbide particles below a critical size dissolve at the recrystallization front while coarser particles further grow in an austenitic stainless steel, the result being a reduction in number density and volume fraction of these particles together with an increase in mean size [364]. The grain boundary interaction with precipitates was also carefully addressed during recrystallization of ODS ferritic steels [365]. The precipitation along twin and grain boundaries, as well as its subsequent coarsening and dissolution, was directly observed using the combination of in-situ TEM, quasi-in-situ EBSD and SEM methods during annealing at 490°C in a cold-rolled Mg-Y-Nd alloy [366]. The dissolution and coarsening of particles modifies the local Zener pinning effect through the variations in particle size and volume fraction.

One typical example that illustrates well the interaction between recrystallization and these unstable particles is the annealing of fine-grained particle-containing Al-Sc alloy [367]. In this study, an Al-0.2 wt.% Sc alloy was solution heat treated to get a single-phase microstructure, the material was then processed by ECAP to an effective true strain of 9.2 which led to a fine-grained microstructure with average grain radius of 0.25μm. The deformed samples were pre-aged at 350°C for 3h to generate an equiaxed grain structure (no recrystallization) with average radius of 0.4 μm, as well as fine coherent Al_3Sc dispersoids of 5 nm size in diameter. These pre-aged materials were then further annealed in the 400-500°C temperatures interval, for which the evolution of grain and particle average sizes are plotted in Fig.27. The microstructure coarsens

both gradually and uniformly, which is often referred to as continuous recrystallization. The evolution of grain size follows the well-known grain growth relation:

$$R^n - R_0^n = K_c t \tag{38}$$

where R and R_0 are the final and initial grain radii, respectively, n is the grain growth exponent. The temperature dependence of grain growth was considered by K_c, where it follows the Arrhenius-type relation $K_c = A\exp(-\mathrm{Q}/\mathrm{RT})$. For ideal grain growth behaviour (i.e., no second-phase particles), n=2, while n=3 was found to give the best fit for the curves shown in Fig.27a in the case where coherent Al_3Sc dispersoids were present. Interestingly, a third order kinetics also fits well the experimental data on particle coarsening (see Fig.27b):

$$r^3 - r_0^3 = \frac{8c_a(1-c_a)\gamma V_m D}{9RT(c_\beta - c_a)^2} t \tag{39}$$

where r_0 and r are the initial particle radius and particle radius after coarsening at time t, respectively. Also involved are the equilibrium concentration of Sc in the Al matrix (c_a) and Al_3Sc (c_β), the partial molar volume of Sc in Al_3Sc (V_m), diffusivity term (D) and the interfacial free energy between Al matrix and Al_3Sc particles (γ). A good agreement was found between the prediction by Eq. (39) and current experimental data, this was also valid for a few data points from another study. Considering that the same growth exponent is used for Eqs. (38) and (39), it implies that $dR/dt \propto dr/dt$, i.e., grain growth is controlled by the coarsening of particles. The limiting grain size which relates to particle size and volume fraction was found to follow Eq. (14) with K=1/6 and m=1. It was also suggested that discontinuous grain coarsening will take place when annealing at higher temperatures due to rapid particle coarsening.

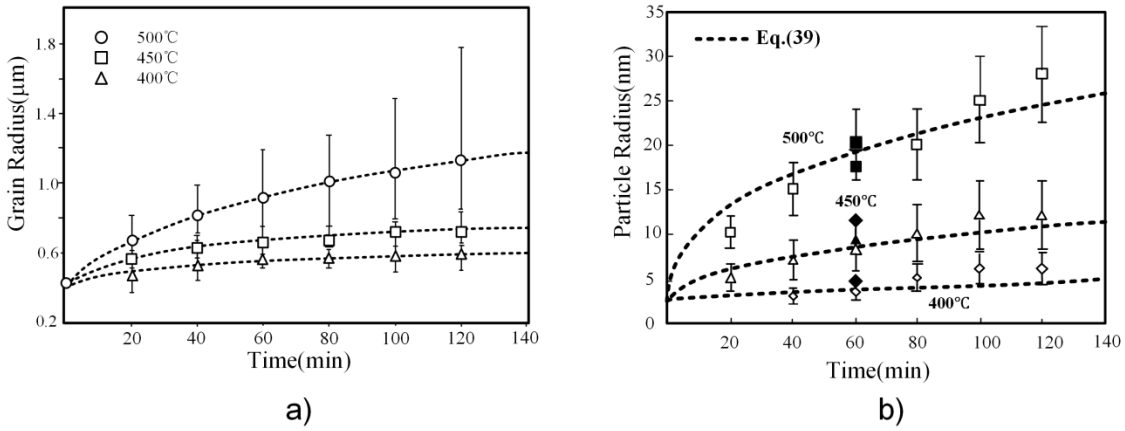

Fig. 27 a) The evolution of grain radius during annealing at different temperatures; b) The evolution of particle radius as a function of annealing time at various temperatures (together with data taken from Jones and Humphreys [60] (filled points)). Superimposed on this figure is particle size evolution predicted by Eq. (39). Reproduced from [367], with permission from Elsevier

It thus appears that the variation of particles structure during annealing could still be understood using the Zener pinning theory, as long as the time dependent particle size and volume fraction are correctly quantified. While particle evolution took place homogeneously in this example, this may not always be the case, in fact particle dissolution and coarsening could take place more rapidly by interacting with moving grain boundaries, see e.g., Refs [364,365]. However, this should in principle pose no problem for calculating grain boundary migration if local Zener pinning is calculated.

4.5.2 Change of particle/matrix coherency

Besides the coarsening and dissolution of particles, the change of particle/matrix interfacial character also plays an important role in recrystallization. The interaction between recrystallization and fine particles in Al-Sc alloys has been investigated by Jones and Humphreys [60], including an Al-0.02 wt.% Sc alloy and two supersaturated alloys with 0.12 and 0.25 wt.% of Sc, respectively. These alloys were 80% cold rolled in the solution treated condition, and then annealed in a salt bath, the recrystallization starting (~5%) and finishing (~95%) temperature as a function of annealing time are shown in Fig.28. The single-phase Al-0.02 wt.% Sc alloy recrystallizes at ~250-300°C with no evidence of precipitation. In the alloy containing the

highest Sc content (Al-0.25wt.%Sc), precipitation always precedes recrystallization, recrystallization does not start until the annealing temperature reaches ~500°C. A more complex situation was found in the Al-0.12wt.%Sc alloy where precipitation was found to precede, follow or occur concurrently with recrystallization, depending on the annealing temperature.

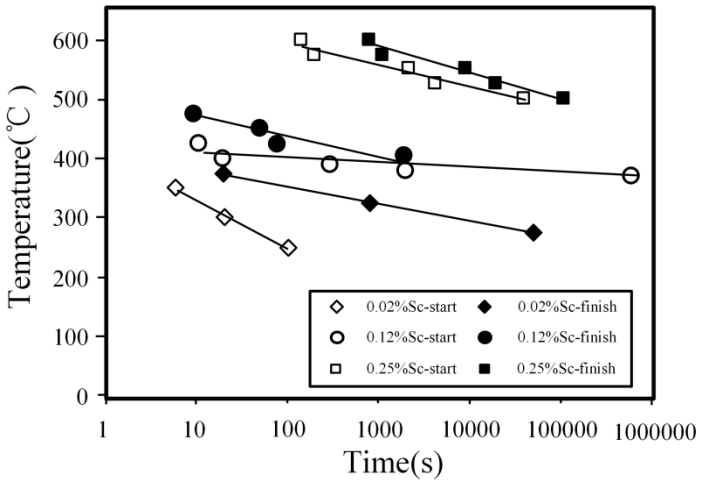

Fig. 28 The starting and finishing time during isothermal annealing of the Al-Sc alloys cold rolled to 80% reduction. Reproduced from [60], with permission from Elsevier.

Fine coherent precipitates are subjected to coarsening and become semi-coherent during the passage of low-angle boundaries during recovery at high temperatures, see Fig.29. The coarsened semi-coherent particles will exert a lower pinning effect on the boundary, and this is why recrystallization could initiate at high temperature for Al-0.25wt.%Sc. The passage of HAGBs through semi-coherent precipitates during recrystallization takes place by migration of the boundary through the particle, and it appears that precipitates can in such case maintain their semi-coherency with the new grain.

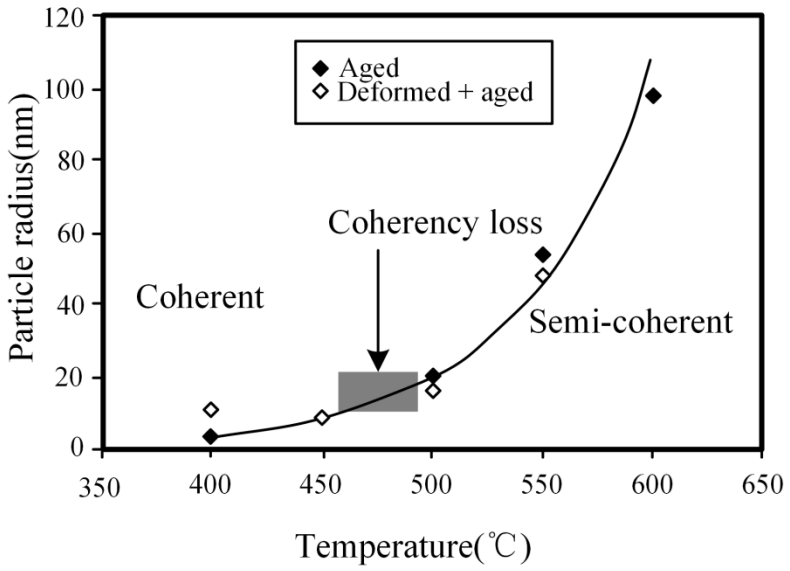

Fig.29 Evolution of precipitates size in Al-0.25wt.%Sc during a 1 h anneal at different temperatures. Reproduced from [60], with permission from Elsevier.

During hot deformation, the particle/matrix coherency may also significantly affect both deformation and recrystallization behaviour, as was reported by Miura et al. [61]. For this purpose, two variants of polycrystalline Cu samples with the same initial grain size, as well as particle size (38nm) and distribution were prepared, the only difference between the two variants being that one variant (Cu-α-Fe) contains incoherent α-Fe precipitates while coherent γ-Fe precipitates are present in the other variant (Cu-γ-Fe). During hot deformation (see Fig.30), it is evident that the yield stress decreases monotonically with decreasing strain rate and increasing temperature for the Cu-α-Fe alloy, suggesting that the same particle bypass mechanism is operative. On the other hand, the yield stress decreases abruptly above 527°C (800K) in the Cu-γ-Fe variant, which was ascribed to the change of particle coherency with the matrix. The much lower yield stress in this variant for all the deformation conditions indicate that the Orowan mechanism is not dominating and another thermally activated bypass mechanism may be involved.

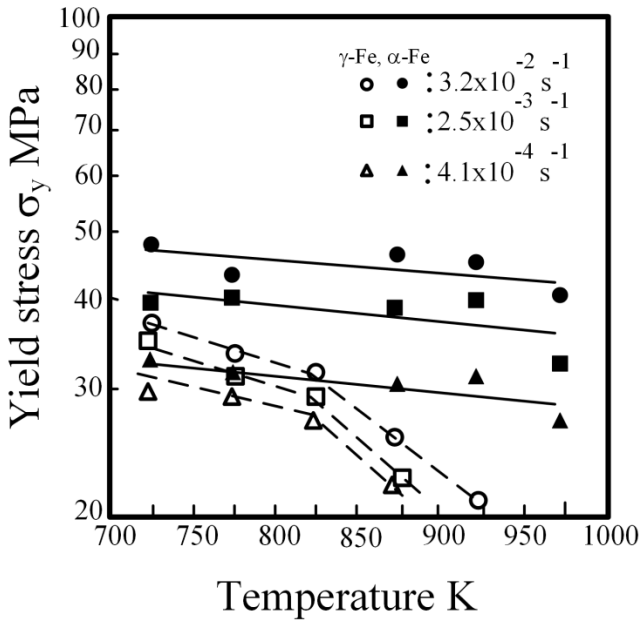

Fig.30 The yield stress of the two variants containing either incoherent α or coherent γ-Fe precipitates in different conditions. Reproduced from [61], with permission from Elsevier.

DRX is completely suppressed in the Cu-γ-Fe when deformed at 700°C with strain rate of $2.5\times10^{-3}s^{-1}$ to a strain of 0.4 due to the suppression of grain boundary migration by coherent particles, while several new grains have been nucleated in the Cu-α-Fe variant, as shown in Fig.31.

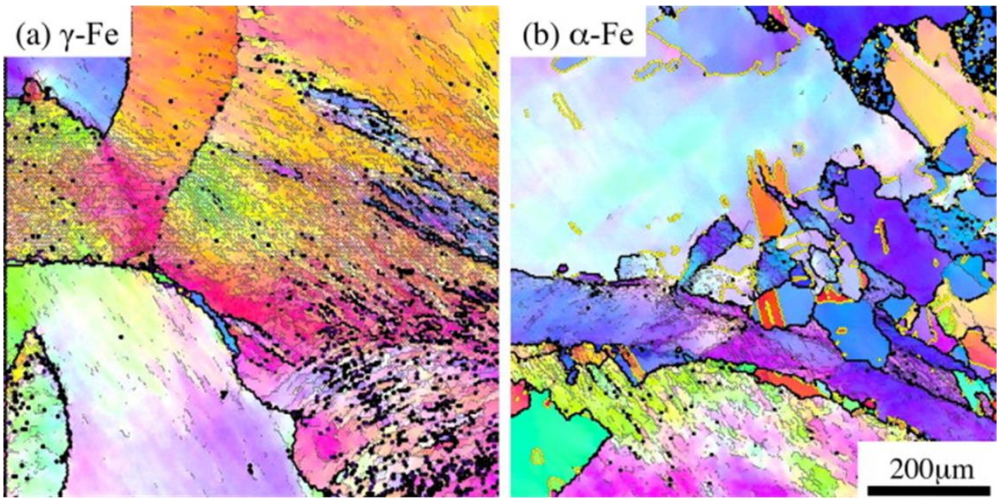

Fig.31 EBSD maps of the two variants containing the (a) coherent α-Fe and (b) incoherent γ-Fe precipitates after deformation to $\varepsilon = 0.4$ at 700°C (973 K) and 2.5×10^{-3} s^{-1}. Low angle, high angle, and twin boundaries are indicated by thin black, bold black, and yellow lines, respectively. Reproduced from [61], with permission from Elsevier.

The effect of deformation on the change of particle coherency is plotted in Fig.32. It can be seen that the coherent precipitates in the Cu-γ-Fe variant gradually lose their coherency and 95% of them become incoherent at a strain of 1. DRX was observed in this variant at higher strains due to the less effective retarding effect on LAGB and HAGB migration from incoherent particles. A small fraction (5%) of very fine coherent γ-Fe precipitates survived, which is probably because dislocations can still bypass these fine precipitates by climb at this temperature. In fact, almost all γ-Fe precipitates are transformed to incoherent ones after a small strain of ~10% at 77K.

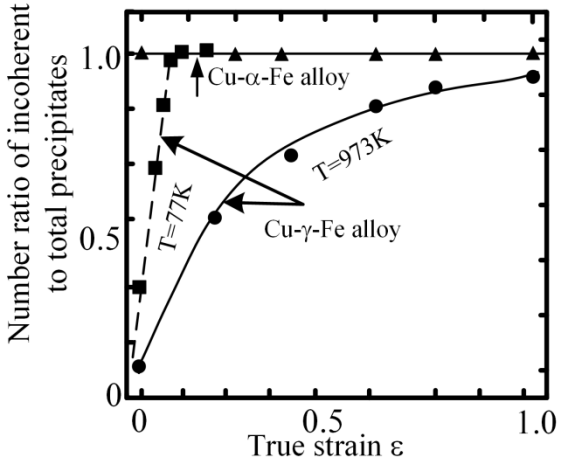

Fig.32 The transformation of the coherent precipitates into incoherent ones in the Cu–γ-Fe alloy during deformation at 3.2×10^{-3} s^{-1} (973 K) and 2.0×10^{-4} s^{-1} (77 K). Reproduced from [61], with permission from Elsevier.

Su et al. [368] reported a good example to further illustrate the complex variations of particles and their interaction with (sub)grain boundaries, during friction stir welding (FSW) of an age-hardenable 7050-T651 Al alloy (i.e. an Al-Zn-Mg-Cu, which was solution heat treated, stress relieved by stretching and then artificially aged). The processed material includes different regions among which the base material (BM), the dynamically recrystallized zone (DXZ), the heat affected zone (HAZ) and the thermo-mechanically affected zones (TMAZ I and II), as shown in Fig.33. Different types of particles are involved such as the strengthening semi-coherent precipitates η' $Mg(Zn, Cu, Al)_2$ and grain boundary incoherent precipitates of η $MgZn_2$ and/or $Mg_3Zn_3Al_2$ in the base material. Moreover, a large constituent phase Al_7Cu_2Fe and fine Al_3Zr dispersoids (due to the trace element of zirconium) formed during solidification also exist.

Localized heating (200-~480°C) caused by the friction-stir process leads to the coarsening or even dissolution of precipitates in the DXZ, TMAZ and HAZ. During the thermo-mechanical cycle, Al_7Cu_2Fe with rod-like shape coarsen to spherical or block shape while the fine coherent Al_3Zr dispersoids are very stable except in the DXZ where they lose coherency due to plastic deformation and subsequent heat treatment.

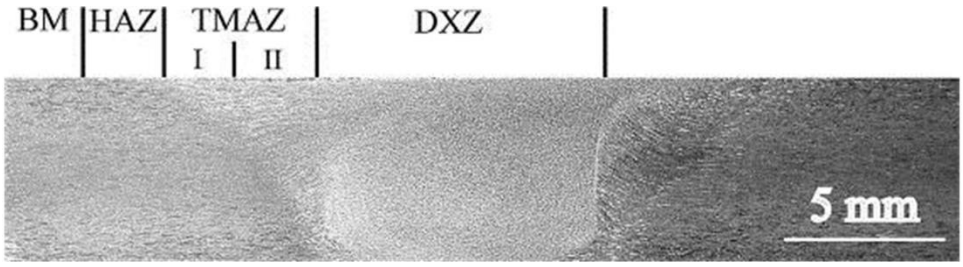

Fig. 33 Micrograph of the cross section of a friction stir weld in 7050 Al, the different weld zone regions from base metal (BM) to DXZ are clearly visible. Reproduced from [368], with permission from Elsevier.

In the base material (Fig.34a), a dense distribution of fine intragranular precipitates (< 50 nm) was observed in the matrix together with coarser precipitates at (sub)grain boundaries. A narrow PFZ is also evident along grain boundaries. Compared to the precipitates in the parent material, the strengthening η' precipitates have severely coarsened in the HAZ, but remain homogeneously distributed. The PFZ along the grain boundaries has increased by a factor of five, as shown in Fig.34b. The distribution of precipitates is inhomogeneous in TMAZ I and a bimodal precipitate structure is obtained with coarse and fine precipitates of size ~100nm and ~10nm, respectively (Fig.34c). The coarse precipitates are a result of coarsening, and the small precipitates are from re-precipitation on dislocations and (sub)grain boundaries during cooling. The precipitates in the matrix are obviously not randomly distributed, it is most likely a result of (sub)grain boundary migration where precipitates on these boundaries are left behind. The strengthening precipitates were completely dissolved and then re-precipitated preferentially along dislocations and (sub)grain boundaries in TMAZ II, see Fig.34d. In the DXZ (Fig.34e) which experienced the highest temperature of ~480°C, precipitates also suffered from dissolution and re-precipitation, with large grain boundary precipitates and fine precipitates on the dislocation structure and/or incoherent Al_3Zr particles in the matrix due to the relatively slow cooling rate.

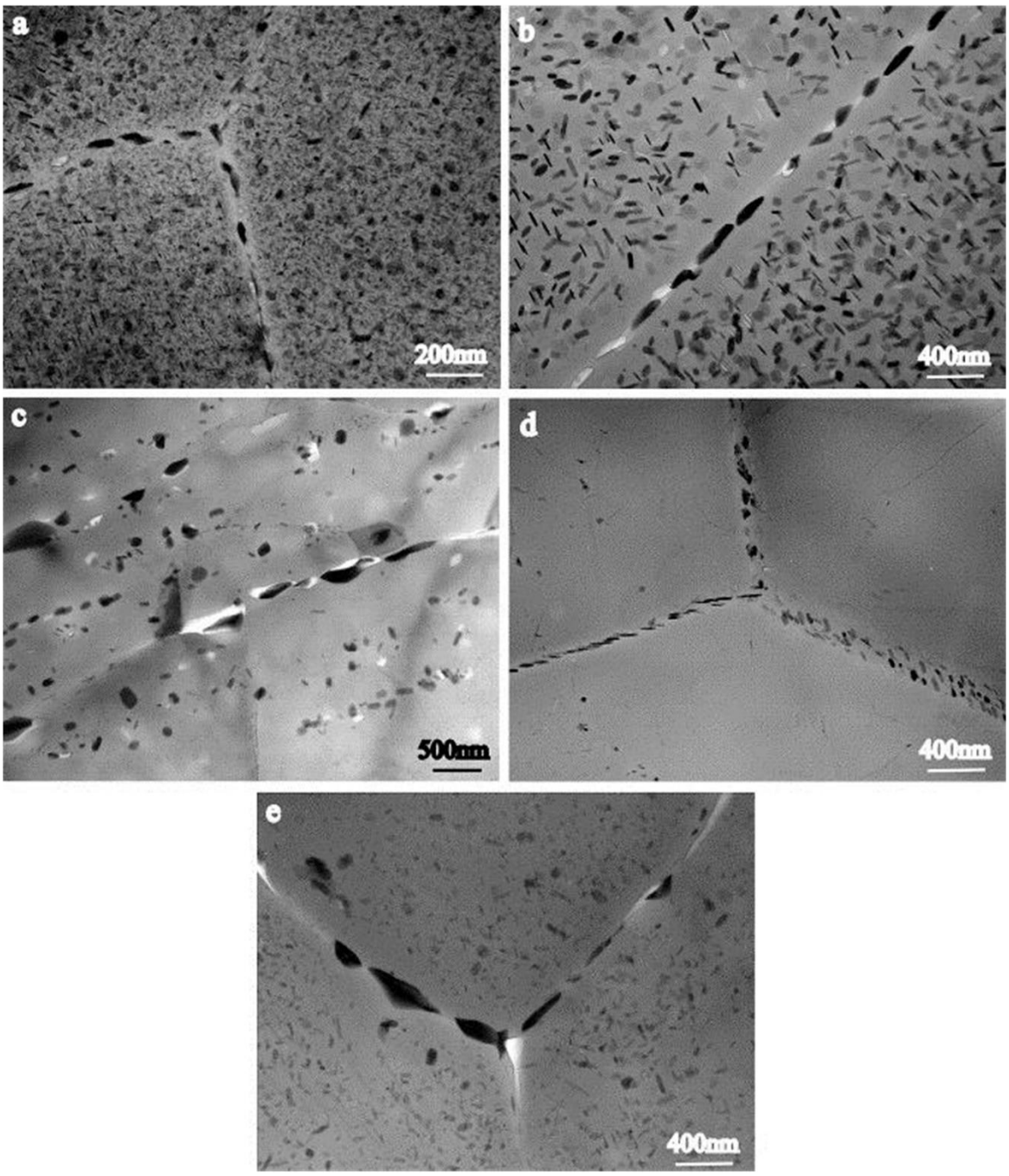

Fig. 34 Precipitate microstructures in (a) parent material, (b) HAZ, (c) TMAZ I, (d) TMAZ II, and (e) DXZ. Reproduced from [368], with permission from Elsevier.

4.6 Numerical modelling

Recrystallization can be substantially influenced by rather small modification in metallurgical state and/or in the TMP conditions. The use of numerical models to describe recrystallization phenomena in terms of grain structure, crystallographic texture and mechanical properties evolutions is already a challenging task in pure metals. The introduction of second-phase particle makes it even more complex. A large number of successful numerical models as well as different simulation approaches exist in the literature focusing on recrystallization with incoherent stable particles, either fine or coarse particles, see e.g. Refs [274,293, 369, 370, 371]. Meanwhile, another group of numerical models solely predicting the evolution of precipitates, i.e., without the involvement of recrystallization, can also be found in the literature [e.g. 372,373,374,375,376]. In this section, modelling of recrystallization with complex particle structures is briefly summarized, a comprehensive review on this topic is however not the main objective. To this end, recrystallization models that predict recrystallization kinetics, grain size and/or recrystallization texture, and at the same time deal with bimodal particle structures and precipitation, respectively, are further discussed below.

4.6.1 Recrystallization with bimodal particle structures

As discussed in the previous sections, recrystallization in alloys containing both coarse and fine stable particles is a very complex phenomenon. Fine dispersoids retard recrystallization by pinning (sub)boundary migration while coarse particles can accelerate recrystallization through PSN, a unified theory on these aspects was given by Humphreys [377]. It should be noted that in these alloys with a bimodal particle structure, recrystallization at other sites typical of single-phase alloys also exists, e.g. nucleation at grain boundaries, deformation bands etc.

Based on a series of extensive experimental investigations, Vatne et al. [302] developed a physically based model to predict recrystallization microstructures and textures after hot deformation of Al alloys containing both coarse and fine particles. The essence of this model lies in the calculation of the number densities of nuclei originated from three different nucleation sites: PSN, nucleation from cube bands and nucleation from pre-existing grain boundaries. In terms of PSN, the critical particle size above which nucleation starts was first calculated (see Eq.

(27)) which already considers the effect from fine particles). The distribution of these overcritical particles was identified, and the number density of PSN nuclei was calculated by assuming that a fraction (C_{PSN}) of these overcritical particles will finally lead to PSN. Nucleation from retained cube bands after hot deformation was then calculated in a very sophisticated way based on experimental observations. The density of cube nuclei was assessed by considering the initial cube grain size and instantaneous volume fraction of cube grains, the surface area per unit volume of cube grains (which was a function of strain), the average cube subgrain size, the density of overcritical subgrains inside the cube regions, and the fraction of cube bands surrounded by the S deformation texture component. The S deformation texture component was considered because the existence of cube-S boundaries promotes nucleation of cube grains, due to their near 40°<111> orientation relationship. Finally, recrystallization from grain boundaries depends on the initial average grain size and subgrain size, deformation strain, as well as the density of overcritical nuclei near grain boundaries. For all three nucleation mechanisms considered, the critical nucleus size follows Eq. (18). The growth rate of these recrystallized grains was calculated using Eq. (15) by neglecting P_C. Combining the calculated total number of nuclei and growth rate, the recrystallized fraction can be easily obtained using the classical JMAK kinetics assuming site saturated nucleation and randomly distributed nucleation sites, which then further determines the average recrystallized grain size. The recrystallization texture is a result of oriented nucleation, i.e., PSN grains, cube grains and grains nucleated at original grain boundaries, each with a specific orientation distribution [378]. Unlike recrystallization after cold deformation, precipitation could be neglected during recrystallization after hot deformation. The model has been validated with AA3xxx and AA1xxx alloys where quantitative agreements with experimental results were obtained. Even though this model was originally developed to predict recrystallization after hot deformation, it can be, with minor modifications, applied to recrystallization after cold deformation [379] or even in multi-pass conditions [380].

An advanced SRX model based on principles of cellular automata was developed by Gottstein et al. [275] for Al alloys. The deformation process was simulated with a deformation texture model and work-hardening model which give local orientations and the dislocation density of each grain. The effect of second-phase particles on the deformation structure was basically neglected. During recrystallization, nucleation from three different sites was considered, i.e., grain boundaries, deformation bands, as well as coarse particles, similar as in the

model developed by Vatne et al. [302]. The effect of fine dispersoids existing before annealing was considered during grain boundary migration by adding a Zener pinning pressure to the driving force from stored energy. As for the coarse particles, their contribution to recrystallization was related to PSN. Overcritical particles were categorized into different size classes, where each class has its own number frequency and deformation zone volume, the latter was assumed to scale with particle size. A constant probability of nucleation per unit volume of the deformation zone was employed to give the absolute number of nuclei. Even though the model was not tested against conditions with concurrent precipitation, it is obvious that concurrent precipitation can be addressed by accounting for the evolution of size and volume fraction of particles with time.

Recrystallization in alloys containing both fine and coarse particles was modelled using a 3D Monte-Carlo method by Song and Rettenmayr [381]. PSN was assumed as the only nucleation mechanism in this model. Different from the two models presented above, the heterogeneous distribution of stored energy introduced by coarse particles was incorporated and fine particles were assumed to have no effects on deformation structure and stored energy. The coarse particles lead to deformation zones after cold deformation and this was considered by introducing additional GNDs (similar to Eq. (3)) and thus additional stored energy (E_D^a). The stored energy in the deformation zone also varies linearly with the distance from the particles, where regions with a distance larger than the particle size were considered as non-affected zone (i.e. with the stored energy of the matrix E_D^M), as schematically shown in Fig.35. No concept of critical particle size for PSN was introduced, nor was the efficiency of nucleation per particle. PSN only occurs when the local stored energy is larger than the sum of the critical stored energy for nucleation in single phase material and the energy barrier that needs to be overcome in the presence of fine dispersoids. The growth of recrystallizing grains was also affected by the retarding force from fine particles, i.e., fine dispersoids reduce both the nucleation rate and growth rate by their pinning effect. The model was tested against experimental results on annealing a cold-rolled Al-Zr alloy containing stable primary particles (0.8-2.0 μm) and fine Al_3Zr particles (150-500 nm), and both the microstructural morphology and recrystallized volume fraction were in good agreement with experimental results.

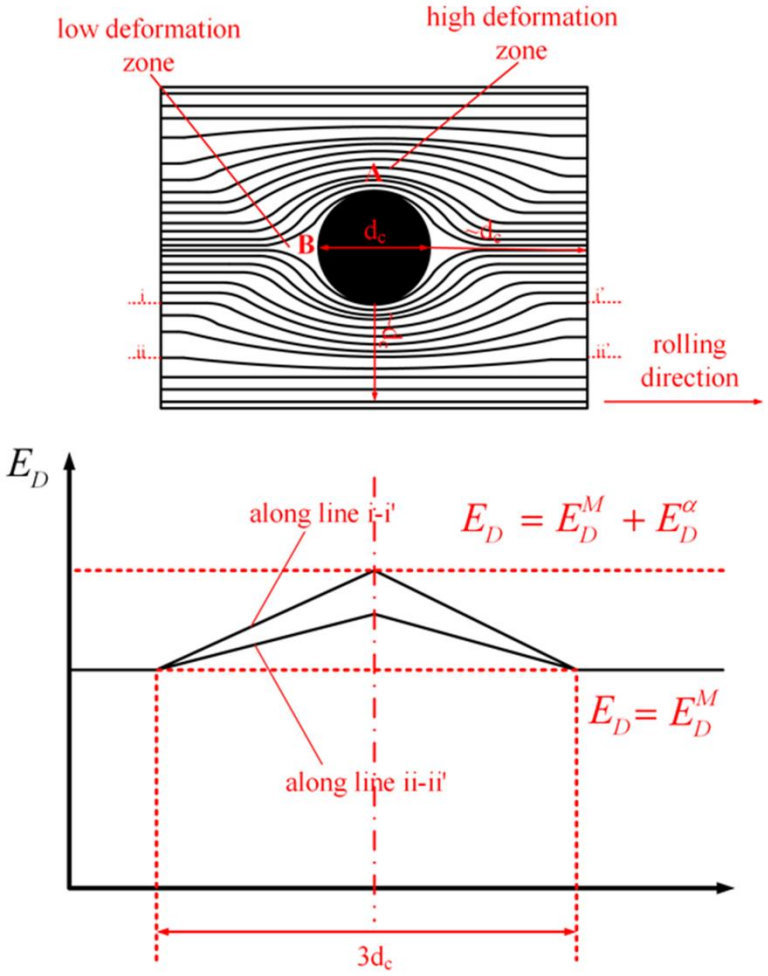

Fig. 35 Schematic graph showing the variations of the deformation and the stored energy E_D near a coarse non-deformable particle; the solid black circle represents the particle with diameter d_c; the square region with a dimension approximately equal to $3d_c$ is the particle-affected region. Reproduced from [381], with permission from Elsevier.

It can be concluded that these recrystallization models, with reasonable assumptions, do provide satisfactory results for the alloys and conditions investigated. However, further improvements are needed such that key aspects for the recrystallization reaction, such as recrystallization kinetics, grain size and recrystallization texture can all be satisfactorily predicted. However, judging from where they stand, it may be challenging for these models to consider more complex situations, e.g. when preferential growth either due to 40°<111> or misorientation dependent Zener pinning appear. As a consequence, they are not expected to be versatile even in the cases of stable bimodal particle structures. Recent simulations do show that both oriented nucleation and growth should be implemented to make satisfactory texture

predictions [369]. It can be noted that all the three models presented are mainly designed for Al alloys. However, bimodal particle structures do also exist in other materials, but it seems that recrystallization is much less studied for these materials, and adequate numerical models are even rarer.

4.6.2 Recrystallization with concurrent precipitation

The situation is even more complex when precipitation is taking place during recrystallization, in which case the size and volume fraction of particles which determine the Zener pinning pressure change with time. The grain boundary mobility can also be drastically influenced by the reduced solute drag effect from solute atoms. A few recently developed recrystallization models coupled with precipitation either through physically based models or with thermodynamic software are summarized below.

The simultaneous variations of recovery, precipitation and recrystallization during annealing of microalloyed Nb-steels were modelled by Zurob et al. [382]. In this model, the progress of recrystallization was based on the JMAK approach assuming site saturated nucleation, i.e., N_{rex} sites per unit volume. The number of nuclei per unit volume N_{rex} is related to the ratio between grain boundary area per unit volume (S_v) and the area of the nucleus (A_c), a geometric factor k is also introduced. The growth rate ($G(t)$) and grain boundary mobility ($M(t)$) (and thus the stored energy $P_D(t)$), are time dependent and vary with recovery and precipitation processes, see Fig.36. When the number of precipitates is higher than the total number of dislocation nodes, $N > N_c$, recovery by dislocation motion is totally suppressed. Otherwise, a pinning term ($1 - N / N_c$) is added to the recovery equation. In terms of precipitation, the mean precipitate radius and the number density of precipitates are predicted. Precipitation is assumed to occur exclusively on dislocations and take place in two steps following the approach of Deschamps and Brechet [372], viz. firstly nucleation and growth, and secondly growth and coarsening. In the first precipitation stage, the variation of precipitate density is given by the nucleation rate (dN / dt). The variation of mean precipitate radius is governed by the combination of the growth of existing precipitates and the nucleation of new precipitates. In the second precipitation stage, size of precipitates increases due to coarsening, and the number of precipitates decreases due to dissolution of small precipitates. When the decrease of the precipitate density by coarsening is

larger than the increase of the precipitate density by nucleation, the transition from the first to the second precipitation stage takes place. The coupling between concurrent recovery, recrystallization and precipitation is shown in Fig.36.

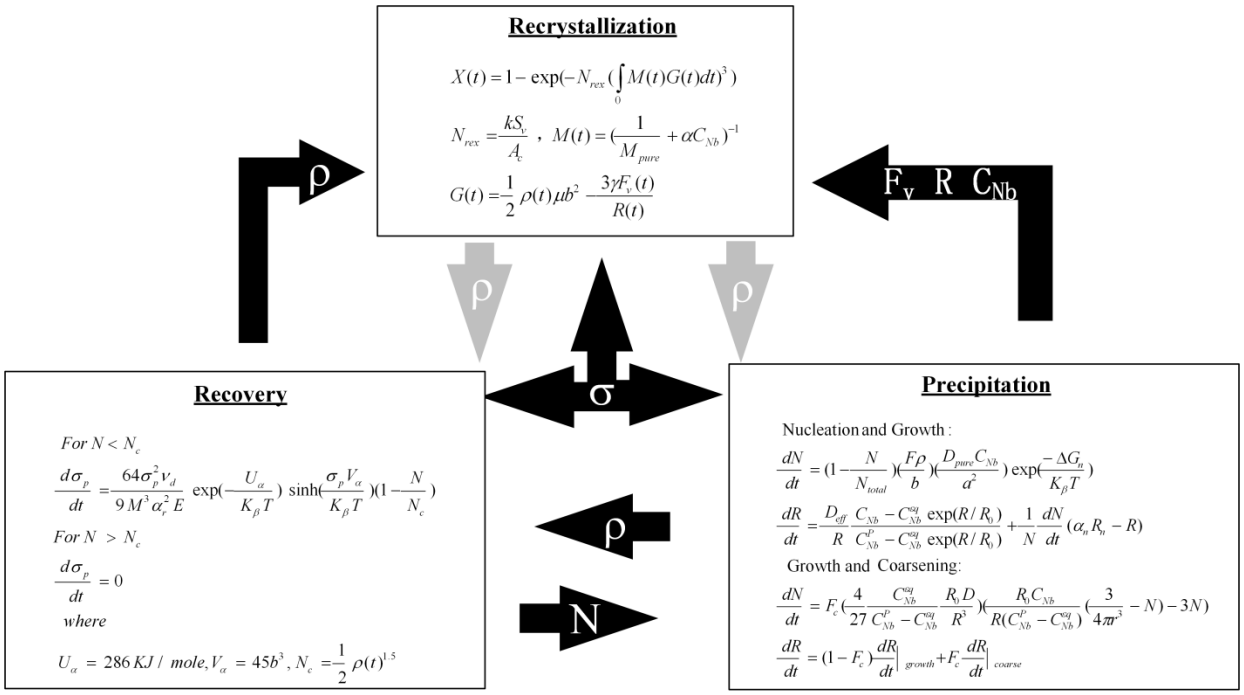

Fig.36 Summary of the recovery, recrystallization and precipitation modules used in the model by Zurob et al. [382]. The variables that provide the coupling between each of the modules are highlighted to emphasize the interdependency of each of these processes. The grey arrows refer to interactions that were not considered in the present model. Reproduced from [382], with permission from Elsevier.

Assuming site saturated nucleation might be a good approximation for some cases, but this is definitely not true in more complex cases such as during low heating rate annealing or step annealing with the first step at very low annealing temperatures where nucleation only takes place when a sufficiently high temperature is reached. A very powerful model for recrystallization during non-isothermal annealing was developed by Schäfer et al. [383,384], which predicts recrystallization kinetics, microstructure and texture. Strictly speaking, the model is a combination of several sub-models developed by the Aachen group led by Prof. G. Gottstein, as shown in Fig.37. This includes: i) the deformation texture and work hardening/softening model GIA-3IVM+ [385,386] which gives orientation dependent dislocation density evolution in

each grain; ii) a nucleation model ReNuc [191,386] which includes nucleation at grain boundaries transition bands and/or shear bands, and PSN where a delay in the start of recrystallization (incubation time) was considered based on recovery kinetics as modelled in the work hardening/softening model 3IVM+; iii) a growth model CORe [275,384] which simulates the growth of recrystallization nuclei in the deformed matrix and considers the preferential growth of grains with 40°<111> orientation relationship to the matrix; iv) a statistical precipitation model ClaNG [387] based on classical nucleation and growth theory to predict solute contents, precipitates size and volume fraction. The fine precipitates induce a Zener pinning pressure opposing the grain boundary migration. More details on each sub-model can be found in the referenced articles, and further discussion is unnecessary at this stage except by noticing that these sub-models can be fully coupled to account for complex phenomena. Based on extensive investigations of the different involved phenomena, this combined model is able to consider the complex interaction between precipitation and recrystallization including precipitation prior to, simultaneous with and after recrystallization. Since both nucleation and precipitation are time- and temperature-dependent, the model can be used in any non-isothermal annealing conditions. The effects of coarse and fine particles on recrystallization were both considered, where the former leads to PSN and the latter retards grain boundary migration. Furthermore, the orientation dependent work hardening and recovery, as well as grain boundary migration lead to more accurate recrystallization texture predictions. This is perhaps one of the most powerful recrystallization models in the literature, it also fully illustrates the complexity of modelling recrystallization in the presence of second-phase particles.

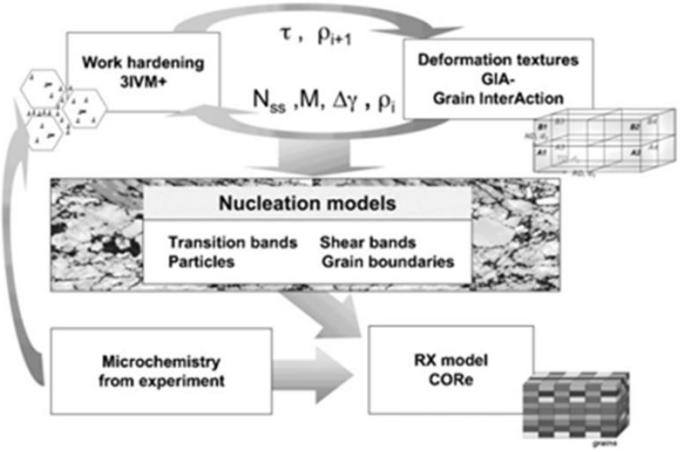

Fig. 37 Schematic graph showing the recrystallization model, where the microchemistry evolution can also be predicted by the precipitation model ClaNG. Reproduced from [384], with permission from Wiley.

While the model by Schäfer et al. [383, 384] considered the complex recrystallization behaviour during non-isothermal annealing, their precipitation model is still of statistical nature. Based on the comprehensive thermokinetic simulation environment provided by MatCalc, precipitation kinetics at different temperatures, deformation conditions and alloy compositions were calculated in an almost parameter-free manner by Buken and Kozeschnik [250, 388]. These authors introduced the concept of local precipitates coarsening at grain boundaries, which was experimentally observed in some microalloyed steels [e.g. 364]. Precipitation also interacts with DRX, which leads to an increase of the critical dislocation density to initiate DRX, as well as a decrease of the HAGB migration as compared to the particle-free case. The principal effects are the same as those encountered in SRX, the interested reader is referred to Ref [389] for more details.

5. The effect of second-phase particles and recrystallization on mechanical properties

Even though the type, size, distribution and volume fraction of second-phase particles (i.e. the microchemistry) in an alloy are largely determined by the alloy composition, these quantities can indeed also be significantly modified by thermo-mechanical processing, which gives additional degrees of freedom for material engineers to control the recrystallization microstructures and textures, as well as mechanical properties. In this section, the mechanical properties of interest are first summarized, examples for improving and deteriorating mechanical properties through the control of recrystallization and second-phase particles are then considered.

5.1 Mechanical properties associated with second-phase particles and recrystallization

5.1.1 Yield strength

Both the yield strength and ultimate tensile strength can be significantly affected by recrystallization and second-phase particles. A common approach consists in linearly adding different contributions to the yield stress (σ_y):

$$\sigma_y = \sigma_0 + \sigma_{ss} + \sigma_{GB} + \sigma_\rho + \sigma_P \tag{40}$$

where σ_0 is a material constant related to the resistance of the lattice to dislocation motion (also known as the Peierls-Nabarro stress), σ_{ss} the solid solution contribution, σ_{GB} the contribution from grain boundaries, σ_ρ the dislocation forest hardening and σ_P the contribution from particles. It has been proved that a linear summation of different strengthening mechanisms in many cases does give good predictions [e.g.390], but other non-linear summation schemes have also been developed, see e.g. Ref [391].

The lattice resistance stress σ_0 is commonly expressed by:

$$\sigma_0 = \frac{2\bar{M}\mu}{1-\nu} exp(\frac{-2\pi a}{b(1-\nu)}) \tag{41}$$

where μ and ν are the shear modulus and the Poisson coefficient, respectively, $\bar{M}$ the Taylor factor and a the lattice parameter of the matrix metal. The solid solution contribution σ_{ss} is usually estimated as follows:

$$\sigma_{ss} = \sum K_i \cdot c_i^z \tag{42}$$

where K_i are hardening constants, c_i the atomic fraction of element i, and z an exponent typically in the range ~0.5-1.

The grain boundary contribution can be described by the Hall-Petch equation:

$$\sigma_{GB} = \frac{k_y}{\sqrt{d}} \tag{43}$$

where k_y is the strengthening factor, and d is the average grain diameter. This equation fails if the grain size drops to ~10nm [392] and below, as schematically shown in Fig.38.

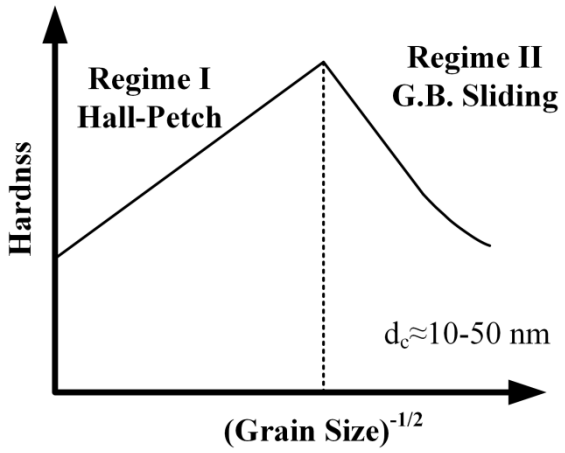

Fig.38 Schematic of the variation of hardness H with grain size d. Reproduced from [393], with permission from Elsevier.

In terms of the contribution from dislocations on material strength, the Taylor equation was one of the first expressions relating the flow stress to dislocation density (ρ). It is still widely used in the literature for FCC, BCC, HCP metals as long as the flow stress is only controlled by interactions between dislocations as shown in Eq. (6). Using the Taylor factor, $\bar{M}$, the dislocation density can be related to the flow stress σ_ρ by the following expression:

$$\sigma_\rho = \alpha \mu b \bar{M} \sqrt{\rho} \tag{44}$$

Subgrain strengthening has long been recognized, Lesuer et al. [394] made this more clear by analysing the effect of nano-scale subgrains in ball-milled iron. The subgrain strengthening is not considered in Eq. (43) nor in (44), but according to Nes [223], the contribution of subgrains can be estimated by converting the subgrain boundary misorientation into a dislocation density. More

details on the strength contribution from low energy dislocation structures can be found in Ref [223, 224,395].

Finally, the contribution of non-deformable particles on shear stress was discussed in **Section 3.1** using the Orowan equation (Eq. (1)). Ashby improved this equation by taking into account the effects of statistically distributed particles and the interparticle spacing (λ); the Ashby-Orowan relationship gives the contribution of particles as [396]:

$$\tau_P = 0.84 \frac{\mu b}{2\pi(1-\nu)^{1/2}\lambda} ln\frac{r}{b} \tag{45}$$

where ν is the Poisson's ratio of the matrix, and the interspacing of particles (λ) can be expressed as

$$\lambda = r \cdot (\frac{2\pi}{3f_V})^{1/2} \tag{46}$$

Combining Eq. (45) and Eq. (46), and using the Taylor factor ($\bar{M}$) for polycrystalline materials, the stress contribution from non-deformable particles is:

$$\sigma_P = \frac{0.84\bar{M}\mu b f_V^{1/2}}{2\pi(1-\nu)^{1/2} r(\frac{2\pi}{3})^{1/2}} ln\frac{r}{b} \tag{47}$$

The contribution of dispersoids on the yield stress thus increases with the shear modulus (μ) and Burgers vector (b), as well as with the volume fraction of dispersoids (f_V). If a typical value of particle radius (r) is used, it can be easily seen from Eq. (47) that the reciprocal of particle radius significantly outweighs that of the logarithmic term, i.e., decreasing particle size increases the yield stress. Further attempts have been made to improve Eq. (47), for instance, the effects of dispersoid shape and orientation on dispersion strengthening was considered by Nie in Ref [397]. In essence, dispersion strengthening is achieved by introducing second-phase precipitates to serve as obstacles to the dislocation motion. Age hardening or precipitation hardening is a special case of dispersion strengthening since it usually involves the strengthening of alloys by fine coherent precipitates which are prone to be sheared by dislocations, of which comprehensive reviews were given by Ardell [398] and Gladman [396]. As stated early, these fine particles will suffer coarsening or dissolution when exposed to high temperature deformation or annealing where recrystallization comes into play, which then makes their contribution to yield stress less important.

The concept of strength anisotropy [399] or yield asymmetry [195], i.e. orientation dependent strength, merits further discussion here. The degree of strength anisotropy is usually limited for common cubic metals thanks to the large number of available slip systems. In hexagonal metals, however, strength anisotropy can be much more significant, in fact this has also been referred to as texture strengthening. These metals have fewer equivalent slip systems which are not always oriented for glide, large variations in the critical shear stress for different slip modes also exist, and deformation twinning can also play an important role. The strength anisotropy can thus be tailored by controlling the crystallographic texture. Due to the lack of generality (with respect to more commonly utilized FCC metals), further discussion in this direction is not proceeded here, but the interested reader is referred to the excellent book by Kocks, Tomé and Wenk, entirely dedicated to texture and anisotropy [400] .

Recrystallization modifies grain size, as well as the total dislocation density of the material, with the former contributing to grain boundary strengthening and the latter leading to work hardening. Large second-phase particles, and especially the insoluble ones, usually make no substantial contribution to the yield strength of the alloy [401]. However, significant contribution from fine dispersoids, i.e., dispersion strengthening, on material strength can be obtained. The precipitation or dissolution of dispersoids also modifies the solution strengthening effect.

5.1.2 Ductility

Ductility is another important material property for most of the structural materials, which is also often correlated with elongation and fracture. The requirements for high yield stress and good ductility are generally contradictory. As it stands, a universal theory of ductile fracture is still lacking, a very recent and comprehensive review on this topic was given by Pineau et al. [402]. For brevity purposes, the effect of deformation conditions such as deformation temperature, strain rate, deformation mode etc. on material ductility will not be discussed (assuming uniaxial tensile test at room temperature with constant strain rate), emphasis is rather placed on the influence from the microstructure parameters on void nucleation. A large increase in ductility can be achieved if void nucleation can be delayed or suppressed. The subsequent void growth, distortion and coalescence are neither discussed, the interested readers are referred to Ref [402] for more details.

It is reasonable to assume that all materials of interest are ductile when recrystallization is of relevance since considerable deformation is needed to induce recrystallization. Fracture could occur by plastic instability such as the formation of shear bands in particle-free materials. In particle-containing ductile materials, fracture may take place prematurely due to void formation at second-phase particles, this could be due to particle decohesion in soft matrix or particle cracking in a hard matrix [403]. The two fracture mechanisms can also coexist in the same sample. Particle fracture occurs instantaneously as soon as the threshold stress is reached, i.e. it is similar to cleavage fracture. On the other hand, interface decohesion develops progressively. Simple models are developed to describe particle fracture and particle decohesion in particle-containing materials, e.g. [403]. The influence of some key parameters on the trend of these two mechanisms is summarized in Table 1 [402]. For instance, particles which are roughly equiaxed tend to generate interfacial decohesion while elongated particles or particles with large aspect ratios often fail by particle fracture. Since most of our previous discussions are based on soft crystalline materials containing hard non-deforming second-phase particles, and since irregular coarse particles tend to decrease their aspect ratio by homogenization, the rest of the discussion is mainly focused on round coarse particles, i.e., fracture by interfacial decohesion. It is then just sufficient to further mention that larger particles are more prone to fracture [404]. The cut-off particle size under which no void nucleation occurs is suggested to be ~0.1μm for the usual dislocation densities encountered in deformed metals, according to Pineau et al. [402].

Table 1 The effect of *increasing* the key parameters in void nucleation. Reproduced from [402], with permission from Elsevier

Parameter	Type	Trend	
		Decohesion	Cracking
Matrix yield strength		↓	↑
Matrix hardening exponent		↓	↑
Particle elongation		↓	↑
Particle stiffness		↑	↑
Load orientation	axial	↓	↑
	transverse	↑	↓
Load triaxiality		↑	↓

A necessary condition for void nucleation is usually derived from energy considerations that are similar to Griffith's theory for brittle fracture [405], i.e., the decrease in elastic strain energy resulting from the formation of a crack must exceed or equal the surface energy of the created new surface:

$$\sigma = (\frac{2E\gamma_s}{\pi c})^{1/2} \tag{48}$$

where E is the Young modulus and c half of the void length. Replacing the void length by the particle size, it is reasonable to conclude that the required stress to cause fracture scales as $1/\sqrt{r}$, r being the particle radius. This implies that a larger stress is needed for materials with fine particles that are well bonded to the matrix to avoid interfacial voids, i.e., improved ductility is achieved. This can be rationalized by the fact that a small particle size minimizes the possibility for multiple slip-band pileups, which will increase the local stress and create fracture. With respect to this, round particles should also be preferred since they reduce stress concentration. Void nucleation is usually observed at much lower stresses than predicted by Eq. (48), implying that stress localization near the particle interface must have occurred.

If the interface between the particle and matrix is weak, the formation of voids at the interface may be possible [406,407], an example has already been shown in Fig.20. Actually, it was found that cold rolling to a true strain of ~0.92 in Ni generated a pair of crescent-shaped voids at *every* coarse silica particle in the analysed volume [408], as shown in Fig.39.

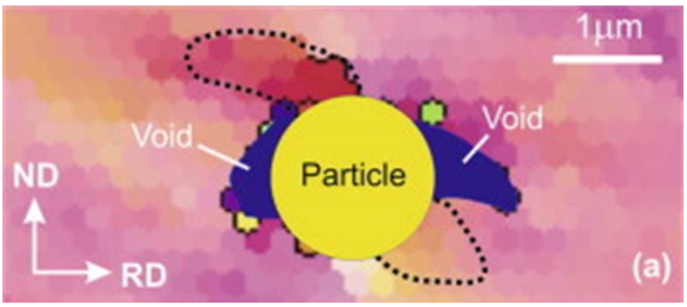

Fig.39 EBSD map showing the interfacial voids and highly rotated matrix zones (bounded by dashed lines) at a coarse silica particle in Nickel. Reproduced from [408], with permission from Elsevier.

Criteria based on critical strain for void nucleation have been also developed. By assuming that decohesion takes place at a critical stress (σ_c) due to local work hardening at particles, Goods and Brown [409] predicted a critical strain for void formation (ε_c), which is proportional to the spherical particle radius (r):

$$\varepsilon_c = \frac{1}{30}\left(\frac{\sigma_c}{\alpha\mu}\right)^2 \cdot \frac{r}{b} \tag{49}$$

where μ and b are the bulk shear modulus and Burgers vector, respectively, and α is a dimensionless constant. The fact that the critical strain is a linear function of the particle radius, is in agreement with experimental results [409]. This means that large widely distributed (in space) second-phase particles are less damaging than fine ones when interfacial fracture is involved. However, when the particle size is large enough, the critical strain for interfacial decohesion becomes independent of particle size. On the other hand, under a minimum particle size, interfacial fracture is energetically not favourable [402]. Void nucleation can also be predicted by the continuum approach depending on the work hardening rate ($d\sigma/d\varepsilon$), if the particles are above a critical size (r_c), of which a typical value is ~1-2μm [409].

$$r_c \approx \frac{\alpha^2\mu^2 b}{\sigma_y}\left(\frac{d\sigma}{d\varepsilon}\right)^{-1} \tag{50}$$

The volume fraction of particles is included in the above equation when expressing the hardening rate term according to the considerations given in **Section 5.1.1**. It is sufficient to say that the void formation strain decreases with increasing the volume fraction of second phase particles [409]. The real fracture behaviour in particle-containing materials is in reality much

more complex, especially when bimodal particles, non-spherical particles or unstable particles are involved, examples can be found in different types of Al alloys [410,411,412,413]. A short review on achieving maximum ductility of two-phase polycrystalline materials including nickel, iron, tungsten, and molybdenum can be found in Ref [414].

Now that the effect of second-phase particles on ductility has been discussed, word must be given on the contribution of grain size effects. According to Goods and Brown [409], void formation at grain boundaries during low temperature deformation is mainly dominated by plasticity, i.e., dislocation pile-up stresses. Materials with a coarser grain size can accumulate higher dislocation pile-up stress and thus promote void formation. In the conventional grain size regime, a reduction in grain size thus usually leads to an increase in ductility. However, it is now clear, both by experiments and molecular dynamic simulations, that the ductility of nano-sized materials is on the contrary low, further discussion on this topic is however not proceeded here, since excellent review papers are available in the literature, e.g. [415]. It is worth mentioning that a bimodal grain structure often proves to give optimal ductility together with high strength: ultra-fine matrix grains contribute to the strength, and micrometre-sized grains provide the needed strain hardening rate [416]. Different approaches to improve the ductility of nanostructured metallic materials are summarized in Ref [417].

5.1.3 Other properties

While strength and ductility are the two most important mechanical properties for most metallic materials, other key material properties such as creep resistance and fatigue life should also be considered in many applications. A very brief introduction to these two properties and their dependences on microstructure parameters are provided below.

Creep is a time-dependent deformation at high homologous temperature under a certain constant applied load. Without going into details of different creep mechanisms, creep is usually divided into three stages according to the creep curve shown in Fig.40: i) creep rate (the slope of this curve) decreases with time in the primary creep regime (or transient creep) stage; ii) limited creep rate changes with time in the so called steady state creep regime (secondary creep); iii) creep rate increases rapidly in the final tertiary creep regime. Not mentioned is the section from

O to A which is supposed to be of elastic origin. It should also be noted that the time scale for creep testing might extend over several months.

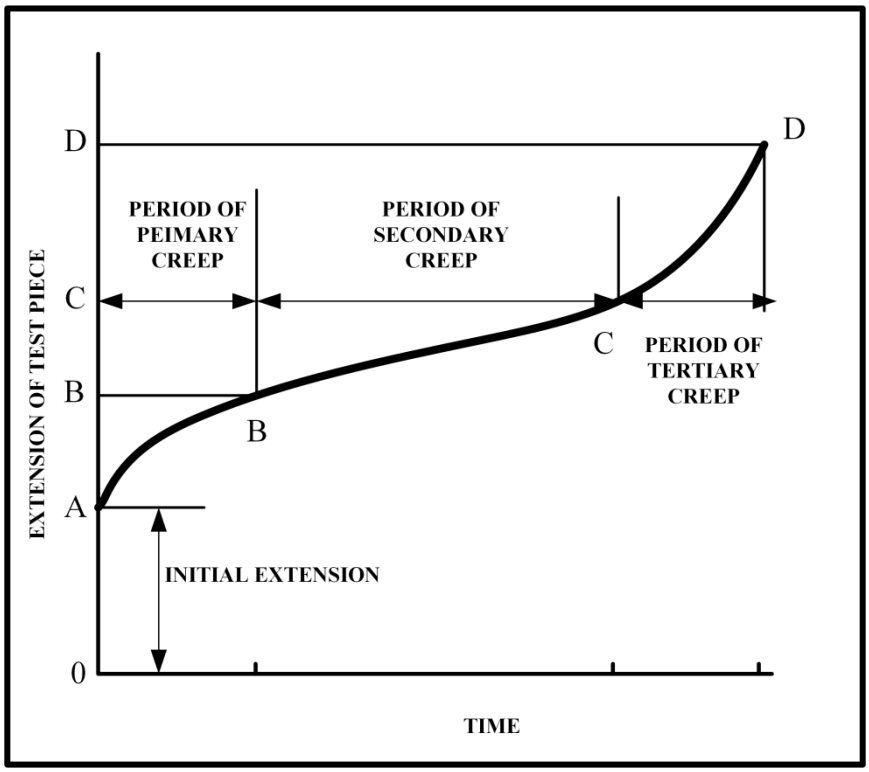

Fig. 40 Typical creep curve showing the three regimes of creep under constant load. Reproduced from [418] with permission of Springer.

The detailed creep behaviour of particle-containing materials can be found in Refs [419,420,421]. It is perhaps sufficient to mention that in order to improve creep resistance, it is usually favourable to increase the melting temperature and grain size of the material and higher creep resistance is achieved with fine and stable particles. The size effect of microstructure, i.e. second-phase particles and grain structures, on creep behaviour is summarized by Arzt [422]. The creep resistance is an extremely important property for high temperature alloys where it is desirable to keep creep deformation to a minimum. As an example, single crystalline Ni-based superalloys with densely distributed second-phase particles are employed in aerospace turbine blades that operate in extremely harsh environments with both high temperature and rotation speed, as will be discussed in more detail in **Section 6.1**.

Fatigue life is another key material property to consider for metallic components during dynamic loading. It has been long recognized that a metal subjected to a repetitive or fluctuating

stress (see Fig.41) can fail at a stress much lower than that required to cause fracture during constant load. The fact that fatigue failure occurs without any obvious warnings, has attracted extensive investigation to predict the fatigue life, which is of statistical nature. Three basic factors act together to cause fatigue failure [423]: i) a maximum tensile stress of sufficiently high value; ii) a large variation or fluctuation in the applied stress; iii) a large number of loading cycles. Other factors that also affect the fatigue behaviour include stress concentration, corrosion, residual stresses and microstructure parameters such as grain size and second-phase particles.

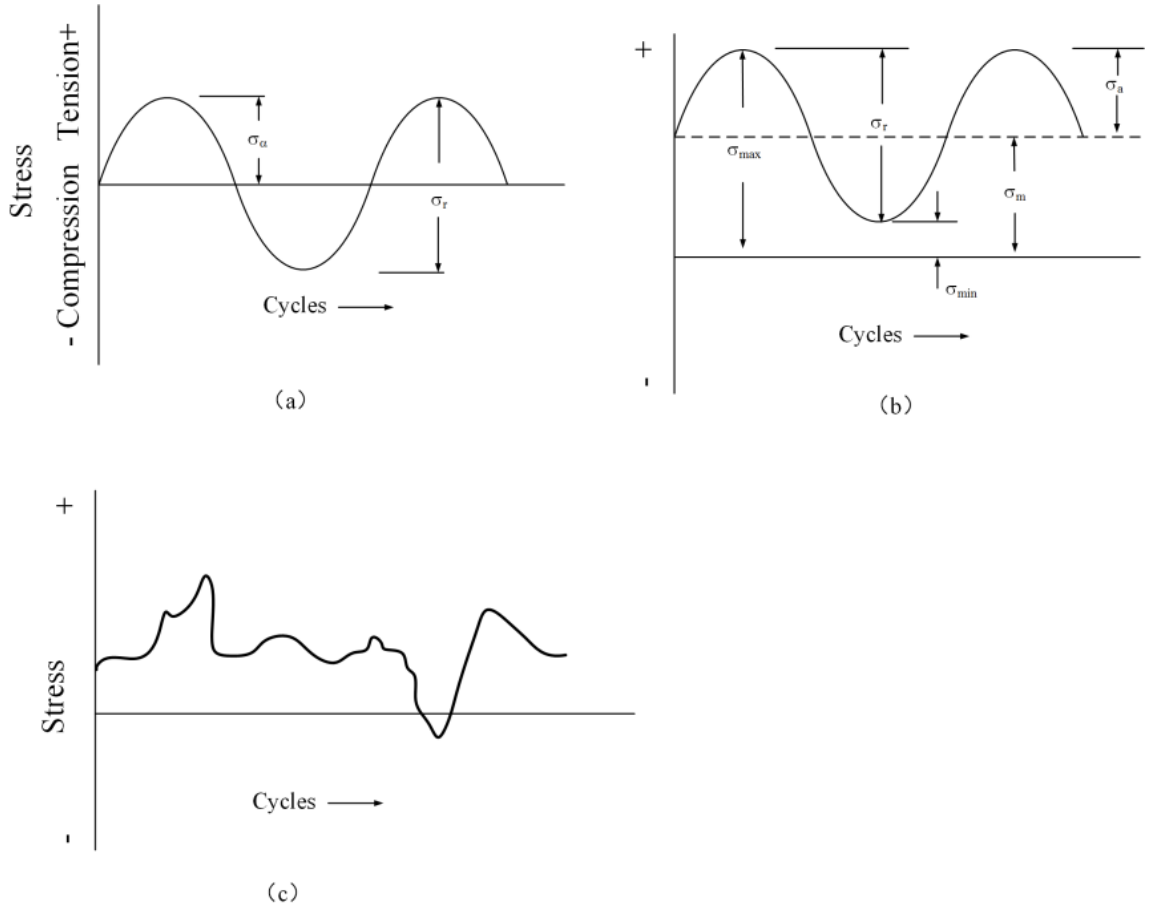

Fig. 41 Examples of typical fatigue stress cycles. a) reversed stress; b) repeated stress; c) irregular or random stress cycle. Reproduced from [423], with permission from McGraw-Hill Education

The typical way to present engineering fatigue data is to plot the stress (S) against the number of cycles to failure (N), usually known as the S-N curve. The fatigue process is usually divided into four steps [423]: i) crack initiation; ii) stage I crack growth which involves the deepening of the initial cracks on planes of high shear stress; iii) stage II crack growth by growing of well-

defined cracks in directions normal to the maximum tensile stress; and iv) ultimate ductile failure where the remaining cross section can no longer support the applied load. As far as metallurgical effects are concerned, the greatest improvements in fatigue performance are to reduce stress concentration or introduce compressive residual stresses. The former could be, for example, achieved by homogenizing slip deformation, in which densely distributed stable fine-dispersoids could be of help. Caution should be taken when using fine-dispersoids since deformable fine dispersoids could easily lead to strain localization or particle dissolution. Most of the fatigue failures start at the surface. Under very high cycle fatigue conditions, cracks can also nucleate inside the specimen, usually at a local stress concentrator such as an inclusion or constituent particle for engineering materials (see Fig.42), or a grain boundary for a pure metal. Note that the effect of second-phase particles on deformation was detailed in **Section 3.1**. The dependence of fatigue life on grain size is not straightforward, but grain size has its largest effect on stage I cracking, according to Thompson and Backofen [424]. In high SFE materials, the fatigue behaviour is mostly related to the cell/substructure size making the effect of grain size less important. On the other hand, materials of low SFE do not readily exhibit substructures and fatigue life is then proportional to $D^{-1/2}$. A detailed description of fatigue of metals can be found in Ref [425], which includes cyclic deformation, crack nucleation and crack propagation.

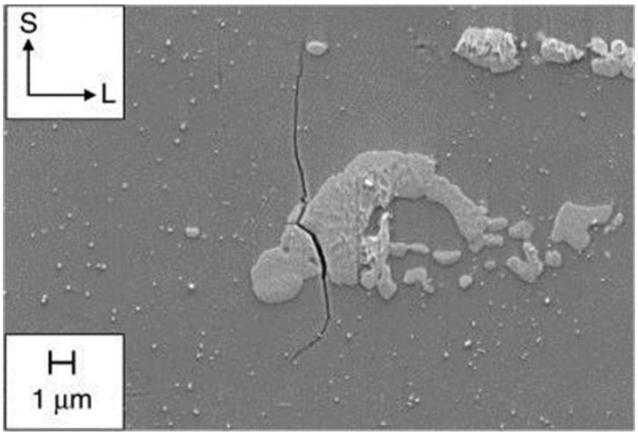

Fig.42 Cracked particle from which a fatigue crack nucleated on the long transverse surface of 7075-T651 aluminium alloy. Reproduced from [426], with permission from Elsevier.

Second-phase particles and microstructure also affect other material properties such as damping behaviour [**427**] and corrosion resistance, both of which are not further discussed here as it is beyond the scope of the present review.

5.2 Controlling mechanical properties of particle-containing metallic materials

As discussed in the last section, the mechanical properties of particle-containing metallic materials are closely related to the obtained microstructures, which can be tailored by appropriate control of grain structure and particle structures. The focus in this section is to discuss the theories behind this approach. The real examples guided by these theories in industrial applications will be given in **Section 6**. While we try to distinguish the contributions from control of grain size, crystallographic texture and second-phase particles, it should be noted that in many cases, the mechanical properties are improved by a combination of all three aspects. An excellent example can be found in the recent work by Wang et al. [428], where high strength and high ductility were simultaneously achieved in a Mg alloy using a single rolling pass. The superior properties were a result of multimodal grain structure, weakened texture, as well as contribution from nanosized second-phase strengthening.

5.2.1 Control of grain size

As discussed in Section 5.1, a large number of the material properties are directly dependent on grain size. The material strength could be significantly increased by reducing the grain size according to the Hall-Patch relation, even though this relation is not valid when reaching grain size levels ~10nm. It appears that ductility follows a similar trend with respect to grain size. A fine grain size is essential for superplastic deformation, as will be further detailed in Section 6.3. Emphasis is here placed on how grain size could be controlled by recrystallization in particle-containing materials.

In materials with negligible second-phase particles content, the control of grain size by SRX is relatively easy: large cold deformation, fast heating rate and high annealing temperature usually lead to a refined grain structure. When second-phase particles are involved, it is generally accepted that coarse particles could accelerate recrystallization and provide a fine and equiaxed

grain structure while densely distributed fine dispersoids tend to retard recrystallization and result in coarse grain structure, as discussed in detail in **Sections 4.1** and **4.2**. Qualitatively, these two opposite effects could also lead to a 'non-particle effect' if they cancel each other. Quantitatively, the complexity brought about by the heterogeneous deformation structure associated with second-phase particles, the structure of the particles themselves in terms of their size, volume fraction and coherency with the matrix, as well as their different interactions with recrystallization, make the prediction or control of grain size difficult. The fact that particle size could evolve with time further adds uncertainty to the final grain size, all these details have been discussed in **Section 4**. In general, a fine grain structure can be reached in particle-containing materials by the following simple procedures: i) solution heat treatment to dissolve all fine particles or very fast solidification to avoid them; ii) large cold deformation to increase the driving force and nuclei density for the subsequent annealing, coarse particles further increase these tendencies; iii) high annealing temperature to avoid the retarding effect from precipitates while PSN can accelerate recrystallization; iv) lower temperature aging to allow precipitation of stable fine particles such as to inhibit grain growth at high temperature applications. The effects of the contributions from fine and coarse particles are thus separated, examples using similar methods could be found in Ref [429].

Significant grain refinement of particle-containing materials can be achieved by SPD at room temperature for materials with good ductility, which strictly speaking does not involve recrystallization since little HAGB migration is involved. Coarse constituent particles have been demonstrated to accelerate the grain refinement process, even though they do not significantly decrease the steady state grain size. Dispute still exists on how fine dispersoids possibly affect the grain refinement, it seems likely that they tend to act against this process, as discussed in **Section 3.3**.

Very often, large deformation at room temperature cannot be achieved for many metallic materials due to their poor ductility. Grain refinement by DDRX during hot deformation is a good alternative. It is generally accepted that the steady state recrystallized size of particle-free materials is a function of the Zener-Hollomon (Z) parameter ($Z = \dot{\varepsilon} exp(\mathrm{Q}/\mathrm{RT})$) which combines the effects of the deformation temperature and strain rate and can furthermore be related to the stress level. This implies that larger strains by severe plastic deformation at high temperatures do not contribute to further grain refinement once the steady state has been reached [9,10]. The

same clarity seems to be absent for particle-containing materials, since the size and volume fraction of particles can also play a role. Watanabe et al. [430] found that the recrystallized grain size could be nicely related to the Z parameter on AZ61 with considerable amount of precipitates. However, Xu et al. [431] reported a breakdown of the relationship between recrystallized grain size and Z parameter as established by Watanabe et al. during hot deformation of particle-containing Mg alloy due to the pinning effect of fine precipitates, which has been later confirmed by Changizian et al. [432]. The coarse particles should in principle accelerate recrystallization and lead to a fine recrystallized grain size, however, this effect is usually small due to the typically low volume fraction of coarse particles in conventional alloys that experience DDRX. This conclusion can be indirectly confirmed by the observation of deformation textures after DDRX since PSN usually leads to a more or less random texture, as will be discussed in the next section. Much less corresponding studies on the relationship between grain size and Z parameter (or stress) can be found for CDRX and GDRX during hot deformation of high SFE materials, which was suggested as one of the few topics for further investigation by Sakai et al. in their review paper on DRX [9]. In these conditions, the presence of fine dispersoids inhibits the (sub)grain boundary migration which yields a larger grain size, however, these fine dispersoids can also stabilize a fine recrystallized grain structure providing a smaller grain size. Coarse particles on the other hand are supposed to give finer grain structure by creating deformation zones and large orientation gradient around them. However, concurrent hot recovery could significantly reduce the PSN efficiency during hot deformation, as discussed in **Section 4.2.1**. More details on different DRX mechanisms and the effect of second-phase particles on grain refinement during DRX can be found in Ref [10].

When multi-pass thermo-mechanical processing steps are involved, the effects of second-phase particles on recrystallized grain size are usually manifested through their combined effects on deformation structures either by cold or hot deformation, as well as by SRX during annealing. If precipitation is involved, an associated decrease of solute drag must also be considered. It remains difficult to separate individual contributions, a good example involving different contributions can be found in Ref [201, 433]. The development of physically based models (see **Section 4.6**) could be of help in this regard, i.e. for a better interpretation of experimental results.

5.2.2 Control of crystallographic texture

Since both the deformation structures [434,435,436] and recovery behaviour [437,438] are orientation dependent, a random recrystallization texture is rarely observed. The developments of textures during recrystallization, as well as the texture control in low carbon steels were reviewed by Hutchinson [439, 440]. The approaches to optimize texture for Al and Mg alloys for automotive applications have been nicely summarized by Hirsch and Al-Samman [188]. As it stands, it seems that deformation texture can be satisfactorily predicted by numerical models, but the quantitative prediction of recrystallization texture usually remains out of reach. A focus is however given here on how to control crystallographic textures through appropriate recrystallization mechanisms. While in most of the applications a random texture is favourable, controlled non-random textures are preferred in some specific cases, as will be detailed below.

We begin with the approaches to randomize recrystallization texture. Weak recrystallization texture can be obtained by PSN, DDRX, control of deformation structure and shear banding. The randomization of recrystallization by PSN has been previously detailed in **Section 4.2.3**, no reiteration is necessary here. In DDRX, nucleation takes place at prior grain boundaries by the conventional serrations and bulging mechanisms [2,441], the deformed original grains are then progressively consumed by the expansion of the freshly formed recrystallized grains with increasing strain, leading to a so called necklace structure [442]. This mechanism does not in itself lead to randomization of texture since the so formed grains have orientations close to that of the adjacent parent grains, as demonstrated by Ponge and Gottstein [443]. These authors reported that at later stages of the recrystallization process the "orientation coherency" rapidly diminishes, owing to the large misorientations in the deformed grains as well as nucleation by twinning, which finally lead to a randomized texture. Most of the studies related to the randomization of textures by DDRX are focused on Mg alloys [e.g. 444], where large lattice rotations take place at prior grain boundaries, which eventually leads to the formation of recrystallized grains with orientations different from that of the grain interior, i.e. texture randomization finally results. In essence, this recrystallization mechanism can also be considered as one type of CDRX, since the formation of HAGBs relies on the progressive increase of misorientation of LAGBs. Rare examples of weakening texture by DDRX in FCC metals such as copper [445] also exist. Less common (or less general) approaches to the weakening of

recrystallization texture include the addition of rare earth elements [188] in Mg alloys, and hot isostatic pressing of powders.

Theories for achieving controlled non-random recrystallization textures are now exemplified. This can be achieved through either oriented nucleation or oriented growth, in many cases both mechanisms are actually involved, see e.g. Ref [446]. Second-phase particles are very often introduced since they can modify the nucleation behaviour by suppressing certain nucleation mechanisms (e.g. nucleation from prior grain boundaries) or give an misorientation dependent Zener pinning effect to some orientations and thus induce oriented growth. It should be acknowledged here that disputes still exist on whether oriented nucleation or growth should be responsible for the development of recrystallization textures, as contradictory results are often reported. A typical example is perhaps the formation of cube texture, which has been reviewed by Hutchinson [447]. Oriented nucleation refers to cube grains from retained cube components after deformation [e.g. 256] or transition bands [185,310], for which their fast recovery [185] gives a size advantage for recrystallization. Nucleation of recrystallization comes from existing embryos that already exist before recrystallization and have a defined orientation. With regard to oriented growth, i.e. nuclei are randomly oriented but some of them can grow faster and eventually dominate the recrystallization texture, cube grains have also been demonstrated to have a close to 40°<111> relationship with certain orientations of the deformed matrix such as the S-orientation and thus experience a growth advantage during recrystallization, see e.g., Ref [308]. Tilt grain boundaries with a close to 40°<111> misorientation were actually measured to have higher mobility by Huang and Humphreys [448,449]. The fact that the number of cube nucleation sites is rather low and limited impingement is expected between the growing cube grains before the completion of recrystallization, can also favour the formation of large cube grains [447]. Examples of cube texture control in industrial practice have been summarized by Hutchinson [447]. Two other very good examples of controlled texture are the production of metallic sheets [450] and grain-oriented silicon steels, the former will be detailed in **Section 6.4**. In fact, the development of many other major recrystallization texture components is explained in a similar way, examples include the formation of P-texture [258,259,262] and R-texture [446]. Recrystallization textures after CDRX, GDRX and continuous SRX have not been equally addressed in the literature. In principle all these recrystallization mechanisms lead to the

formation of a recrystallization texture similar to the deformation texture since only little HAGB migration is involved, as explained in Ref [10].

The formation of a recrystallization texture is usually significantly affected by deformation strain, heating rate and annealing temperature, microchemistry conditions in terms of solute and particle structures etc. The randomization or weakening of recrystallization textures could be strongly affected by these factors. Experimental results in favour of either the oriented nucleation or oriented growth theories should not be taken as evidence to disregard the other one. These factors affect recrystallization textures by modifying the nucleation mechanisms and growth behaviour during recrystallization, distinctly different recrystallization textures can be obtained starting from the same deformed samples just by varying the annealing conditions [451], much of which has been detailed in **Section 4**.

In summary, different factors must be taken into account when interpreting recrystallization textures resulting from thermo-mechanical processing. Deformation strain is important in determining recrystallization texture since: i) deformation texture intensity increases with strain; ii) it affects the grain boundary density (i.e. area per unit volume); iii) it influences the remaining texture components which could act as nucleation embryos; iv) precipitation is generally accelerated by increasing strain; v) it also affects the temperature at which recrystallization starts and interacts with precipitation, as well as the nucleation rate of recrystallization. The effect of annealing temperature is mainly manifested through its influence on activation of different recrystallization mechanisms and precipitation behaviour. The second-phase particles set in because: i) coarse particles can lead to PSN which generally leads to a weak texture; ii) fine dispersoids, preferentially located at (sub)grain boundaries, can suppress nucleation at prior grain boundaries, which may remove some recrystallization texture components; iii) fine dispersoids increase the critical nucleus size such that only orientations with a size advantage can further grow, e.g. cube grains [284]; iv) fine dispersoids are also less effective in selectively pinning special grain boundaries with low energies [255, 258, 260].

5.2.3 Control of particles

As mentioned in **Section 5.2.1**, large second-phase particles in general deteriorate the mechanical properties of metallic materials while small dispersoids tend to improve mechanical

properties if appropriately introduced. Use of second-phase particles in the design of alloys was reviewed already by Decker in 1973 [452]. The most obvious way to change the particle structures is by controlling the type and amount of alloying elements [e.g., 453] which is however not the main focus of this section, we are more interested in controlling particles through thermomechanical processing.

Bearing in mind that not all applications require mechanical properties such as long fatigue life and high fracture toughness, alloy systems with large particles can still find a wide range of applications in different industrial sectors. A good example is the successful application of the AA3004 alloy to produce commercial beverage cans, where a careful control of size, volume fraction and spatial distribution of constituent particles is vital. Large constituent particles, which form by a eutectic reaction during solidification, are present to different extents in almost all conventional Al alloys [454], most notably in Al-Si alloys. Due to their large sizes, constituent particles have incoherent interfaces with the matrix, contribute little to the pinning of dislocations or grain boundaries, provide almost no strength increase, however they can contribute to PSN. Constituent particles, which do not contain iron, may be dissolved into the matrix, typical homogenization procedures in industrial practice help to dissolve the network of soluble constituent particles. However, some of them have a low solubility, e.g. Al_7Cu_2Fe. In fact, the solubility of one element in Al can be modified by the addition of other elements, for example, although silicon has appreciable solubility in aluminium, its solubility is decreased by alloying elements such as magnesium. The sizes of insoluble and undissolved particles can be largely reduced by severe plastic deformation, a good example was already shown in Fig.8 (**Section 3.4**) [206]. The presence of large constituent particles is not an exclusive characteristic of Al alloys, e.g. an eutectic network of large particles also exist in other alloy systems, such as Mg-Zn-Y alloys [455].

Improving material properties by the control of fine dispersoids has been widely studied, well-known examples include the age hardenable high strength Al alloys [164], high strength low alloy (HSLA) steels [456,457] and particle containing austenitic steels (to avoid phase transformation during cooling) [24,458,459], Ni-based superalloys [460], Mg alloys [461], to list a few. While these might be considered as well established old approaches, a few more recent excellent examples are given below.

It is desirable to simultaneously achieve high strength and ductility in conventional structural materials. However, most of the earlier approaches to improve ductility are accompanied by a sacrificed strength. In the last decade, effective thermomechanical processing steps have been successfully designed in achieving both high strength and high ductility by a careful control of the second-phase particles [462,463]. The principle itself does not involve any complex theory. Take 2024 Al alloy as an example, it consists of three steps: i) a solution-treatment to *partially* dissolve T-phase particles, the remaining T-phase particles were deliberately kept to accumulate dislocations during cryo-rolling in the next step; ii) cryo-rolling at liquid nitrogen temperature to produce ultrafine-grain microstructures with high dislocation density; and finally iii) an appropriate aging procedure to generate closely dispersed nano-particles (S′ precipitates), which is enhanced by the high dislocation density generated in step ii), together with a low dislocation density in the matrix. The high density of S′ precipitates is responsible for the increase in strength, while both the dramatic decrease in dislocation density in the matrix and high density of S′ precipitates promote increased ductility. This promising approach or modified versions of it may be applicable to many other precipitation-hardening alloys for different purposes, such as to improve fatigue life in the Cu-Cr-Zr alloy [464].

Another illustrative example is related to the oxide dispersion-strengthened (ODS) alloys [465], which exhibit good radiation resistance and superior creep rupture strength at elevated temperature due to finely distributed oxide particles (e.g.,Y_2O_3) in the matrix. They are considered as potential materials for high-temperature applications. Reducing the oxide particles size in ODS alloys could help further improving their properties. In this type of alloys, the powder of the base material and the oxide are usually mechanically alloyed [20], the result is an ultrafine grained structure with high dislocation density, which facilitates the decomposition of the oxide particles. During subsequent annealing process, oxide particles can re-precipitate and their size can be reduced by adding appropriate minor alloying elements [466]. The size of these oxide particles can of course also be varied by changing the annealing temperatures during which re-precipitation takes place [391]. The formation and evolution of oxide particles in ODS steels during the multi-stage processing steps and the resulting impact on the microstructures were investigated in detail in Ref [467].

Besides the control of size and volume fraction of second-phase particles, the effect of particle shape can also be controlled to improve material properties. A very detailed study on

improving room and high temperature fracture in AA6xxx alloys by the control of coarse particles was conducted by Pardoen et al. [468]. AA6xxx alloys contain a large volume fraction of intermetallic particles with size ranging from 1-10μm, including the plate-like Al_5FeSi and rounded $Al_{12}(Fe, Mn)_3Si$ particles. These two types of particles give rise to damage, and the damage evolution consists of nucleation, growth and coalescence of different voids. These authors illustrated that the conversion of the elongated constituent particles into round ones can significantly improve the room temperature fracture strain by up to a factor of two. The effect of precipitate shape on the deformation behaviour of Mg alloys has also been extensively investigated [469,470,471], since precipitates in Mg alloys usually are of rod or plate like shape, with their morphology and habit plane depending on the alloy system and thermal treatment [397], i.e. these can be tailored by thermo-mechanical processing design. Also of relevance is the alignment of second-phase particles after deformation on the formation of fracture [399].

6. Industrial applications

Application examples involving the control of recrystallization have been reviewed by Bhatia [472] 20 year ago. This section does not claim to exhaustively review all the applied aspects with respect to particle-containing metallic materials. Rather, emphasis is placed on advanced manufacturing technologies such as production of high temperature alloys, additive manufacturing of metallic alloys, and new superplastic materials with fine grain structures obtained by severe plastic deformation etc. Typical traditional applications are also briefly discussed.

6.1 High temperature alloys

One of the most important properties for high temperature alloys is their creep strength, i.e. the maximum stress that can be applied to a material at a prescribed temperature without causing more than a specified strain in a given time. A large grain size (or even single crystal in some cases) and closely dispersed fine dispersoids are usually the favourable microstructure.

High temperature alloys find their wide application in aircraft engines, where safety, fuel efficiency and strict emission requirements must be met at the same time, motivating for

developing new alloys with higher melting temperatures, higher toughness and lower density. An overview of the alloy design for aircraft engines was recently given by Pollock [473] and it is summarized below. The aircraft engines usually consist of the fan at the intake, the compressor, combustor, turbine and exhaust sections, see Fig.43. The fan operates at low temperatures, so the materials used to construct it will not be addressed here (low-density materials such as titanium alloys, polymer matrix composites, Al alloys). The temperature of the compressed air through the compressor can rise up to ~700 °C, and here Ti alloys are the priority choice for both blades and disks. Ni- and Co-based alloys are mainly used in the combustor section where combustion takes place. The gas temperatures in the high-pressure turbine can reach to 1400-1500°C, the turbine blades, made in Ni-based single crystals, could reach up to 1100-1200°C (~90% of the onset melting temperature) with the help of proper thermal barrier coating and internal cooling systems [473]. The blades are assembled to turbine disks comprised of polycrystalline Ni-based alloys. These disks are often fabricated from powders that are subsequently consolidated and formed by extrusion and superplastic forging. The temperatures of the air fall again below 800 °C after passing the turbine to the exhaust section. The rotating and static components in the later stages of the turbine section (i.e. exhaust section) are dominated by polycrystalline cast Ni-based superalloys. The engine shafts, which must possess both very high strength and fatigue resistance, are typically fabricated with either high-strength steels or Ni-based superalloys. Of all these high temperature materials, we choose to illustrate the production of turbine blades and turbine discs, made in Ni-based single crystals and polycrystalline Ni-based alloys, respectively. The reason of the choice is simply because they are operating at the highest temperatures, even though the production routes of other mentioned alloys also involves both second-phase particles and recrystallization, interested readers are referred to Ref [474] for more details.

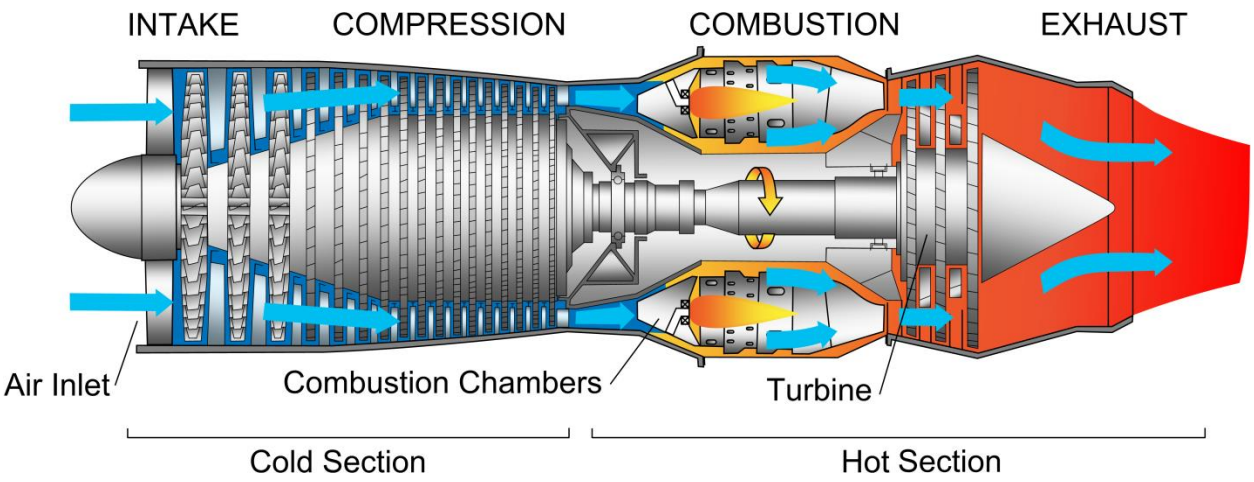

Fig. 43 Diagram of a typical gas turbine jet engine [475]. By Jeff Dahl [GFDL (http://www.gnu.org/copyleft/fdl.html) or CC BY-SA 4.0-3.0-2.5-2.0-1.0 (http://creativecommons.org/licenses/by-sa/4.0-3.0-2.5-2.0-1.0)], via Wikimedia Commons.

Turbine blades made in single crystals are free from grain boundaries. Grain boundaries are preferential sites for easy diffusion paths and therefore the removal of grain boundaries improves the creep resistance of the material. The strength of single crystals comes from fine precipitates. The essential solutes in Ni-based superalloys are aluminium and/or titanium. The single crystal alloys are usually heat treated to high temperatures to dissolve the coarse particles inherited from the solidification process. This is followed by heat treatment at lower temperature to achieve a controlled and fine-scale precipitation of γ'-Ni_3(Al,Ti), which is particularly resistant to high temperature, in a highly concentrated Ni solid-solution matrix (γ phase). Intensive efforts have been invested to tune alloy compositions, in order to optimize parameters of γ' intermetallic strengthening particles in terms of volume fraction, composition, morphology, and their spatial distribution. As a result, a typical Ni-based single crystal alloy now contains 8–10 major alloying elements [476]. While it may seem that the production of turbine blades is irrelevant to the recrystallization phenomenon, avoiding recrystallization during solution heat treatment of single crystal Ni-based superalloys is actually an essential problem in investment casting industry. A recent study focused on this topic can be found in Ref [477]. Grain boundaries produced by recrystallization lead to a catastrophic drop in creep rupture life, as well as to an increase of fatigue crack nucleation and propagation rates.

Concerning the turbine discs made by polycrystalline Ni-based superalloys, the powder metallurgy routes are usually employed due to the fact that a higher alloy content is desired in these materials, with conventional casting and wrought routes inevitably leading to segregation and workability issues. The Ni-based superalloys in the form of powders are consolidated by hot extrusion or hot isostatic pressing (HIP). The consolidated billet is then subjected to isothermal forging, where the tight control of heating and forging steps is essential to get the desired microstructure, and that is where static and dynamic recrystallization come into play. Whether second-phase particles are involved at this stage depends on the processing temperature since particles are dissolved if it is processed above the super-solvus temperature (i.e., the temperature at which γ' particles dissolve). The process route is followed by a heat treatment procedure since the microstructures produced from hot working operation are not yet appropriate for service application. Solution heat treatment is performed just below the γ' solvus such that the coarse γ' particles are dissolved while small number of γ' particles are kept in the matrix to pin grain boundaries. By careful control of the cooling rate after solution heat treatment or with a separate aging process, high volume fractions of very fine secondary γ' particles can be obtained [478].

Oxide dispersion-strengthened (ODS) steels are potential candidates for applications in nuclear environments [465], which require improved cladding and core structural materials with high-temperature performance (~600°C) in terms of thermal and irradiation creep deformation, irradiation-induced swelling etc. Although the production routes may slightly change depending on researchers/manufacturers, the principle remains approximately similar. A homogeneous distribution of yttrium in the steel powder is obtained by high-energy mechanical alloying of Y_2O_3 and base steel powder which also introduces a high dislocation density and nano-sized elongated grains. The material after mechanical alloying is subsequently consolidated by hot isostatic pressing or extrusion, during which yttrium in solid solution precipitates rapidly below the recrystallization temperature. These yttrium oxides (Y_2O_3) are mainly heterogeneously precipitated at triple and quadruple grain boundary junctions due to the small grain sizes which then maximizes the Zener pinning pressure. The size of oxide particles can also be controlled by addition of other alloying elements like Ti, Nb, V, Zr etc. The fine yttrium oxide dispersions act as pinning points that impede boundary movement and reduce irradiation swelling by acting as tripping sites for point defects induced by radiation displacement, giving excellent high temperature strength and creep resistance. The fuel claddings are cold-rolled, with intermediate

heat treatment, after consolidation, which leads to elongated grain morphology and deformation textures that are detrimental to creep rupture strength. Making equiaxed grains is a key technology for realizing ODS steel cladding. Two different approaches can be used to obtain equiaxed and homogeneous grain structure depending on the materials: i) recrystallization of cold rolled cladding tubes for ferritic steels (Cr>12%); ii) phase transformation of ferrite-martensite into austenite phase with fine grain structure due to the existence of Y_2O_3 particles for ferritic/martensitic steels (low Cr%). One of the current problems in producing ODS ferritic steel is the potential triggering of heterogeneous grain structures, including some amount of coarse grains after high temperature recrystallization, due to the similar magnitudes of high driving and retarding forces that oppose each other, which then result in anisotropic microstructures and detrimental consequences on properties in nuclear applications [479].

Refractory metals, with melting point above 2000°C, are another type of high temperature materials. Tungsten (W) has the highest melting point (3422°C) among all metals. Tungsten heavy alloys (WHAs) possess high strength at both room and elevated temperature. The widespread application of WHAs is, however, limited by their poor plasticity at room temperature, due to grain boundary brittleness induced by the soluble interstitial impurities segregated at grain boundaries. Improved compressive strength (2078 MPa at room temperature with a strain rate of 5×10^{-4} s^{-1}) and strain-to-failure (>40%) of tungsten alloys by the concurrent formation of intragranular tungsten oxide nanoparticles during low temperature (1200°C) spark plasma sintering (SPS) with high pressure of 1 GPa has been recently realized [480]. High strength and good plasticity were simultaneously achieved since these second phase particles inhibit grain growth and strongly interact with dislocations. A similar approach was used to improve the strength and ductility of another molybdenum alloy, which is also a typical refractory metal, where microstructure of submicrometer grains with nanometric oxide particles uniformly distributed in grain interior is the key [481].

6.2 Additive manufacturing

There is no need here to reiterate on the fast development of additive manufacturing techniques. The reader is referred to recent review papers [482,483,484] for more details on additive manufacturing (AM) of metallic materials. Laser-based AM processes are currently

regarded as the most versatile AM processes [483]. We will show in this section, with a few typical examples, how microstructure and mechanical properties could be tailored by controlling second-phase particles and recrystallization during laser-based AM and/or after subsequent thermo-mechanical processing. Ti alloys, Ni-based superalloys and Al alloys are the three types of most widely used metallic materials for laser-based AM. Since Ti alloys, Ti-6Al-4V and Ti-6Al-7Nb in particular, are often two-phase materials usually involving fine acicular α' martensite and some β grains, they are not further discussed below, interested readers are referred to Refs [485,486] for more details.

As already mentioned in the previous section, the control of second-phase particles is essential in fabricating Ni-based superalloys. These precipitates are not only tunable by AM process optimisation, they are also influenced by the subsequent thermo-mechanical treatments where both recrystallization and precipitation occur. Take the widely used Inconel 718 (Ni-Fe-Cr) as an example, in its wrought form it has three intermetallic precipitation phases in its austenitic matrix (γ): γ'-Ni_3(Al, Ti, Nb) with cubic (ordered face-centred) Ll_2 crystal structure, γ''-Ni_3Nb with a body-centred tetragonal crystal structure (DO_{22}), and an orthorhombic (DO_a) δ-Ni_3Nb. With respect to the microstructure and properties control, the strength level of the fabricated sample is highly dependent on the precipitation structures (i.e., size and volume fraction of precipitates), so does the recrystallization process. A very good example to illustrate this was conducted by Amato et al. [487] where Inconel 718 was fabricated by selective laser melting (SLM), the as-built samples were further subjected to either hot isostatic pressing (HIP) or annealing. The as-built samples exhibited columnar grains and arrays of γ'' oblate ellipsoidal precipitates (100 nm in the major axis and 25nm in the minor axis). After HIP at 1163°C for 4h, the γ'' (~250 nm in major axis) columns become more regular and a partially (5-10%) recrystallized grain structure was observed. Inside these recrystallized grains, columnar γ'' were dissolved. On the other hand, the samples annealed at 1160°C for 4h lead to ~50% of recrystallization, with spheroidal γ' homogeneously distributed in a dense field of much finer coherent γ'' (~35nm ~7nm), some δ precipitates were observed at the interface between recrystallized and non-recrystallized grains. Due to the fine γ'' precipitates, the micro-indentation hardness of the annealed sample was lower than the HIPed samples, but 18% higher than the as-built samples.

Laser-based AM is not yet a merited choice for all Al alloys. Most of the studies are focused on AlSi12 and AlSi10Mg alloys where the high Si content appears to be necessary to improve the melt properties to avoid defects. A brief review of AM of Al alloys was given in Ref [488] focusing on the microstructure and mechanical properties aspects. The mechanical properties of these so-produced alloys are usually inferior to conventionally produced high strength Al alloys such as AA7xxx alloys. One potential way to improve this is by adding second-phase particles to the metal matrix by mechanical mixing process (e.g. mechanical alloying) which however also introduces inherent drawbacks. The most important ones include the decreasing flowability of the matrix powder [483], the difference in thermal history between second-phase particles and matrix metals [489], as well as difficulties in ensuring good interfacial bonding between the matrix and second-phase particle [486]. In a very recent study, a novel in-situ preparation method of nano-TiB_2 decorated AlSi10Mg composite (NTD-Al) was fabricated for SLM by Li et al. [490]. This in-situ preparation method did not involve mechanical alloying and consisted of two steps: i) nano-TiB_2 was melted into pure Al at 900°C, the molten composite was solidified during casting to get a nano-TiB_2 reinforced pure Al composite master alloy; ii) pure Mg and Al-Si master alloys were introduced into the re-molten alloy prepared in i), and the NTD-Al composite powder was gas-atomised. The morphology and microstructure of the NTD-Al powder are shown in Fig. 44. SLM was performed using the so-produced powders under inert argon gas atmosphere to minimise oxidation, fully dense and crack-free samples were fabricated with optimised SLM parameters. It was found that the SLMed NTD-Al material possessed random texture and a fine microstructure, where *coherent* nano-TiB_2 particles were uniformly distributed along the grain/cell boundaries together with internal rod-like *coherent* nano-Si precipitates. More importantly, the SLMed samples using NTD-Al composite powder exhibit a high strength of 530±16 MPa together with superior ductility of ~15.5±1.2%, which are comparable to or higher than most conventionally fabricated wrought and tempered Al2xxx to AA7xxx alloys. It is worth mentioning that other types of Al alloys have also been used in non-laser-based AM techniques such as ultrasonic AM, where metal foils were bonded together using ultrasonic welding technology, examples include particle-containing AA3xxx and AA6xxx alloys [491, 492, 493, 494]. The material properties could also be further improved by subsequent heat treatments to modify the second-phase structures [488].

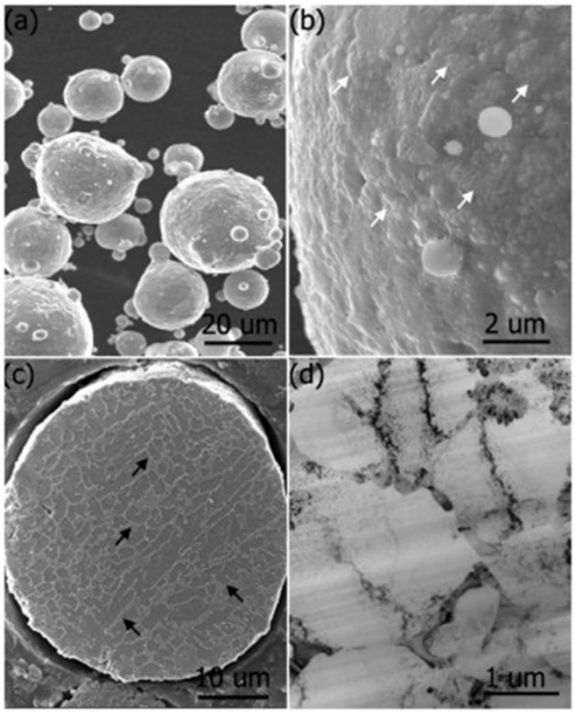

Fig. 44 SEM images of the (a) morphology, (b) surface and (c) cross-section of the NTD-Al composite powder. (d) TEM bright field (BF) image showing the grain structure and distribution of nano-TiB_2 in the NTD-Al powder. White arrows in (b) point to the TiB_2 particles on the surface of the NTD-Al composite powder. Black arrows in (c) point to the reticulated-distributed TiB_2 particles inside the NTD-Al composite powder. Reproduced from [490], with permission from Elsevier.

Even though examples were only given with two types of metallic materials, the theories described above are also valid in other alloy systems. For instance, a good combination of strength and ductility was obtained by the control of DRX and precipitation during friction stir AM of a Mg-based alloy [495], the control of fine dispersoids during SLM and subsequent heat treatment of an ODS ferritic steel [496] and Cu-4.3 % Sn [497] was also recently reported, together with the mechanical properties and microstructures. With the fast development of AM techniques, even more particle-containing metallic materials are expected to be used.

6.3 Superplastic metallic materials with ultrafine-grained structure

By definition, superplasticity refers to [498] "the ability of a polycrystalline material to exhibit, in a generally isotropic manner, very high elongations prior to failure. The measured

elongations in superplasticity are generally at least 400% and the measured strain rate sensitivities are close to ~0.5." It is now generally accepted that superplasticity can only be obtained during deformation when the following two requirements are fulfilled: i) a fine grain structure with size <~10 μm; ii) at high deformation temperatures above ~0.5T_m, where T_m is the absolute melting temperature of the material. Finer grain size or higher deformation temperature promotes superplasticity and could lower the requirement on the other. The high deformation temperature, however, tends to lead to grain growth for the fine-grained microstructure, that is why a fine dispersion of second-phase particles is usually introduced to inhibit grain growth in single-phase materials. Superplastic forming (SPF) is a way to reduce manufacturing cost since it lends itself to the manufacture of very complicated parts. Here, we are mainly concerned with the microstructure control during SPF of metallic materials, other aspects of SPF processes are out of the scope of this review.

Commercially available superplastic sheets were summarized by Barnes [499], where it can be seen that Al alloys, Ti alloys and Mg alloys are the three main categories. We choose to treat here the principles of microstructure control of superplastic Al alloys. Traditionally, SPF of Al alloys was performed at high temperatures (>500°C) and with low strain rates (<$10^{-3}s^{-1}$) [500]. Microstructures suitable for SPF can be obtained by appropriate thermomechanical processing, a four-step procedure is usually employed to obtain high strength aerospace AA7xxx alloys with superplastic microstructures of [501,502]: i) solution heat treatment of the material; ii) over-aging to have a uniform distribution of large particles (~1μm) and a stable dispersion of small dispersoids (~0.1 μm); iii) large rolling reductions to introduce deformation zones around the particles; iv) annealing treatment at high temperatures to trigger PSN, which leads to a fine grain structure, its growth being inhibited by the small particles. More recent examples using a similar approach to produce fine grained structures of AA5xxx (Al-Mg-Mn) and AA6xxx (Al-Mg-Si-Cu) can be found in Ref [503] and Ref [504], respectively. Alternatively, a fine grained structure can be achieved by DRX. For AA2xxx alloys, such as the Al-Cu-Zr Supral-type alloys, this involves several steps [2]: i) fast cooling during solidification to get small grain size and avoid precipitation of primary $ZrAl_3$ (or Al_3Zr); ii) heat treatment at ~350°C to introduce a fine dispersion of stable $ZrAl_3$ (volume fraction of 5%, size of ~10nm); iii) solution treatment at ~500°C where large $CuAl_2$ (or Al_2Cu) particles (>1 μm) are formed; iv) warm deformation at ~300°C with small $ZrAl_3$ particles preventing static recrystallization during inter-pass time; v)

cold rolling to further reduce the sheets; vi) superplastic forming at ~460°C where a fine grained structure of ~5 μm (depending on the strain rate) is obtained by continuous DRX during the initial stages of this deformation. Examples to achieve superplasticity by this method can be found in Refs [505,506].

The slow rate of the forming process significantly restricts the commercial applications of superplastic forming, therefore extensive work has been conducted to achieve superplasticity at elevated strain rates. Superplasticity is promoted at faster strain rates when the material grain size is reduced or when the temperature is increased [507]. Due to the possible grain growth at high temperatures, decreasing the grain size of the material seems to be a better option. Conventional thermo-mechanical processing cannot be used to obtain a grain size below ~2-3 μm. One typical way to achieve ultrafine-grained metallic materials for SPF is through SPD, of which a recent review was given by Langdon [508] where it can be seen that ECAP and high-pressure torsion (HPT) are the most common approaches. Some examples of fine-grained microstructures produced by ECAP were previously shown in **Section 3.3**, where the grain refinement is a result of high dislocation densities from large deformation, which subsequently re-arrange themselves and finally produce an array of high angle grain boundaries. However, the materials produced by these SPD techniques suffer from their small sizes and other processes must be considered when large scale industrial applications are of concern.

General Motor (GM) developed a so called quick plastic forming (QPF) process (hereafter referred to as GM QPF) [500,509] for the production of high volumes of aluminium panels for use in automotive applications at high strain rates ($>10^{-3}s^{-1}$ up to $10^{-1}s^{-1}$) and low temperatures (~450°C). The preferred alloy is AA5083 with 4-5 wt.% of Mg, 0.3-1 wt.% of Mn, <0.25 wt.% of Cr, ~0.1 wt.% of Cu, <0.3 wt.% of Fe, <0.2 wt.% of Si, and the balance Al. The alloy is first hot and then cold rolled to a thickness of ~1-4mm. It is then recrystallized to get a fine-grained Al matrix (7-8 μm) with Mg in solid solution and well-distributed finely dispersed second-phase particles. More details on microstructure control for the GM QPF process are not freely available. At high strain rates and low temperatures, both grain boundary sliding and solute drag creep were reported to be active mechanisms.

6.4 Traditional applications

Recrystallization plays a vital role in the manufacture of almost all metallic materials, which contain, to different extent, second-phase particles. Steels and Al alloys are the two most popular metallic materials in metal forming industry. A few more industrially important examples are discussed to illustrate the control of microstructure and texture of these two types of materials.

The production of HSLA Steels, which have been widely used for structural applications and pipeline industry, is a good example to reveal the interactions between recrystallization and second-phase particles. Even though HSLA steels have already been mentioned several times in the previous sections, a common definition was not yet provided. HSLA steels are a group of low carbon steels (0.05-0.25% C) that introduce small amounts of alloying elements, such as Nb, Mo, Ti and V, to the matrix to achieve high yield strengths (>275 MPa) in the as rolled condition [456]. As discussed previously, the effect of Nb is perhaps the most studied one in modern steels and this has been nicely summarized in Ref [510]. The production of HSLA steels usually consists of the following steps: i) slabs are reheated to dissolve most of the second-phase particles such as Nb(C,N), but stable TiN particles could still survive and they limit the austenite grain growth; ii) if necessary, repeated deformation steps at high temperature ($T>T_{nr}$ where T_{nr} is the non-recrystallization temperature, i.e., the temperature below which inhibition of *complete* SRX occurs during cooling between rolling passes) to refine the austenite grain size by SRX during inter-pass time, the microalloying elements mainly remaining in solution; iii) deformation in the low temperature austenite region ($A_{r3}<T<T_{nr}$ where A_{r3} is the temperature at which austenite begins to transform to ferrite during cooling) which leads to the formation of pancaked grains and deformation bands such that a large number of nucleation sites for the austenite to ferrite transformation are available, as well as strain induced precipitation of Nb (C, N) of size ~20 nm to retard SRX during inter-pass time; iv) accelerated cooling to get finer grain structure, as well as precipitation of finer Nb(C, N) of size ~1.5nm and V(C,N) as strengthening particles. Suitable understanding of the T_{nr} is the key to optimize the rolling process, a schematic graph showing the different obtained microstructures by changing the deformation temperature (and thus annealing temperature during inter-pass time) is given in Fig.45. The T_{nr} temperature is, however, influenced by the interaction between four different mechanisms: recovery, recrystallization, solute drag and precipitation. In industrial practice, it is desirable for a material

to have the highest possible T_{nr}. This provides less cooling time between the high and low temperature deformation, i.e., rough rolling and finish rolling. It also leaves a large temperature interval for low temperature deformation which makes it possible to conduct final rolling at higher temperatures with lower force. The total yield strength of HSLA steels is dependent on multiple strengthening mechanisms including the intrinsic strength of the iron lattice, the contribution of precipitation strengthening, solid solution strengthening and grain size effect. For a complete review on this topic, the reader is referred to Ref [456].

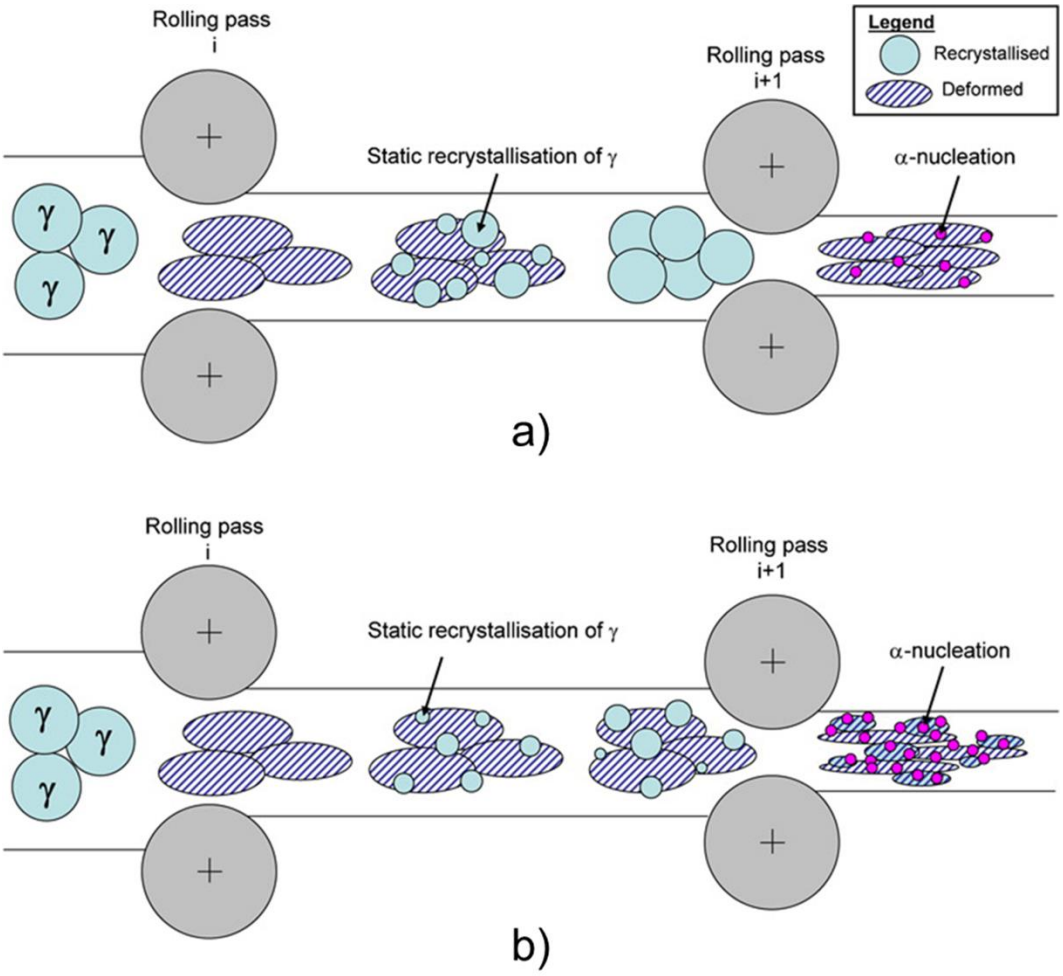

Fig.45 Schematic graph of thermomechanical controlled processing (TMCP) and microstructures that result from this process, particles are not displayed here. a) deformation above T_{nr} with complete recrystallization during inter-pass time and the resultant ferrite nucleation; b) deformation below T_{nr} with partial recrystallization during inter-pass time and the accelerated nucleation of ferrite. Reproduced from [456], with permission from Taylor & Francis.

While most of the industrial examples discussed above emphasized the control of recrystallization kinetics and grain size, further discussion on how the recrystallization texture can be controlled by the interactions of recrystallization and second-phase particles seems to be appropriate. The development of strong crystallographic textures during thermo-mechanical processing of sheet metals may lead to the formation of pronounced plastic anisotropy [399]. An excellent example is the formation of earing during deep drawing of Al beverage cans. The drawability is given by the r value (note that r is used throughout the paper as the radius of particles), which is the ratio of the true strains in the width (ε_w) and thickness directions (ε_t) when pulling along the third direction:

$$\mathrm{r} = \frac{\varepsilon_w}{\varepsilon_t} \tag{51}$$

As far as the anisotropy coming from crystallographic texture is concerned, an average r value, $\bar{\mathrm{r}}$ is calculated by considering three different directions:

$$\bar{\mathrm{r}} = \frac{\mathrm{r}_0 + 2\mathrm{r}_{45} + \mathrm{r}_{90}}{4} \tag{52}$$

High values of $\bar{\mathrm{r}}$, which correlate with good drawability, are desirable. The extent of earing in deep drawing from planar anisotropy is given by:

$$\Delta\mathrm{r} = \frac{\mathrm{r}_0 + \mathrm{r}_{90} - 2\mathrm{r}_{45}}{2} \tag{53}$$

In a rolled Al sheet starting from more or less random crystallographic texture, pronounced typical deformation texture usually leads to ears at the four positions ±45° to the rolling direction (RD) around the drawn cup. If a strong cube texture is present for the Al sheet before deep drawing, 0° / 90° earing is expected. However, if Al sheet with cube texture is further deformed by cold rolling, this modifies the deformation textures, and, as a consequence, it then gradually transforms to 45° earing with increasing rolling strain. For those who are not familiar with the concept of earing, an example is shown in Fig.46. Microstructures with a mixture of deformation texture components and the cube component can result in a balanced earing profile, e.g. see the texture optimization using a texture component crystal plasticity finite element method proposed by Raabe et al. [511]. The recrystallization texture is usually dominated by the cube grains and other grains of random orientations, where the former is thought to originate at retained cube bands or transition bands and the latter are mainly a result of PSN at the constituent particles.

More details on the microstructure control during production of can beverage body can be found in Refs [450,512,513], where it is seen that both coarse particles and fine dispersoids play a role in determining the final recrystallization texture. A few more industrially important examples were illustrated by Humphreys and Hatherly in their textbook on recrystallization [2], including the production of grain-oriented silicon steels and cold rolled and annealed steel sheets, and different types of Al alloys from commercial purity AA1xxx to AA6xxx automotive sheets.

Fig.46 Cups produced by deep drawing from circular blanks of an AA3104 alloy with different textures. (a) mixed cube and rolling texture, showing little earing; (b) strong cube texture, showing extensive 0°/90° earing. Reproduced from [2], with permission from Elsevier.

Finally, it is worth mentioning that extensive investigations have been conducted on Mg alloys for improving their strength anisotropy and low ductility; very often second-phase particles are involved, but their industrial production at present is rather limited compared to steels and Al alloys, they are therefore not discussed further here.

7. Summary and future work

7.1 Summary

The effects of second-phase particles on recrystallization and mechanical properties of particle-containing materials are discussed together in this paper, most of the discussion is related to SRX, even though DRX was also covered whenever available. Slight overlap with the textbook of Humphreys and Hatherly [2] is regrettably unavoidable because the necessary groundwork must be laid.

The important terminologies related to recrystallization and second-phase particles are explained. The methods used to characterize recrystallization and second-phase particles are introduced, including both the traditional techniques and the most recent ones. Much information can be obtained using the powerful 2D/3D in-situ studies or 3D-EBSD techniques such as to characterize the deformation zones around coarse particles. These techniques are, however, not yet fully applicable to the study of interaction between recrystallization and fine dispersoids.

The effects of second-phase particles on deformation structure and deformation texture have been discussed, with a focus on their influence on subsequent recrystallization behaviour. Moreover, the effect of different types of second-phase particles on microstructure evolution during SPD was illustrated, together with the particle evolution induced by deformation.

Emphasis is placed on the effect of second-phase particles on recrystallization, including the retarding effect from fine dispersoids, accelerating effect from coarse particles, as well as more complex situations involving bimodal particle structures and unstable particles. The effects of pre-existing particles before deformation, particles precipitated before onset of recrystallization, as well as concurrent precipitation on recrystallization were discussed separately, focusing on their influence on recrystallization kinetics, grain structure and texture. Typical numerical models, which are capable of considering complex conditions with bimodal particle structures and concurrent precipitation, are discussed in terms of their strengths and disadvantages.

The effect of second-phase particles on material properties is summarized. Theories to improve material properties by controlling grain size, crystallographic texture and particle structures are illustrated, together with real industrial applications.

7.2 Existing unresolved problems and future outlooks

There still exist many unresolved problems for recrystallization of single phase materials [1], these issues are of course inherited when dealing with recrystallization of particle-containing materials. The lack of systematic experimental data makes our understanding of the interaction between second-phase particles and recrystallization incomplete. The complex interaction between second-phase particles and recrystallization has been demonstrated in the previous sections. The overall complexity points to the need for the study of model alloy systems where systematic experiments can be conducted to separate the various possible mechanisms. Some important aspects that are worth further investigations for particle-containing materials are listed below:

1) Much of our current understanding of the effect of second-phase particles on deformation structure is essentially of qualitative nature. A better understanding of the deformation structure is vital for studying the subsequent recrystallization behaviour, this includes quantification of the deformation zone around coarse particles and homogenization of slip by densely distributed fine dispersoids etc. These effects involve dislocation reactions, which makes it difficult to be treated by finite element analysis. Moreover, the incorporation of the effect of middle sized particles effects on deformation structure remains challenging.

2) Current models for the interaction between recrystallization and second-phase particles are mostly based on the highly idealized assumptions of randomly distributed spherical particles. More realistic descriptions of second-phase particles are needed, this not only affects the deformation structure and microstructure evolution during recrystallization, but also very much determines the final mechanical properties.

3) In situ and/or 3D characterization of recrystallization and second-phase particles are still very much needed. Regarding recrystallization, the highest interest goes to the early stages of nucleation and growth, i.e. where nuclei of recrystallization come from and how they grow. The same questions arise for second-phase particles. Concerning the interaction between recrystallization and second-phase particles, the essential questions are the efficiency of PSN, why certain grain orientations are less affected by fine dispersoids, how the moving grain boundary modifies the particle structure etc. As far as fine dispersoids are concerned, we are expecting that an improved spatial resolution could be obtained in the near future for 3D

characterization techniques to resolve both grain structure and second-phase particles, or complementary characterization techniques (such as EBSD and BSE) can be conveniently combined.

4) During recrystallization of particle-containing materials, the reduced driving force from recovery should be quantified [382]. The interaction between recovery and second-phase particles also merits more investigation. The neglected recovery could frequently be taken as an unjustified enhanced retarding force from fine dispersoids. Experiments can be conducted at cryogenic temperature to avoid recovery, which then can be compared with other experiments performed at higher temperatures where recovery is active.

5) The effect of solute drag and particle drag should not be mixed up, since both of them induce different retarding effects on (sub)grain boundary migration. The decrease of solute drag during concurrent precipitation and particle coarsening should be properly considered, while particle dissolution obviously increases solute drag.

6) While the majority of recrystallization and particle interaction studies are focused on SRX, further investigation related to DRX should be conducted. The influence of second-phase particles on critical dislocation density (or strain) for DDRX is not well-established. The relationship between recrystallized grain size and Z parameter (or stress level) at steady state for CDRX and GDRX is of both academic and industrial interest. The complex dynamic precipitation behaviour and its interaction with DRX is also worth further investigation, proper alloy systems should be chosen such as to avoid issues related to phase transformation (e.g. during cooling of HSLA steels).

7) Physically based numerical models at different scales should be further developed. It is of our opinion that an advanced recrystallization model should start at least from the subgrain level since this is where nucleation of recrystallization and precipitation of particles are of relevance. While some of them, particularly those running at the atomic scale, may not yet be applicable to industrial scale problems, invaluable information such as the effect of misfit energy of coherent particles on grain boundary migration can still be obtained. Recrystallization kinetics and grain size can generally be predicted with satisfactory accuracy, however, the successful quantitative prediction of recrystallization textures is still a challenge, particularly in conditions involving second-phase particles. It is also desirable to extend existing numerical models to handle the full

complexity of non-isothermal conditions, since this provides additional potential for thermo-mechanical process design.

8) The effect of second-phase particles on microstructure evolution has been extensively investigated, much less effort has been placed on their influence on material properties. Some work remains in order to better relate material properties (e.g. yield strength, see Eq.(46)), in an analytical or even empirical way, to particle parameters. The individual contributions of coarse and fine particles to material properties should also be identified and better quantified.

This review paper is a contribution the authors wanted to bring in order to promote further the field of design of microstructures and associated mechanical properties, in the context of metallic alloys processed at low and high temperatures, and in which second-phase particles interact with recrystallization phenomena.

Acknowledgements

K.H and R.E.L acknowledge financial support from PX Group, Switzerland. The authors acknowledge with great gratitude the help from Q.Q. Zhang and H.D. Zhang for preparing some of the figures. The constructive and detailed comments from the reviewers are also highly appreciated.

Appendix A. Abbreviations

ACOM -TEM	Automated crystal orientation mapping technique based on TEM
AM	Additive manufacturing
APT	Atom probe tomography
BF	(TEM)Bright field
BM	Base material
BSE	Backscattered electron
CDRX	Continuous dynamic recrystallization
CPFEM	Crystal Plasticity Finite Elemetn Method
CSL	Coincident site lattice
DAXM	Differential aperture X-ray microscopy
DDRX	Discontinuous Dynamic Recrystallization
DRV	Dynamic recovery
DRX	Dynamic recrystallization
DSC	Differential scanning calorimetry
DXZ	Dynamically recrystallized zone
EBSD	Electron backscattering diffraction
ECAE	Equal channel angular extrusion
ECAP	Equal-Channel Angular Pressing
ECCI	Electron channelling contrast imaging
EDS	Energy Dispersive Spectrdmeter
FC	Full constraint
FEM	Finite element models
FIB	Focused ion beam
FSW	Friction stir welding
GDRX	Geometric dynamic recrystallization
GM	General Motor
GND	Geometrically necessary dislocation
HAGB	High angle grain boundary
HAZ	Heat affected zone

HIP	Hot isostatic pressing
HPR	Hard-plate rolling
HPT	High-pressure torsion
HRTEM	High-resolution transmission electron microscopy
HSLA	High strength low alloy (steel)
IPF	Inverse pole figure
JMAK	Johnson- Mehl- Avrami- Kolmogorov kinetic model
LAGB	Low angle grain boundary
LM	Layer manufacturing
MAGB	Medium angle grain boundary
MDRX	Metadynamic recrystallization
ND	Normal direction
ODS	Oxide dispersion-strengthened
PDRX	Post-dynamic recrystallization
PFZ	Particle free zone
PSN	Particle stimulated nucleation
QPF	Quick plastic forming
RC	Relaxed constraint
RD	Rolling direction
RE	Rare earth
SANS/SAXS	Small-angle neutron/X-ray scattering
SAP	Sintered aluminium powder
SEM	Scanning electron microscope
SIBM	Strain induced boundary migration
SFE	Stacking fault energy
SIBM	Strain induced grain boundary motion
SLM	Selective laser melting
SPD	Severe plastic deformation
SPF	Superplastic forming
SPS	Spark plasma sintering
SRV	Static recovery

SRX	Static recrystallization
SSD	Statistically stored dislocation
T-EBSD	Transmission EBSD
TEM	Transmission electron microscope
TKD	Transmission Kikuchi diffraction
TMAZ	Thermo-mechanically affected zone
TMCP	Thermomechanical controlled processing
TMP	Thermomechanical processing
WHA	Tungsten heavy alloy
XRD	X-ray diffraction

Appendix B. Symbols

a	Lattice parameter of the matrix metal; Shorter axis of ellipsoid
A	Pre-exponential factor
A_c	Area of the nucleus
A_{r3}	Temperature at which austenite begins to transform to ferrite during cooling
b	Burgers vector of a dislocation; Longer axis of ellipsoid
c	Half of the void length
c_1, c_2	Constant
c_a	Equilibrium concentration of Sc in the Al matrix
c_i	Atomic fraction of element i
c_β	Equilibrium concentration of Sc in the Al_3Sc
d	Average diameter of second phase particles
$d_{crit}, r_{crit}, d_c, r_c$	Critical particle size ($d_{crit} = 2r_{crit}$)
D	Average grain size
D_{Lim}	Limiting grain size
e	Particle shape parameter
E	Young modulus
E_D^a	Additional stored energy
E_D^M	Stored energy of the matrix
f_V	Volume fraction of the particles
$f(r)$	Distribution of particle size
$F, F_{\max}$	Pinning force, maximum value of the force
F_B	Pinning force on the boundary
F_P	Retarding force
$G(t)$	Growth rate
h	Width of considered ledge
k	Nucleation efficiency

k_y	Strengthening factor
K	Dimensionless parameter depends on dislocation structure
K_c	Reaction rate constant
K_i	Hardening constants
$\overline{l}$	Average LAGB intercept length
L	Average distance over which the mobile dislocations can migrate before being stored
L_g	Geometric slip distance
m	Constant
M	Grain boundary mobility
$\overline{M}$	Taylor factor
M_0	Constant of boundary mobility
n	Grain growth exponent; Avrami exponent
N	Number of remaining nucleation site for recrystallization
$\dot{N}$	Rate of disappearance of the remaining nucleation sites
$N(r_c)$	Total number of potential nucleation sites per unit volume
N_c	Total number of dislocation nodes
N_{rex}	Number of nuclei per unit volume
N_S	Number of particles per unit area of boundary
N_{SB}	Number of particles per unit subboundaries
N_V	The number of particles per unit volume
P_C	Driving pressure due to boundary curvature
P_D	Driving pressure due to stored energy
P_D^{Rex}	Stored energy for recrystallization
P_D^{LAGB}	Stored energy in the cellular microstructure
P_N	Driving pressure
P_r	Retarding force
P_Z	Zener pressure
q	Pressure ratio

Q	Apparent activation energy
r, r_i	Radius of particles
r_0	Initial particle radius
R, R_{crit}	Radius of the bulging boundary; Radius of grain; Critical nucleus size
R_0	Initial grain radius
r_0, r_{45}, r_{90}	The ratio of the true strains in the width and thickness directions
R_0^{LAGB}	Initial values of subgrain size
R_{crit}^{LAGB}	Critical subgrain size of nucleation
S_v	Grain boundary area per unit volume
t_f	Time needed to complete recrystallization
T_m	Absolute melting temperature
T_{nr}	Non-recrystallization temperature
V	Boundary migration rate
V_m	Partial molar volume of Sc in Al_3Sc
x	Distance from the particle
$X_V(t)$	Volume fraction of transformed material
z	Exponent typically in the range ~ 0.5-1
Z	Atomic number of elements; Zener-Hollomon parameter
α_2	Ti_3Al precipitation
β''	Particles in Al-Mg-Si alloy
γ	Shear strain; Interfacial free energy
$\gamma_{AB}, \gamma_{AC}, \gamma_{BC}$	Grain boundary energy
γ_m	Boundary energy for transition anlge from LAGB to HAGB
δ	Particle distribution parameter
Δr	Extent of earing in deep drawing from planar anisotropy
ε_c	Critical strain for void formation
ε_t	True strains in the thickness direction
ε_w	True strains in the width direction

$\dot{\varepsilon}$	Strain rate
θ	Misorientation angle
$\theta'_{\max}$	Maximum misorientation of smaller particles
θ_0	Initial values of subgrain misorientation
θ_m	Misorientation for transition anlge from LAGB to HAGB
$\theta_{\max}$	Maximum misorientation
λ	Interspacing of particles
μ	Shear modulus
ν	Poisson coefficient
ρ	Dislocation density
ρ_G	Density of the GNDs
ρ_{tot}	Total dislocation density
σ_0	Peierls-Nabarro stress
σ_c	Critical stress
σ_{GB}	Stress from grain boundaries contribution
σ_P	Stress from particles strengthening
σ_{ss}	Stress from solid solution strengthening
σ_y	Yield stress
σ_ρ	Dislocation forest hardening
τ	Shear stress
τ_0	Shear flow shear stress of the material in the absence of dislocation interactions; Orowan stress
τ_p	Particle-induced shear stress
ξ	Variable representing the location in a grain
Ω	Orientation gradient
Σn	Coincidence site lattice (CSL) grain boundaries. 1/n is the fraction of sites common to both grains

References

[1] Doherty RD, Hughes DA, Humpheys FJ, Jonas JJ, Juul Jensen D, Kassner ME, King WE, McNelley TR, McQueen HJ, Rollett AD. Current issues in recrystallization. Mater Sci Eng A 1997;238: 219–274

[2] Humphreys FJ, Hatherly M. Recrystallization and related annealing phenomena, Elsevier, 2nd Edition, 2004.

[3] Robertson IM, Schuh CA, Vetrano JS, Browning ND, Field DP etc. Towards an integrated materials characterization tool box. J Mater Res 2011;26:1341-1383

[4] Raabe D. Recovery and recrystallization: phenomena, physics, models, simulation. In: D.E. Laughlin, K. Hono (Eds.), Physical Metallurgy, fifth ed. Elsevier, Amsterdam 2014, 2291–2397

[5] Rollett A. Overview of modeling and simulation of recrystallization. Prog Mater Sci 1997;42: 79–99.

[6] Hallberg H. Approaches to modeling of recrystallization. Metals 2011;1 :16-48

[7] Rios PR, Siciliano F, Sandim HRZ, Plaut RL, Padilha AF. Nucleation and growth during recrystallization. Mater Res 2005;8:225-238

[8] Hansen N, Juul Jensen D. Deformed metals – structure, recrystallisation and strength. Mater Sci Technol 2011;27:1229-1240

[9] Sakai T, Belyakov A, Kaibyshev R, Miura H, Jonas JJ. Dynamic and post-dynamic recrystallization under hot, cold and severe plastic deformation conditions. Prog Mater Sci 2014;60:130–207

[10] Huang K, Logé RE. A review of dynamic recrystallization phenomena in metallic materials. Mater Des 2016 ;111:548-574

[11] Smith CS. Introduction to grains, phases, and interfaces: An interpretation of microstructure. T Am Min Met Eng.1948;175: 15–51

[12] Baker I. Recovery, recrystallization and grain growth in ordered alloys. Intermetallics 2000;8:1183-1196

[13] Herwegh M, Linckens J, Ebert A, Berger A, Brodhag SH. The role of second phases for controlling microstructural evolution in polymineralic rocks: A review. J Struct Geol 2011;33:1728-1750

[14] Urai JL, Means WD, Lister GS. Dynamic recrystallization of minerals. in: B.E. Hobbs, H.C. Heard (Eds.), Mineral and Rock Deformation: Laboratory Studies, Geophysical Monograph 36, The Paterson Volume , American Geophysical Union, Washington, DC 1986 :161–199

[15] Backerud L, Krol E, Tamminen J. Solidification characteristics of aluminium alloys, vol.1:Wrought alloys. Oslo Skanaluminium 1986;93-97

[16] Nie J-F. Physical metallurgy of light alloys. In: D.E. Laughlin, K. Hono (Eds.), Physical Metallurgy, 5th ed. Elsevier, Amsterdam 2014, pp. 2209–2156.

[17] Bhadeshia HKDH, Honeycombe R. Steels microstructure and properties. 3rd Ed, Elsevier, 2006

[18] Preston O, Grant NJ. Dispersion strengthening of copper by internal oxidation Trans. Met. Soc. AIME 1961:22;164-173

[19] Stott FH, Wood GC. Internal oxidation. Mater Sci Technol 1988;4:1072-1078

[20] Suryanarayana C. Mechanical alloying and milling. Prog Mater Sci 2001;46 :1-184

[21] Alborn H, Hornbogen E, Köster U. Recrystallisation mechanism and annealing texture in aluminium-copper alloys, J. Mater. Sci 1969;4:944-950

[22] Hin C, Bréchet Y, Maugis P, Soisson F. Kinetics of heterogeneous grain boundary precipitation of NbC in α-iron: A Monte Carlo study. Acta Mater 2008;56:5653-5667

[23] Hin C, Bréchet Y, Maugis P, Soisson F. Kinetics of heterogeneous dislocation precipitation of NbC in alpha-iron. Acta Mater 2008;56:5535-5543

[24] Rainforth WM, Black MP, Higginson RL, Palmiere EJ, Sellars CM, Prabst I, Warbichler P, Hofer F. Precipitation of NbC in a model austenitic steel. Acta Mater 2002 ;50:735-747

[25] Nes E, Ryum N, Hunderi O. On the Zener drag. Acta Metall 1985; 33:11-22

[26] Kelly A, Nicholson RB. Precipitation hardening. Prog Mater Sci 1963;10:151-391

[27] Ashby MF, Harper J, Lewis J. The interaction of crystal boundaries with second-phase particles. Trans Metall Soc AIME 1969;245:413.

[28] Ashby MF, Centamore RMA. The dragging of small oxide particles by migrating grain boundaries in copper. Acta Metall 1968;16:1081-1092.

[29] Onaka S, Hashimoto S, Miura S, Kato M. Effect of diffusional relaxation on the shape change of liquid B_2O_3 particles in a deformed Cu matrix. Acta Metall Mater. 1995 ;43 :1577-1585

[30] Miura H, Sakai T, Tamura H, Gottstein G. Effect of dispersed liquid B_2O_3 particles on high-temperature mechanical behavior of copper. Acta Mater 1999;47:757-768

[31] Palmer IG, Ashby MF. The dragging of solid particles through metals by grain boundaries. Acta Metall. 1967 ; 15:420-423

[32] Spitzig WA, Kelly JF, Richmond O. Quantitative characterization of second-phase particles. Metallogr 1985;18:523-261

[33] Atkinson HV, Shi G. Characterization of inclusions in clean steels: a review including the statistics of extremes. Prog Mater Sci 2003;48:457-520

[34] Gupta AK, Marois PH, Lloyd DJ. Review of the techniques for the extraction of second-phase particles from aluminum alloys. Mater Charact 1996;37:61-80.

[35] Li YJ, Arnberg L. Quantitative study on the precipitation behavior of dispersoids in DC-cast AA3003 alloy during heating and homogenization. Acta Mater 2003 ; 51 :3415-3428.

[36] Konrad J, Zaefferer S, Raabe D. Investigation of orientation gradients around a hard Laves particle in a warm-rolled Fe_3Al-based alloy using 3D EBSD-FIB technique. Acta Mater 2006;54:1369-1380

[37] Xu W, Ferry M, Cairney JM, Humphreys FJ. Three-dimensional investigation of particle-stimulated nucleation in a nickel alloy. Acta Mater 2007 ;55 :5157-5167

[38] Li M, Ghosh S, Richmond O, Weiland H, Rouns TN. Three dimensional characterization and modeling of particle reinforced metal matrix composites:part I: Quantitative description of microstructural morphology. Mater Sci Eng A 1999;265:153-173

[39] Zhang Y, Juul Jensen D, Zhang Y, Lin F, Zhang Z, Liu Q. Three-dimensional investigation of recrystallization nucleation in a particle-containing Al alloy. Scr Mater 2012 ;67 :320-323

[40] Dwyer L, Robson J, Quinta da Fonseca J, Kamp N, Hashimoto T, Thompson G. Constituent particles and dispersoids in an Al-Mn-Fe-Si alloy studied in three-dimensions by serial sectioning. Mater Sci Forum 2013;765 :451-455

[41] Nielsen SF, Lauridsen EM, Juul Jensen D, Poulsen HF. A three-dimensional X-ray diffraction microscope for deformation studies of polycrystals. Mater Sci Eng A 2001;319-321:179-181

[42] Larson BC, Yang W, Ice GE, Swadener JG, Budai JD, Tischler JZ. Three-dimensional X-ray structural microscopy with submicrometre resolution. Nature 2002;415:887-890

[43] Miller MK. Atom Probe Tomography : Analysis at the atomic level. Kluwer Academic/Plenum. New York. 2000.

[44] Miller ML, Russell KF, Hoelzer DT. Characterization of precipitates in MA/ODS ferritic alloys. J. Nucl Mater. 2006 ;351 :261-268

[45] Midgley PA, Weyland M. 3D electron microscopy in the physical sciences: the development of Z-contrast and EFTEM tomography. Ultramicoscopy 2003;96:413-431

[46] Starink MJ. Analysis of aluminium based alloys by calorimetry: quantitative analysis of reactions and reaction kinetics. Int Mater Rev 2004;49:191-226

[47] Noble B, Thompson GE. Precipitation characteristics of aluminium-lithium alloys. Metal Sci J1971 ;5 :114-120

[48] Eivani AR, Ahmed H, Zhou J, Duszczyk J. Correlation between Electrical Resistivity, Particle Dissolution, Precipitation of Dispersoids, and Recrystallization Behavior of AA7020 Aluminum Alloy. Metall Mater Trans A 2009;40:2435-2446

[49] Jiang F, Zurob H, Purdy G, Zhang H. Characterizing precipitate evolution of an Al–Zn–Mg–Cu-based commercial alloy during artificial aging and non-isothermal heat treatments by in situ electrical resistivity monitoring. Mater Charact 2016;117:47-56

[50] Rossiter PL. The Electrical Resistivity of Metals and Alloys. Cambridge University Press, Cambridge, United Kingdom, 1987.

[51] Boulnat X, Sallez N, Dadé M, Borbély A, Béchade J-L, de Carlan Y, Malaplate J, Bréchet Y, de Geuser F, Deschamps A, Donnadieu P, Fabrègue D, Perez M. Influence of oxide volume fraction on abnormal growth of nanostructured ferritic steels during non-isothermal treatments: An in situ study. Acta Mater 2015;97:124-130

[52] Odette GR, Lucas GE. Recent progress in understanding reactor pressure vessel steel embrittlement. Radiat. Eff. Defects Solids, 1998;144:189-231

[53] Fratzl P. Small-angle scattering in materials science - a short review of applications in alloys, ceramics and composite materials. J Appl Cryst 2003;36:397-404

[54] Bardel D, Perez M, Nelias D, Deschamps A, Hutchinson CR, Maisonnette D, Chaise T, Garnier J, Bourlier F.

Coupled precipitation and yield strength modelling for non-isothermal treatments of a 6061aluminium alloy. Acta Mater 2014;62 :129-140

[55] Nicolas M, Deschamps A. Characterisation and modelling of precipitate evolution in an Al–Zn–Mg alloy during non-isothermal heat treatment. Acta Mater 2003;51 :6077-6094

[56] Eckold G, Schober H, Nagler S.E. (Eds.), Studying kinetics with neutrons, 2010, Springer-Verlag, Berlin

[57] Zhang S, Kohlbrecher J, Tichelaar FD, Langelaan G, Brück E, van der Zwaag S, van Dijk NH. Defect-induced Au precipitation in Fe–Au and Fe–Au–B–N alloys studied by in situ small-angle. Acta Mater 2013;61:7009-7019

[58] Glatter O, Kratky O. Small Angle X-ray Scattering. Academic Press, London, 1982

[59] Deschamps A, Livet F, Bréchet Y. Influence of predeformation on ageing in an Al–Zn–Mg alloy—I. Microstructure evolution and mechanical properties. Acta Mater 1998;47:281-292

[60] Jones MJ, Humphreys FJ. Interaction of recrystallization and precipitation: The effect of Al_3Sc on the recrystallization of deformed aluminium. Acta Mater 2003;51 :2149-2159

[61] Miura H, Tsukawaki H, Sakai T, Jonas JJ. Effect of particle/matrix interfacial character on the high-temperature deformation and recrystallization behavior of Cu with dispersed Fe particles. Acta Mater 2008;56:4944-4952

[62] Tsivoulas D, Prangnell PB. The effect of Mn and Zr dispersoid-forming additions on recrystallization resistance in Al–Cu–Li AA2198 sheet. Acta Mater 2014;77:1-16

[63] Li YJ, Muggerud AMF, Olsen A, Furu T. Precipitation of partially coherent α-Al(Mn,Fe)Si dispersoids and their strengthening effect in AA 3003 alloy. Acta Mater 2012 ;60 :1004-1014

[64] Li YJ, Zhang WZ, Marthinsen K. Precipitation crystallography of plate-shaped Al6(Mn,Fe) dispersoids in AA5182 alloy. Acta Mater 2012 ;60 :5963-5974

[65] Zhang W-Z, Weatherly GC. On the crystallography of precipitation. Prog Mater Sci 2000 ;50:181-292

[66] Zhang MX, Kelly PM. Crystallographic features of phase transformations in solids. Prog Mater Sci 2009;54:1101-1170

[67] Wang N, Ji Y, Wang Y, Wen Y, Chen LQ. Two modes of grain boundary pinning by coherent precipitates. Acta Mater 2017;135:226-232

[68] Wenner S, Holmestad R. Accurately measured precipitate–matrix misfit in an Al–Mg–Si alloy by electron microscopy. Scr Mater 2016;118 :5-8

[69] Williams CA, Unifantowicz P, Baluc N, Smith GDW, Marquis EA. The formation and evolution of oxide particles in oxide-dispersion-strengthened ferritic steels. Acta Mater 2013;61:2219-2235

[70] Edwards GA, Stiller K, Dunlop GL, Couper MJ. The precipitation sequence in Al–Mg–Si alloys. Acta Mater 1998; 46:3893-3904

[71] Miller MK, Wirth BD, Odette GR. Precipitation in neutron-irradiated Fe–Cu and Fe–Cu–Mn model alloys: a comparison of APT and SANS. Mater Sci Eng A 2003;353:133-139.

[72] Briggs SA, Edmondson PD, Littrell KC, Yamamoto Y, Howard RH, Daily CR, Terrani KA, Sridharan K, Field KG. A combined APT and SANS investigation of α' phase precipitation in neutron-irradiated model FeCrAl alloys. Acta Mater 2017;129:217-228.

[73] Andrade HL, Akben MG, Jonas JJ. Effect of molybdenum, niobium, and vanadium on static recovery and recrystallization and on solute strengthening in microalloyed steels. Metall Trans A 1983 ;14 :1967-1977

[74] Palmiere EJ, Garcia CI, DeArdo AJ. The influence of niobium supersaturation in austenite on the static recrystallization behavior of low carbon microalloyed steels. Metall Mater Trans A 1996;27:951-960

[75] Drury MD, Humphreys FJ. The development of microstructure in Al-5% Mg during high temperature deformation. Acta Metall 1986 :34 :2259

[76] Gardner KJ, Grimes R. Recrystallization during hot deformation of aluminium alloys. Metal Sci 1979 ;13 :216-222

[77] Le Gall R, Jonas JJ. Solute drag effects during the dynamic recrystallization of nickel. Acta Mater 1999;47:4365-4374

[78] Luton MJ, Sellars CM. Dynamic recrystallization in nickel and nickel-iron alloys during high temperature deformation. Acta Metall 1969;17:1033-1043

[79] Porter A, Ralph B. The recrystallization of nickel-base superalloys. J Mater Sci 1981;16 :707-713

[80] Dahlén M, Winberg L. The influence of γ'-precipitation on the recrystallization of a nickel base superalloy. Acta Metall 1980;28 :41-50

[81] Cram DG, Fang XY, Zurob HS, Bréchet YJM, Hutchinson CR. The effect of solute on discontinuous dynamic recrystallization. Acta Mater 2012; 60:6390-6404

[82] Cottrell AH, Bilby BA. Dislocation theory of yielding and strain ageing of iron. Proc. Phys. Soc. Sect. A 1949;62:49-62

[83] Leyson GPM, Curtin WA, Hector LG, Woodward CF. Quantitative prediction of solute strengthening in aluminium alloys. Nature Mater 2010 ;9 :750-755

[84] Lücke K, Detert K. A quantitative theory of grain-boundary motion and recrystallization in metals in the presence of impurities. Acta Metall 1957;5:628-637

[85] Cahn JW. The impurity-drag effect in grain boundary motion. Acta Metall 1962;10:789-798

[86] Lücke K, Stüwe HP. On the theory of impurity controlled grain boundary motion. Acta Metall 1971;19:1087-1099

[87] Hillert M, Sundman B. A treatment of the solute drag on moving grain boundaries and phase interfaces in binary alloys. Acta Metall 1976;24:731-743

[88] Mendelev MI, Srolovitz DJ. A regular solution model for impurity drag on a migrating grain boundary. Acta Mater 2001;49:589-597

[89] Bréchet YJM, Purdy GR. Solute drag in ternary solid solutions. Acta Mater 2003;51:5587-5592

[90] Hersent E, Marthinsen K, Nes E. The effect of solute atoms on grain boundary migration: A solute pinning approach. Metall Mater Trans A 2013;44:3364-3375

[91] Gallagher PCJ. The influence of alloying, temperature, and related effects on the stacking fault energy. Metall Trans 1970;1:2429-2461

[92] Engler O, Deformation and texture of copper-manganese alloys. Acta Mater 2000;48:4827-4840

[93] Stanford N, Atwell D, Barnett MR. The effect of Gd on the recrystallisation, texture and deformation behaviour of magnesium-based alloys. Acta Mater 2010;58:6773-6783

[94] Lücke K, Stüwe HP. Effect of Al and Gd solutes on the strain rate sensitivity of magnesium alloys. Acta Metall 1971;19:1087-1099

[95] Stanford N, Marceau RKW, Barnett MR. The effect of high yttrium solute concentration on the twinning behaviour of magnesium alloys. Acta Mater 2015;82:447-456

[96] Griffiths D. Explaining texture weakening and improved formability in magnesium rare earth alloys. Mater Sci Technol 2015;31:10-24

[97] Basu I, Pradeep KG, Mießena Ck, Barrales-Mora LA, Al-Samman T. The role of atomic scale segregation in designing highly ductile magnesium alloys. Acta Mater 2016;116:77-94

[98] Zhang Y, Zuo TT, Tang Z, Gao MC, Dahmen KA, Liaw PK, Lu ZP. Microstructures and properties of high-entropy alloys. Prog Mater Sci 2014;61:1-93

[99] Tsai MH, Yeh JW. High-Entropy alloys: A critical review. Mater Res Lett 2014;2:107-123

[100] Kwon O, DeArdo AJ. Interactions between recrystallization and precipitation in hot-deformed microalloyed steels. Acta Metall Mater 1991;39:529-538

[101] Bhatia ML, Cahn RW. Recrystallization of Porous Copper. Proc R Soc Lond A 1978;362:341-360

[102] Osetsky YN, Bacon DJ. Atomic-scale mechanisms of void hardening in bcc and fcc metals. Philos Mag 2010; 90:945-961

[103] Osetsky YN, Bacon DJ. Comparison of void strengthening in fcc and bcc metals: Large-scale atomic-level modelling. Mater Sci Eng A 2005;400-401: 374-377

[104] Beck PA, Sperry P R. Strain induced grain boundary migration in high purity aluminium. J Appl Phys 1950;2:150-152

[105] Dillamore I L, Smith CJE, Watson TW. Oriented Nucleation in the Formation of Annealing Textures in Iron. Met Sci J 1967;1:49-54

[106] Faivre P, Doherty RD. Nucleation of recrystallization in compressed aluminium: studies by electron microscopy and Kikuchi diffraction. J Mater Sci 1979;14:897-919

[107] Jones AR, Ralph B, Hansen N. Subgrain coalescence and the nucleation of recrystallization at grain-boundaries in aluminum. Proc R Soc A 1979;368:345-357

[108] Doherty RD, Szpunar J. Kinetics of sub-grain coalescence – a reconsideration of the theory. Acta Metall 1984;32:1789-1798

[109] Bailey JE, Hirsch PB. The Recrystallization Process in Some Polycrystalline Metals. Proc R Soc Lond A 1962;267:11-30

[110] Jazaeri H, Humphreys FJ. The transition from discontinuous to continuous recrystallization in some aluminium alloys: II – annealing behavior. Acta Mater 2004;52:3251-3262

[111] Gourdet S, Montheillet F. A model of continuous dynamic recrystallization Acta Mater 2003 ;51 :2685-2699

[112] McQueen HJ, Solberg JK, Ryum N, Nes E. Evolution of flow stress in aluminium during ultra-high straining at elevated temperatures. Part II. Philos Mag A 1989;60:473-485

[113] Kassner ME, Barrabes SR. New developments in geometric dynamic recrystallization. Mater Sci Eng A 2005;410-411 : 152-155

[114] Zaefferer S, Elhami N-N.Theory and application of electron channelling contrast imaging under controlled diffraction conditions. Acta Mater 2014;75:20-50

[115] Sun S, Adams BL, King WE. Observations of lattice curvature near the interface of a deformed aluminium bicrystal. Philos Mag A 2000 ;80:9-25

[116] Pantleon W, Resolving the geometrically necessary dislocation content by conventional electron backscattering diffraction. Scr Mater 2008;58:994-997

[117] Jiang J, Britton TB, Wilkinson AJ. Measurement of geometrically necessary dislocation density with high resolution electron: Effects of detector binning and step size. Ultramicroscopy 2013;125:1-9

[118] Moussa C, Bernacki M, Besnard R, Bozzolo N. Statistical analysis of dislocations and dislocation boundaries from EBSD data. Ultramicroscopy 2017;179:63-72

[119] Keller RR, Geiss RH. Transmission EBSD from 10 nm domains in a scanning electron microscope. J Microscopy 2012;245:245-251

[120] Trimby PW. Orientation mapping of nanostructured materials using transmission Kikuchi diffraction in the scanning electron microscope. Ultramicroscopy 2012;120:16-24.

[121] Trimby PW, Cao Y, Chen Z, Han S, Hemker KJ, Lian J, Liao X, Rottmann P, Samudrala S, Sun J, Wang JT, Wheeler J, Cairney JM. Characterizing deformed ultrafine-grained and nanocrystalline materials using transmission Kikuchi diffraction in a scanning electron microscope. Acta Mater 2014:62;69–80

[122] Hull D, Bacon DJ. Introduction to dislocations, 5th Edition, Elsevier, 2011

[123] Liu Q, Juul Jensen D, Hansen N. Effect of grain orientation on deformation structure in cold-rolled polycrystalline aluminium. Acta Mater 1998;46:5819-5838

[124] Zaefferer S. New developments of computer-aided crystallographic analysis in transmission electron microscopy. J Appl Cryst 2000;33:10-25

[125] Schwarzer RA, Sukkau J. Automated Crystal Orientation Mapping (ACOM) with a computer controlled TEM by interpreting transmission Kikuchi patterns. Mater Sci Forum 1998;273-275:215-222

[126] Rauch EF, Automated crystal orientation and phase mapping in TEM. Mater Charact 2014;98:1-9

[127] http://www.nanomegas.com/

[128] Cizek P, Sankaran A, Rauch EF, Barnett MR. Microstructure and Texture of Electrodeposited Nanocrystalline Nickel in the As-Deposited State and After In-Situ and Ex-Situ Annealing. Metall Mater Trans A 2016;47:6655-6670

[129] Ghamarian I, Samimi P, Rohrer GS, Collins PC. Determination of the five parameter grain boundary character distribution of nanocrystalline alpha-zirconium thin films using transmission electron microscopy. Acta Mater 2017;130:164-176

[130] Ghamarian I, Liu Y, Samimi P, Collins PC. Development and application of a novel precession electron diffraction technique to quantify and map deformation structures in highly deformed materials—as applied to ultrafine-grained titanium. Acta Mater 2014;79:203-215

[131] Zha M, Li Y, Mathiesen RH, Bjørge R, Roven HJ. Microstructure evolution and mechanical behavior of a binary Al–7Mg alloy processed by equal-channel angular pressing. Acta Mater 2015 ;84 :42-54

[132] Wolfenden A, The energy stored in polycrystalline copper deformed at room temperature. Acta Metall 1971;19:1373-1377

[133] Steffen H, Gottstein G, Wollenberger. Stored energy measurements in copper single crystals tensile deformed at 20°C. Acta Metall 1973;21:683-689

[134] Zhou F, Liao XZ, Zhu YT, Dallek S, Lavernia EJ. Microstructural evolution during recovery and recrystallization of a nanocrystalline Al-Mg alloy prepared by cryogenic ball milling. Acta Mater 2003;51:2777-2791

[135] Scruby CB, Bull CE, Young RMK, Humphreys FJ, In-situ monitoring of recrystallization of cold rolled copper by non-contact ultrasonics. Mater Sci Technol 2003;19:163-172

[136] Sarkar A, Moreau A, Militzer M, Poole WJ, Evolution of austenite recrystallisation and grain growth using laser ultrasonics, Metall Mater Trans A 2008;39:897–907

[137] Bate P, Lundin P, Lindh-Ulmgren E, Hutchinson B. Application of laser-ultrasonics to texture measurements in metal processing. Acta Mater 2017;123:329-336

[138] Freudenberger J, Kauffmann A, Klauß H, Marr T, Nenkov K, Subramanya Sarma V, Schultz L. Studies on recrystallization of single-phase alloys by resistance measurements. Acta Mater 2010;58:2324-2329

[139] Coates DG. Kikuchi-like reflection patterns obtained with the scanning electron microscope, Phil. Mag 1967;16:1179-1184

[140] Booker GR, Shaw AMB, Whelan MJ, Hirsch PB. Some comments on the interpretation of the 'kikuchi-like reflection patterns' observed by scanning electron microscopy. Phil Mag 1967;16:1185-1191

[141] Rollett AD, Lee S-B, Campman R, Rohrer GS. Three-Dimensional Characterization of Microstructure by Electron Back-Scatter Diffraction. Annu Rev Mater Sci 2007;37:627-658

[142] Patala S, Mason JK, Schuh CA. Improved representations of misorientation information for grain boundary science and engineering. Prog Mater Sci 2012;57:1383-1425

[143] Kelly MN, Glowinski K, Nuhfer NT, Rohrer GS. The five parameter grain boundary character distribution of α-Ti determined from three-dimensional orientation data. Acta Mater 2016;111:22-30

[144] Fan GH, Zhang YB, Driver JH, Juul Jensen D, Oriented growth during recrystallization revisited in three dimensions. Scr Mater 2014;72-73;9-12

[145] Pirgazi H, Glowinski K, Morawiec A, Kestens LAI. Three-dimensional characterization of grain boundaries in pure nickel by serial sectioning via mechanical polishing. J Appl Cryst 2015; 48:1672-1678

[146] Rowenhorst DJ, Gupta A, Feng CR, Spanos G. 3D Crystallographic and morphological analysis of coarse martensite: Combining EBSD and serial sectioning. Scr Mater 2006;55:11-16

[147] Saylor DM, Morawiec A, Rohrer GS. Distribution of grain boundaries in magnesia as a function of five macroscopic parameters. Acta Mater 2003:51:3663-3674

[148] http://dream3d.bluequartz.net/

[149] Kremer JR, Mastronarde DN, Mclntosh JR. Computer visualization of three-dimensional image data using IMOD. J Struct Biol 1996;116:71-76

[150] Zaefferer S, Wright SI, Raabe D. Three-dimensional orientation microscopy in a focused ion beam-scanning electron microscope : A new dimension of microstructure characterization. Metall Mater Trans A 2008 ;39: 374-389

[151] Zhong X, Rowenhorst DJ, Beladi H, Rohrer GS. The five-parameter grain boundary curvature distribution in an austenitic and ferritic steel. Acta Mater 2017;123 :136-145

[152] Konijnenberg PJ, Zaefferer S, Raabe D. Assessment of geometrically necessary dislocation levels derived by 3D EBSD. Acta Mater 2015;99:402-414

[153] Liu HH, Schmidt S, Poulsen HF, Godfrey A, Liu ZQ, Sharon JA, Huang X. Three-Dimensional Orientation Mapping in the Transmission Electron Microscope. Science 2011;332:833-834

[154] Poulsen HF, Nielsen SF, Lauridsen EM, Schmidt S, Suter RM, Lienert U, Margulies L, Lorentzen TD, Juul Jensen D. Threedimensional maps of grain boundaries and the stress state of individual grains in polycrystals and powders. J Appl Crystallogr 2001;34:751–756

[155] Margulies L, Winther G, Poulsen HF. In situ measurement of grain rotation during deformation of polycrystals. Science 2001;291:2392–2394.

[156] Larsena AW, Poulsen HF, Margulies L, Gundlach C, Xing Q, Huang X, Juul Jensen D. Nucleation of recrystallization observed in situ in the bulk of a deformed metal. Scr Mater 2005;53:553-557

[157] West SS, Schmidt S, Sørensen HO, Winther G, Poulsen HF, Margulies L, Gundlach C, Juul Jensen D. Direct non-destructive observation of bulk nucleation in 30% deformed aluminum. Scr Mater. 2009;61:875–878

[158] Schmidt S, Nielsen SF, Gundlach C, Margulies L, Huang X, Juul Jensen D. Watching the growth of bulk grains during recrystallization of deformed metals. Science 2004;305:229-232

[159] Poulsen HF. Three-Dimensional X-Ray Diffraction Microscopy: Mapping Polycrystals and their Dynamics. Springer, New York, 2004

[160] Xu C, Zhang Y, Godfrey A, Wu G, Liu W, Tischler JZ, Liu Q, Juul Jensen D. Direct observation of nucleation in the bulk of an opaque sample. Sci Rep 2017;7:42508

[161] Larson BC, Yang W, Ice GE, Budai JD, Tischler JZ. Three-dimensional X-ray structural microscopy with submicrometer resolution. Nature 2002;415:887–890

[162] Manohar PA, Ferry M, Chandra T. Five decades of the Zener equation. ISIJ Int 1998;38: 913–924

[163] Huang K, Logé RE. Zener Pinning. In: Hashmi S ed. Reference Module in Materials Science and Materials Engineering, Elsevier, 2016

[164] Weiss M, Taylor AS, Hodgson PD, Stanford N. Strength and biaxial formability of cryo-rolled 2024 aluminium subject to concurrent recovery and precipitation. Acta Mater 2013;61:5278-5289

[165] Jain J, Cizek P, Poole WJ, Barnett MR. Precipitate characteristics and their effect on the prismatic-slip-dominated deformation behaviour of an Mg–6 Zn alloy. Acta Mater 2013;61:4091-4102

[166] Gleiter H, Hornbogen E. Precipitation hardening by coherent particles. Mater Sci Eng 1967/68;2:285-302

[167] Hornbogen E, Gahr KHZ. Distribution of plastic strain in alloys containing small particles. Metallogr 1975;8:181-202

[168] Engler O, Hirsch J, Lücke K. Texture development in Al 1.8wt% Cu depending on the precipitation state—I. Rolling textures. Acta Metall. 1989;37:2743–2753.

[169] Lücke K, Engler O. Effects of particles on development of microstructure and texture during rolling and recrystallisation in fcc alloys. Mater Sci Technol 1990;6:1113–1130.

[170] Engler O, Lücke K. Influence of the precipitation state on the cold rolling texture in 8090 Al-Li material. Mater Sci Eng. A 1991;148 :15–23.

[171] Gerold V, Karnthaler HP, On the origin of planar slip in f.c.c. alloys. Acta Metall. 1989;37:2177–2183.

[172] Lunt D, Busolo T, Xu X, Quinta da Fonseca J, Preuss M. Effect of nanoscale α2 precipitation on strain localisation in a two-phase Ti-alloy. Acta Mater 2017;129:72-82

[173] Barlow CY, Hansen N, Liu YL. Fine scale structures from deformation of aluminum containing small alumina particles. Acta Mater. 2002;50:171–182.

[174] Apps PJ, Berta M, Prangnell PB. The effect of dispersoids on the grain refinement mechanisms during deformation of aluminium alloys. Acta Mater 2005;53:499-511

[175] Ashby MF. The deformation of plastically non-homogeneous materials. Philos Mag 1970;21:399–424

[176] Karamched PS, Wilkinson AJ. High resolution electron back-scatter diffraction analysis of thermally and mechanically induced strains near carbide inclusions in a superalloy. Acta Mater 2011;59:263-272

[177] Humphreys FJ, Hirsch PB., The Deformation of Single Crystals of Copper and Copper-Zinc Alloys Containing Alumina Particles. II. Microstructure and Dislocation-Particle Interactions. Proc R Soc Lond A. 1970;318: 73–92.

[178] Baker I, Martin JW. Effect of fine second phase particles on stored energy and recrystallization kinetics of cold rolled copper single crystals. Metal Sci 1983;17:469-474

[179] Roumina R, Sinclair CW. Recovery kinetics in the presence of precipitates: The softening response of an Al–Mg–Sc alloy. Acta Mater 2010;58:111-121

[180] Mandal D, Baker I. On the effect of fine second-phase particles on primary recrystallization as a function of strain. Acta Mater 1997:45:453-461

[181] Lewis MH, Martin JW. Yielding and work-hardening in internally oxidised copper alloys. Acta Metall. 1963;11: 1207–1214.

[182] Brimhall JL, Klein MJ, Huggins RA. Influence of a finely dispersed second phase on recrystallization. Acta Metall 1966;14 :459–466.

[183] Humphreys FJ. Local lattice rotations at second phase particles in deformed metals. Acta Metall 1979;27:1801-1814

[184] Barlow CY, Hansen N. Deformation structures in aluminum containing small particles. Acta Metall. 1989;37:1313–1320.

[185] Ridha AA, Hutchinson WB. Recrystallisation mechanisms and the origin of cube texture in copper. Acta Metall 1982;30:1929-1939

[186] Duckham A, Engler O, Knutsen RD. Moderation of the recrystallization texture by nucleation at copper-type shear bands in Al-1Mg. Acta Mater 2002;50:2881-2893

[187] Engler O, Yang P, Kong XW. On the formation of recrystallization textures in binary Al-1.3% Mn investigated by means of local texture analysis. Acta Mater 1996;44:3349-3369

[188] Hirsch J, Al-Samman T. Superior light metals by texture engineering: Optimized aluminum and magnesium alloys for automotive applications. Acta Mater 2013;61:818-843

[189] Engler O, Kong XW, Lücke K. Development of microstructure and texture during rolling of single-phase and two-phase cube-oriented Al-Cu single crystals. Scr Mater 1999;41:493-503

[190] Kim HW, Kang SB, Tsuji N, Amino YM. Deformation textures of AA8011 aluminum alloy sheets severely deformed by accumulative roll bonding. Metall Mater Trans A 2005;36:3151-3163

[191] Schäfer C, Song J, Gottstein G. Modeling of texture evolution in the deformation zone of second-phase particles. Acta Mater 2009;57:1026-1034

[192] Higginson R, Bate P. Substructure drag effects and recrystallization textures in aluminium. Acta Mater 1999;47:1079-1090

[193] Bate PS, Huang Y, Humphreys FJ. Development of the “brass” texture component during the hot deformation of Al–6Cu–0.4Zr. Acta Mater 2004;52:4281-4289

[194] Barlow CY, Hansen N, Liu YL. Fine scale structures from deformation of aluminium containing small alumina particles. Acta Mater 2002;50:171-182

[195] Ball EA, Prangnell PB. Tensile-compressive yield asymmetries in high strength wrought magnesium alloys. Scr Metall Mater 1994;31:111-116

[196] Bohlen J, Dobron P, Swiostek J, Letzig D, Chmelik F, Lukac P, Kainer KU. On the influence of the grain size and solute content on the AE response of magnesium alloys tested in tension and compression. Mater Sci Eng A 2007;462:302-306

[197] Stanford N, Geng J, Chun YB, Davies CHJ, Nie JF, Barnett MR. Effect of plate-shaped particle distributions on the deformation behaviour of magnesium alloy AZ91in tension and compression. Acta Mater 2012;60:218-228

[198] Jain J, Poole WJ, Sinclair CW, Gharghouri MA. Reducing the tension–compression yield asymmetry in a Mg–8Al–0.5Zn alloy via precipitation. Scr Mater 2010;62:301-304

[199] Li X, Jiao F, Al-Samman T, Ghosh Chowdhury S. Influence of second-phase precipitates on the texture evolution of Mg–Al–Zn alloys during hot deformation. Scr Mater 2012;66:159-162

[200] Miller VM, Pollock TM. Texture Modification in a Magnesium-Aluminum-Calcium Alloy During Uniaxial Compression. Metall Mater Trans A 2016;47:1854-1864

[201] Nikulin I, Kipelova A, Malopheyev S, Kaibyshev R. Effect of second phase particles on grain refinement during equal-channel angular pressing of an Al–Mg–Mn alloy. Acta Mater 2012;60:487-497

[202] Schmidt CW, Knieke C, Maier V, Höppel HW, Peukert W, Göken M. Accelerated grain refinement during accumulative roll bonding by nanoparticle reinforcement. Scr Mater 2011;64:245-248

[203] Shen YF, Guan RG, Zhao ZY, Misra RDK. Ultrafine-grained Al–0.2Sc–0.1Zr alloy: The mechanistic contribution of nano-sized precipitates on grain refinement during the novel process of accumulative continuous extrusion. Acta Mater 2015;100:247-255

[204] Apps PJ, Bowen JR, Prangnell PB. The effect of coarse second-phase particles on the rate of grain refinement during severe deformation processing. Acta Mater 2003;51:2811-2822

[205] Pippan R, Scheriau S, Taylor A, Hafok M, Hohenwarter A, Bachmaier A. Saturation of Fragmentation During Severe Plastic Deformation. Annu Rev Mater Res 2010;40:319-343

[206] Gutierrez-Urrutia I, Munoz-Morris MA, Morris DG. Contribution of microstructural parameters to strengthening in an ultrafine-grained Al–7% Si alloy processed by severe deformation. Acta Mater 2007;55 :1319-1330

[207] Jazaeri H, Humphreys FJ. The transition from discontinuous to continuous recrystallization in some aluminium alloys: I – the deformed state. Acta Mater 2004;52:3293-3250

[208] Gutierrez-Urrutia I, Munoz-Morris MA, Morris DG. The effect of coarse second-phase particles and fine precipitates on microstructure refinement and mechanical properties of severely deformed Al alloys. Mater Sci Eng A 2005;394;399-410

[209] Zha M, Li Y, Mathiesen RH, Roven HJ. Dispersion of soft Bi particles and grain refinement of matrix in an Al–Bi alloy by equal channel angular pressing. J Alloy Compd 2014;605:131-136

[210] Tsuchiyama T, Yamamoto S, Hata S, Murayama M, Morooka S, Akama D, Takaki S. Plastic deformation and dissolution of ε-Cu particles by cold rolling in an over-aged particle dispersion strengthening Fe-2mass%Cu alloy. Acta Mater 2016;113:48-55

[211] Hutchinson CR, Loo PT, Bastow TJ, Hill AJ, da Costa Teixeira J. Quantifying the strain-induced dissolution of precipitates in Al alloy microstructures using nuclear magnetic resonance. Acta Mater 2009;57:5645-5653

[212] Murayama M, Horita Z, Hono K. Microstructure of two-phase Al-1.7 at% Cu alloy deformed by equal-channel angular pressing. Acta Mater 2001;49 :21-29

[213] Buranova Y, Kulitskiy V, Peterlechner M, Moucheva A, Kaibyshev R, Divinski SV, Wilde G. Al_3(Sc,Zr)-based precipitates in Al–Mg alloy: Effect of severe deformation. Acta Mater 2017;124:210-224

[214] Deschamps A, Fribourg G, Bréchet Y, Chemin JL, Hutchinson CR. In situ evaluation of dynamic precipitation during plastic straining of an Al-Zn-Mg-Cu alloy. Acta Mater 2012;60:1905-1916

[215] Teichmann K, Marioara CD, Pedersen KO, Marthinsen K. The effect of simultaneous deformation and annealing on the precipitation behaviour and mechanical properties of an Al-Mg-Si alloy. Mater Sci Eng A 2013;565:228–235.

[216] Kloc L, Spigarelli S, Cerri E, Evangelista E, Langdon TG. Creep behavior of an aluminum 2024 alloy produced by powder metallurgy. Acta Mater. 1997;45:529–540.

[217] Roven HJ, Liu M, Werenskiold JC. Dynamic precipitation during severe plastic deformation of an Al-Mg-Si aluminium alloy. Mater Sci Eng A 2008;483–484:54–58.

[218] Lumley RN, Polmear IJ. The effect of long term creep exposure on the microstructure and properties of an underaged Al–Cu –Mg–Ag alloy. Scr Mater 2004;50:1227–1231.

[219] Lumley RN, Morton AJ, Polmear IJ. Enhanced creep performance in an Al–Cu–Mg–Ag alloy through underageing. Acta Mater. 2002;50:3597–3608.

[220] Guo F, Zhang D, Yang X, Jiang L, Pan F. Strain-induced dynamic precipitation of $Mg_{17}Al_{12}$ phases in Mg–8Al alloys sheets rolled at 748K. Mater Sci Eng A 2015;636:516–521.

[221] Dogan E, Wang S, Vaughan MW, Karaman I. Dynamic precipitation in Mg-3Al-1Zn alloy during different plastic deformation modes. Acta Mater 2016;116:1–13.

[222] Su J, Kaboli S, Kabir ASH, Jung I, Yue S. Effect of dynamic precipitation and twinning on dynamic recrystallization of micro-alloyed Mg–Al–Ca alloys. Mater Sci Eng A 2013;587:27–35.

[223] Nes E. Modelling of work hardening and sress saturation in FCC metals. Prog Mater Sci 1998;41:129-193.

[224] Kocks UF, Mecking H. Physics and phenomenology of strain hardening : the FCC case. Prog Mater Sci 2003;48:171-273

[225] da Costa Teixeira J, Bourgeois L, Sinclair CW, Hutchinson CR. The effect of shear-resistant, plate-shaped precipitates on the work hardening of Al alloys: Towards a prediction of the strength–elongation correlation. Acta Mater. 2009;57:6075–6089.

[226] Fribourg G, Bréchet Y, Deschamps A, Simar A. Microstructure-based modelling of isotropic and kinematic strain hardening in a precipitation hardened aluminium alloy. Acta Mater. 2011;59:3621–3635.

[227] Zhao Q, Holmedal B, Li Y. Influence of dispersoids on microstructure evolution and work hardening of aluminium alloys during tension and cold rolling. Philos Mag 2013;93:2995–3011.

[228] Proudhon H, Poole WJ, Wang X, Bréchet Y. The role of internal stresses on the plastic deformation of the Al–Mg–Si–Cu alloy AA6111. Philos Mag 2008;88:621–640.

[229] Marthinsen K, Nes E. Modelling strain hardening and steady state deformation of Al–Mg alloys. Mater Sci Technol 2001;17:376-388

[230] Roters F, Raabe D, Gottstein G. Work hardening in heterogeneous alloys—a microstructural approach based on three internal state variables. Acta Mater 2000;48:4181-4189

[231] Zhao Q, Holmedal B. Modelling work hardening of aluminium alloys containing dispersoids. Philos Mag 2013;93:3142–3153.

[232] Brown LM, Stobbs WM. The work-hardening of copper-silica I. A model based on internal stresses, with no plastic relaxation. Philos Mag 1971;23:1185–1199.

[233] Brown LM, Stobbs WM. The work-hardening of copper-silica. Philos Mag 1971;23:1201–1233.

[234] Ashby MF. Work hardening of dispersion-hardened crystals. Philos Mag 1966;14:1157–1178.

[235] Embury JD, Poole WJ, Lloyd DJ. The work hardening of single phase and multi-phase aluminium alloys. Mater Sci Forum 2006;519–521:71–78.

[236] V. Gerold, in:, F.R.N. Nabarro (Ed.), Dislocations in Solids, North-Holland, New York, 1979.

[237] Humphreys FJ, Kalu PN. The plasticity of particle-containing polycrystals. Acta Metall Mater 1990;38:917-930

[238] Humphreys FJ, Ardakani MG. The deformation of particle-containing aluminium single crystals. Acta Metall Mater 1994;42:749-761

[239] Kobayashi S, Zambaldi C, Raabe D. Orientation dependence of local lattice rotations at precipitates: Example of κ-Fe_3AlC carbides in a Fe_3Al-based alloy. Acta Mater 2010;58:6672-6684.

[240] Sidor JJ, Decroos K, Petrov RH, Kestens LAI. Evolution of recrystallization textures in particle containing Al alloys after various rolling reductions: Experimental study and modeling. Int J Plast 2015;66:119–137

[241] da Fonseca JQ, Ko L. The kinematics of deformation and the development of substructure in the particle deformation zone. IOP Conf Ser Mater Sci Eng 2015;89:12012.

[242] Smith CS. Introduction to grains, phases, and interfaces: an interpretation of microstructure. Transactions of the American Institute of Mining Engineers 1948;175: 15–51.

[243] Bernacki M, Chastel Y, Coupez T, Logé RE. Level set framework for the numerical modelling of primary recrystallization in polycrystalline materials. Scr Mater 2008;58:1129-1132

[244] Bernacki M, Resk H, Coupez T, Logé RE. Finite element model of primary recrystallization in polycrystalline aggregates using a level set framwork. Model Simul Mater Sci Eng 2009;17:064006

[245] Agnoli A, Bozzolo N, Logé R, Franchet J-M, Laigo J, Bernacki M. Development of a level set methodology to simulate grain growth in the presence of real secondary phase particles and stored energy – Application to a nickel-base superalloy. Comp Mater Sci 2014;89:233-241

[246] Scholtes B, Shakoor M, Settefrati A, Bouchard P-O, Bozzolo N, Bernacki M. New finite element developments for the full field modeling of microstructural evolutions using the level-set method. Comp Mater Sci 2015;109:388-398

[247] Morere B, Shahani R, Maurice C, Driver J. The influence of Al_3Zr dispersoids on the recrystallization of hot-deformed AA 7010 alloys. Metall Mater Trans A 2001;32:625-632

[248] Eivani AR, Valipour S, Ahmed H, Zhou J, Duszczyk J. Effect of the Size Distribution of Nanoscale Dispersed Particles on the Zener Drag Pressure. Metall Mater Trans A 2011;42:1109-1116

[249] Fullman RL. Metal Interface. American Society for Metals, 1952, 179–259.

[250] Buken H, Kozeschnik E. A Model for Static Recrystallization with Simultaneous Precipitation and Solute Drag. Metall Mater Trans A 2017;48:2812-2818

[251] Hansen N, Bay B.The effect of particle content, particle distribution and cold deformation on the recrystallization of low oxide Al-Al_2O_3 products. J Mater Sci 1972;7:1351-1362

[252] Rohrer GS. The role of grain boundary energy in grain boundary complexion transitions. Curr Opin Solid State Mater Sci 2016;20:231-239

[253] Huang K, Logé RE, Marthinsen K. On the sluggish recrystallization of a cold-rolled Al–Mn–Fe–Si alloy. J Mater Sci 2016 ;51 :1632-1643

[254] Bacon DJ, Osetsky YN, Rodney D. Dislocation–Obstacle Interactions at the Atomic Level. In: Hirth JP, Kubin L Ed. Dislocations in solids. Elsevier, 2009

[255] Humphreys FJ, Ardakani MG. Grain boundary migration and Zener pinning in particle-containing copper crystals. Acta Mater 1996;44:2717-2727

[256] Daaland O, Nes E. Recrystallization texture development in commercial Al–Mn–Mg alloys. Acta Mater 1996;44:1413-1435

[257] Engler O. Nucleation and growth during recrystallization of aluminium alloys investigated by local texture analysis, Mater Sci Tech 1996;12:859-872

[258] Tangen S, Sjølstad K, Furu T, Nes E. Effect of concurrent precipitation on recrystallization and evolution of the P-texture component in a commercial Al-Mn alloy. Metall Mater Trans A 2010;41A:2970-2983

[259] Schäfer C, Gottstein G. The origin and development of the P{011}<111> orientation during recrystallization of particle-containing Alloys. Int J Mater Res 2011;102:1106-1114

[260] Huang K, Engler O, Li YJ, Marthinsen K. Evolution in microstructure and properties during non-isothermal annealing of a cold-rolled Al–Mn –Fe–Si alloy with different microchemistry states. Mater Sci Eng A 2015;628:216-229

[261] Jung J, Yoon JI, Lee DN, Kim HS. Numerical analysis on the formation of P-orientation near coarse precipitates in FCC crystals. Acta Mater 2017;131:363-372

[262] Huang K, Zhang K, Marthinsen K, Logé RE. Controlling grain structure and texture in Al-Mn from the competition between precipitation and recrystallization. Acta Mater 2017;141:360-373

[263] Zhou J, Zhang S, Wang X, B Zhao, X Dong, Zhang L. Interaction between coherent second-phase particles and migrating boundaries: Boundary effect and particle reorientation. Scr Mater 2016;116:100-103

[264] Homma H, Hutchinson B. Orientation dependence of secondary recrystallisation in silicon–iron. Acta Mater 2003;51:3795-3805

[265] Raabe D, Lücke K. Selective particle drag during primary recrystallization of Fe-Cr alloys. Scr Metall Mater 1992;26:19-24

[266] Gleiter H. Theory of grain boundary migration rate. Acta Metall 1969;17:853-862

[267] Chan HM, Humphreys FJ. The recrystallisation of aluminium-silicon alloys containing a bimodal particle distribution. Acta Metall 1984;32:235-243

[268] Köster U. Recrystallization involving a second phase. Metal Sci 1974;8:151-160

[269] Williams DB, Butler EP. Grain boundary discontinuous precipitaiton reaction. Int Mater Rev 1981;26:153-183

[270] Rettberg LH, Pollock TM. Localized recrystallization during creep in nickel-based superalloys GTD444 and René N5. Acta Mater 2014;73:287-297

[271] Moelans N, Blanpain B, Wollants P. Phase field simulations of grain growth in two-dimensional systems containing finely dispersed second-phase particles. Acta Mater 2006;54:1175-1184.

[272] Daaland O, Nes E. Recrystallization texture development in commercial Al-Mn-Mg alloys. Acta Mater 1996;44:1413-1435

[273] Baker I, Martin JW. The effect of particle size and spacing on the retardation of recrystallization in two-phase copper crystal. J Mater Sci 1980;15:1533-1538

[274] Raabe D, Hantcherli L. 2D cellular automaton simulation of the recrystallization texture of an IF sheet steel under consideration of Zener pinning. Comput Mater Sci 2005;34:299-313

[275] Mukhopadhyay P, Loeck M, Gottstein G. A cellular operator model for the simulation of static recrystallization. Acta Mater 2007;55.551-564

[276] Hallberg H, Svendsen B, Kayser T, Ristinmaa. Microstructure evolution during dynamic discontinuous recrystallization in particle-containing Cu. Comput Mater Sci 2014;84:327-338

[277] Luton MJ, Dorvel R, Petkovic RA. Interaction between deformation, recrystallization and precipitation in Niobium steels. Metall Trans A 1980;11:411-420

[278] Doherty RD, Martin JW. Effect of a dispersed second phase on recrystallization of aluminium-copper alloys. J Inst Metals 1962-1963;91:332-338

[279] Humphreys FJ, Martin JW. The effect of dispersed phases upon the annealing behaviour of plastically deformed copper crystals. Philos Mag 1968;17:365-403

[280] Clegg MA, Lund JA. Substructure strengthening in dispersion-strengthened nickel alloys. Metall Trans 1971;2:2495-2507

[281] Humphreys FJ, Martin JW. The effect of dispersed silica particles on the recovery and recrystallization of deformed copper crystals. Acta Metall 1966;14:775-781

[282] Humphreys FJ. Recrystalliaztion mechanisms in two-phase alloys. Metal Sci 1979;13:136-145

[283] Chopra OK, Niessen P. Recrystallization in internally oxidized Cu-Ag-Al alloys. J Mater Sci 1974;9:279-288

[284] Benum S, Nes E. Effect of precipitation on the evolution of cube recrystallisation texture. Acta Mater 1997;45:4593-4602

[285] Yamagata H. Microstructural evolution of single-crystalline aluminum during multipeak stress oscillation at 623K. Scr Metall Mater 1992;27:1157-1160

[286] Ponge D, Bredehoft M, Gottstein G. Dynamic recrystallization in high purity aluminum. Scr Mater 1997;37:1769-1775

[287] Yamagata H, Ohuchida Y, Saito N, Otsuka M. Nucleation of new grains during discontinuous dynamic recrystallization of 99.998 mass% Aluminum at 453 K. Scr Mater 2001;45:1055-1061

[288] Castro-Fernandez FR, Sellars CM. Static recrystallisation and recrystallisation during hot deformation of Al–1Mg–1Mn alloy. Mater Sci Technol 1988;4:621-627

[289] Sheppard T, Tutcher MG. Development of duplex deformation substructure during extrusion of a commercial Al-5Mg-0.8Mn alloy. Metal Sci 1980;14:579-590

[290] De Siqueira RP, Sandim HRZ, Raabe D. Particle Stimulated Nucleation in Coarse-Grained Ferritic Stainless Steel. Metall Mater Trans A 2013;44:469-478

[291] Robson JD, Henry DT, Davis B. Particle effects on recrystallization in magnesium–manganese alloys: Particle-stimulated nucleation. Acta Mater 2009;57:2739-2747

[292] Kubin LP Mortensen A. Geometrically necessary dislocations and strain-gradient plasticity: a few critical issues. Scr Mater 2003;48:119-125

[293] Humphreys FJ. The nucleation of recrystallization at second phase particles in deformed aluminium. Acta Metall 1977;25:1323-1344

[294] Gawne DT, Higgins GT. Associations between spherical particles of two dissimilar phases. J Mater Sci 1971;6:403-412

[295] Ardakani MG, Humphreys FJ. High temperature deformation and dynamic recrystallization of some two-phase copper alloys. Mater Sci Forum 1993; 113-115:213-218

[296] Semiatin SL, Weaver DS, Kramb RC, Fagin PN, Glavicic MG, Goetz RL, Frey ND, Antony MM. Deformation and recrystallization behavior during hot working of a coarse-grain, nickel-base superalloy ingot material. Metall Mater Trans A 2004;35:679-693

[297] Pereloma EV, Mannan P, Casillas G, Saleh AA. Particle stimulated nucleation during dynamic and metadynamic recrystallisation of Ni-30%Fe-Nb-C. Mater Charact 2017; 125:94-98

[298] Humphreys FJ, Kalu PN. Dislocation-particle interactions during high temperature deformation of two-phase aluminium alloys. Acta Metall 1987;35:2815-2829

[299] Castro-Fernández FR, Sellars CM. Static recrystallisation and recrystallisation during hot deformation of Al–1Mg–1Mn alloy. Mater Sci Technol 1988;4:621-627

[300] Goetz RL. Particle stimulated nucleation during dynamic recrystallization using a cellular automata model. Scr Mater 2005;52:851-856

[301] Charpagne M-A, Billot T, Franchet J-M, Bozzolo N. Heteroepitaxial recrystallization: A new mechanism discovered in a polycrystalline γ-γ’ nickel based superalloy. J Alloy Compd 2016;688:685-694

[302] Vatne HE, Furu T, Ørsund R, Nes E. Modelling recrystallization after hot deformation of aluminium. Acta Mater 1996;44:4463-4473

[303] Hansen N, Bay B. Initial stages of recrystallization in aluminium containing both large and small particles. Acta Metall 1981;29:65-77

[304] Humphreys FJ. Particle stimulated nucleation of recrystallization at silica particles in nickel. Scr Mater 2000;43:591-596

[305] Ørsund R, Nes E. Effect of particles on recrystallization textures in aluminium-manganese alloys. Scr Metall 1988;22:665-669

[306] Ørsund R, Nes E. A model for the nucleation of recrystallization from particles: The texture aspect. Scr Metall 1988;22:671-676

[307] Ferry M, Humphreys FJ. The deformation and recrystallization of particle-containing {011}〈100〉 aluminium crystals. Acta Mater 1996;44:3089-3103

[308] Juul Jensen D, Hansen N, Humphreys FJ. Texture development during recrystallization of aluminium containing large particles. Acta Metall 1985;33:2155-2162

[309] Engler O, Hirsch J, Lücke K. Texture development in Al-1.8 wt% Cu depending on the precipitation state—II. Recrystallization textures. Acta Metall Mater 1995;43:121-138

[310] Dillamore IL, Katoh H. The Mechanisms of Recrystallization in Cubic Metals with Particular Reference to Their Orientation-Dependence. Metal Sci 1974;8:73-83

[311] Juul Jensen D. Growth of nuclei with different crystallographic orientation durirng recrystallization. Scr Metall Mater 1992;27:533-538

[312] Nes E, Embury JD. Influence of a fine particle dispersion on the recrystallization behaviour of a two phase aluminium alloy. Z Metallk 1975;66:589-593

[313] Nes E. The effect of a fine particle dispersion on heterogeneous recrystallization. Acta Metall 1976;24:391-398

[314] Nes E, Wert JA. Modeling of recrystallization in alloys with a bimodal particle size distribution. Scr Metall 1984;18:1433-1438

[315] Kolmogorov AN. On the statistical theory of metal crystallization, Isv Akad Nauk USSR Ser Matemat 1937;1: 355-359

[316] Johnson WA, Mehl RF. Reaction Kinetics in Processes of Nucleation and Growth. Trans Metall Soc AIME 1939;135:416-442

[317] Avrami M. Kinetics of phase change. I: General Theory. J Chem Phy 1939;7:1103-1112

[318] Avrami M. Kinetics of phase change II. Transformation-time relations for random distribution of nuclei. J Chem Phys 1940;8:212-224

[319] Avrami M. Kinetics of phase change III. Granulation, phase change and microstructure. J Chem Phys 1941;9:177-184 .

[320] Deng K, Shi J, Wang C, Wang X, Wu Y, Nie K, Wu K. Microstructure and strengthening mechanism of bimodal size particle reinforced magnesium matrix. Compos Part A Appl Sci Manuf 2012;43:1280-1284

[321] Morris MA, Leboeuf M, Morris DG. Recrystallization mechanisms in a Cu-Cr-Zr alloy with a bimodal distribution of particles. Mater Sci Eng A 1994;188:255-265

[322] Paul H, Morawiec A, Baudin T. Early Stages of Recrystallization in Equal-Channel Angular Pressing (ECAP)-Deformed AA3104 Alloy Investigated Using Scanning Electron Microscopy (SEM) and Transmission Electron Microscopy (TEM) Orientation Mappings. Metall Mater Trans A 2012;43:4777-4793

[323] Marthinsen K, Fridy J, Rouns T, Lippert K, Nes E. Characterization of 3-D particle distributions and effects on recrystallization kinetics and microstructure. Scr Mater. 1998;39:1177-1183

[324] Marthinsen K, Daaland O, Furu T, Nes E. The the spatial distribution of nucleation sites and its effect on the recrystallization kinetics. Metall Mater Trans A 2003;34:2705-2715

[325] Godfrey A, Juul Jensen D, Hansen N. Recrystallisation of channel die deformed single crystals of typical rolling orientations. Acta Mater 2001;49:2429-2440

[326] Miszczyk M, Paul H, Driver JH, Maurice C. New orientation formation and growth during primary recrystallization in stable single crystals of three face-centred cubic metals. Acta Mater 2015;83:120-136

[327] Srolovitz J, Andersen MP, Grest GS, Rollett AD. Computer simulation of recrystallization-II. Heterogeneous Nucelation and growth. Acta metall. 1988;36: 2115-2128

[328] Furu T, Marthinsen K, Nes E. Modelling recrystallization. Mater Sci Technol. 1990;6:1093-1102.

[329] Marthinsen K. Repeated grain boundary and grain corner nucleated recrystallization in one- and two-dimensional grain structures. Model Simul Mater Sci Eng 1996;4:87-100

[330] Mahin KW, Hanson K, Morris J.W. Comparative analysis of the cellular and Johnson-Mehl microstructures through computer simulation, Acta Metall. 1980;28:443-453.

[331] Marthinsen K, Lohne O, Nes E. The development of recrystallization microstructures studied experimentally and by computer simulation. Acta Metall 1989;37:135-145

[332] Vandermeer RA. Microstructural descriptors and the effects of nuclei clustering on recrystallization path kinetics. Acta Mater 2005;53:1449-1457

[333] Villa E, Rios PR. Transformation kinetics for nucleus clusters. Acta Mater 2009;57:3714-3724

[334] Villa E, Rios PR. Transformation kinetics for inhomogeneous nucleation. Acta Mater 2009;57:1199-1208

[335] Hansen SS, Vander Sander JB, Cohen M. Niobium carbonitride precipitation and austenite recrystallization in hot-rolled microalloyed steels. Metall Trans A 1980;11:387-402

[336] Somerday M, Humphreys FJ. Recrystallization behavior of supersaturated Al-Mn alloys Part I- Al-1.3 wt-% Mn. Mater Sci Technol 2003;19:20-29

[337] Huang K, Wang N, Li YJ, Marthinsen K. The influence of microchemistry on the softening behaviour of two cold-rolled Al-Mn-Fe-Si alloys. Mater Sci Eng A 2014;601:86-96

[338] Huang K, Marthinsen K. The effect of heating rate on the softening behaviour of a deformed Al–Mn alloy with strong and weak concurrent precipitation. Mater Charact 2015;110:215-221

[339] Huang K, Li YJ, Marthinsen K. Effect of heterogeneously distributed pre-existing dispersoids on the recrystallization behavior of a cold-rolled Al–Mn–Fe–Si alloy. Mater Charact 2015;102 :92-97

[340] Tian B, Zickler GA, Lind C, Paris O. Local microstructure and its influence on precipitation behavior in hot deformed Nimonic 80a. Acta Mater 2003;51:4149-4160

[341] Dutta B, Valdes E, Sellars CM. Mechanism and kinetics of strain induced precipitation of Nb(C,N) in austenite. Acta Metall Mater 1992;40:653-662

[342] Gladman T. On the Theory of the Effect of Precipitate Particles on Grain Growth in Metals. Proc Roy Soc A 1996;294:298-309

[343] Vatne HE, Engler O, Nes E. Influence of particles on recrystallization textures and microstructures of aluminium alloy 3103. Mater Sci Technol1997; 13:93-102

[344] Bréchet YJM, Zurob HS, Hutchinson CR. On the effect of pre-recovery on subsequent recrystallization, Int J Mater Res. 100 (2009) 1446-1448.

[345] Decreus B, Zurob HS, Bréchet YJM. Effect of low-temperature recovery treatments on subsequent recrystallization in Al-2.5%Mg, Mater Sci Forum. 550(2007) 381-386.

[346] Primig S, Leitner H, Knabl W, Lorich A, Clemens H, Stickler R. Influence of the heating rate on the recrystallization behavior of molybdenum. Mater Sci Eng A 2012;535:316-324

[347] Huang L, Huang G, Gao L, Wu X, Jia Z, Xia M, Liu Q. Influence of pre-recovery on the subsequent recrystallization and mechanical properties of a twin-roll cast Al-Mn alloy, Mater Sci Eng A 2017;682:63-72

[348] Morris JG, Liu WC. Al alloys: The influence of concurrent precipitation on recrystallization behavior, kinetics, and texture. JOM 2005;57:44-47

[349] Dutta B, Sellars CM. Effect of composition and process variables on Nb(C, N) precipitation in niobium microalloyed austenite. Mater Sci Technol 1987;3:197-206

[350] Ryum N. Precipitation and recrystallization in an A1-0.5 wt.% Zr-alloy. Acta Metall 1969;17:269-278

[351] Ryu J-H, Lee DN. The effect of precipitation on the evolution of recrystallization texture in AA8011 aluminum alloy sheet. Mater Sci Eng A 2002;336:225-232

[352] Sasaki TT, Yamamoto K, Honma T, Kamado S, Hono K. A high-strength Mg–Sn–Zn–Al alloy extruded at low temperature. Scr Mater 2008;59:1111-1114

[353] Schinhammer M, Pecnik CM, Rechberger F, Hänzi AC, Löffler JF, Uggowitzer PJ. Recrystallization behavior, microstructure evolution and mechanical properties of biodegradable Fe –Mn–C(–Pd) TWIP alloys. Acta Mater 2012;60:2746-2756

[354] Liu WC, Morris JG. Evolution of recrystallization and recrystallization texture in continuous-cast AA 3015 aluminum. Metall Mater Trans A 2005;36:2829-2848

[355] Liu WC, Li Z, Man C-S, Raabe D, Morris JG. Effect of precipitation on rolling texture evolution in continuous cast AA 3105 aluminum alloy. Mater Sci Eng A 2006;434:105-113

[356] Wen W, Liu WC, Morris JG. The effect of precipitation of Mg2Al3 and of MnAl6 on texture evolution during isothermal annealing and subsequently on formability of CC AA5182 Al alloy. Mater Sci Eng A 2004;380:191-207

[357] Zhao Q, Huang K, Li Y, Marthinsen K. Orientation preference of recrystallization in supersaturated aluminum alloys influenced by concurrent precipitation. Metall Mater Trans A 2016;47:1378-1388

[358] Lok ZJ, Miroux A, van der Zwaag S. Solute and second phase evolution during industrial processing of AA3103. Mater Sci Forum 2007;539-543:281-286.

[359] Jonas JJ, Weiss I. Effect of precipitation on recrystallization in microalloyed steels. Metal Sci 1979;13:238-245

[360] Yazawa Y, Furuhara T, Maki T. Effect of matrix recrystallization on morphology, crystallography and coarsening behavior of vanadium carbide in austenite. Acta Mater 2004;52:3727-3736

[361] Doherty RD. Role of interfaces in kinetics of internal shape changes. Metal Sci 1982;16:1-14

[362] Kreye H, Hornbogen E, Haessner F. Recrystallization of supersaturated and plastically deformed solid solutions of nickel. Phys Stat Sol A 1970;1:97-108

[363] Bee JV, Jones AR, Howell PR. The interaction of recrystallizing interfaces with intragranular precipitate dispersions in a nickel-base superalloy. J Mater Sci 1981;16:1471-1476

[364] Jones AR, Ralph B. The influence of recrystallization on carbide particle distribution in a fully stabilized austenitic steel. Acta Metall 1975;23.355-363

[365] Sallez N, Hatzoglou C, Delabrouille F, Sornin D, Chaffron L, Blat-Yrieix M, Radiguet B, Pareige P, Donnadieu P, Bréchet Y. Precipitates and boundaries interaction in ferritic ODS steels. J Nucl Mater 2016;472:118-126

[366] Guan D, Nutter J, Sharp J, Gao J, Rainforth WM. Direct observation of precipitation along twin boundaries and dissolution in a magnesium alloy annealing at high temperature. Scr Mater 2017;138:39-43

[367] Ferry M, Hamilton NE, Humphreys FJ. Continuous and discontinuous grain coarsening in a fine-grained particle-containing Al–Sc alloy. Acta Mater 2005;53:1097-1109

[368] Su J-Q, Nelson TW, Mishra R, Mahoney M. Microstructural investigation of friction stir welded 7050-T651 aluminium. Acta Mater 2003;51:713-729

[369] Sidor JJ, Petrov RH, Kestens LAI. Modeling the crystallographic texture changes in aluminum alloys during recrystallization. Acta Mater 2011;59:5735-5748

[370] Rollett AD, Srolovitz DJ, Anderson MP, Doherty RD. Computer simulation of recrystallization—III. Influence of a dispersion of fine particles. Acta Metall Mater 1992;40:3475-3495

[371] Alves ALM, Villa E, Rios PR. Transformation kinetics for nucleation on second-phase particles: analytical solution and computer simulation. Acta Mater 2017;131:523-533

[372] Deschamps A, Brechet Y. Influence of predeformation and agEing of an Al–Zn–Mg alloy—II. Modeling of precipitation kinetics. Acta Mater 1998;47:293-305

[373] Myhr OR, Grong Ø, Andersen SJ. Modelling of the age hardening behaviour of Al–Mg–Si alloys. Acta Mater 2001;49:65-75

[374] Robson JD, Prangnell PB. Dispersoid precipitation and process modelling in zirconium containing commercial aluminium alloys. Acta Mater 2001;49:599-613

[375] Perez M, Dumont M, Acevedo-Reyes D. Implementation of classical nucleation and growth theories for precipitation. Acta Mater 2008;56:2119-2132

[376] Svoboda J, Fischer FD, Fratzl P, Kozeschnik E. Modelling of kinetics in multi-component multi-phase systems with spherical precipitates: I: Theory. Mater Sci Eng A 2004;385:166-174

[377] Humphreys FJ. A unified theory of recovery, recrystallization and grain growth, based on the stability and growth of cellular microstructures—II. The effect of second-phase particles. Acta Mater 1997;45:5031-5039

[378] Engler O, Löchte L, Hirsch J. Through-process simulation of texture and properties during the thermomechanical processing of aluminium sheets. Acta Mater 2007;55:5449-5463

[379] Wang N, Huang K, Li Y, Marthinsen K. The influence of processing conditions on microchemistry and the softening behavior of cold rolled Al-Mn-Fe-Si alloys. Metals 2016;6:61

[380] Vatne HE, Ørsund R, Marthinsen K, Nes E. Modeling recrystallization kinetics, grain sizes, and textures during multipass hot rolling. Metall Mater Trans A 1996;27:4133-4144

[381] Song X, Rettenmayr M. Modeling recrystallization in a material containing fine and coarse particles. Comput Mater Sci 2007;40:234-245

[382] Zurob HS, Hutchinson CR, Brechet Y, Purdy G. Modeling recrystallization of microalloyed austenite: effect of coupling recovery, precipitation and recrystallization. Acta Mater 2002;50:3077-3094

[383] Schäfer C, Mohles V, Gottstein G. Modeling of non-isothermal annealing: Interaction of recrystallization, recovery, and precipitation. Acta Mater 2011;59:6574-6587

[384] Schäfer C, Pomana G, Mohles V, Gottstein G, Engler O, Hirsch J. Recrystallization Modeling of AA8XXX Alloys with Cellular Automata Considering Recovering Kinetics. Adv Eng Mater 2010;12:131-140

[385] Prasad GVSS., An Improved Dislocation Density Based Work-Hardening Model for Al Alloys, PhD Thesis, IMM, RWTH Aachen, 2007

[386] Crumbach M, Goerdeler M, Gottstein. Modelling of recrystallisation textures in aluminium alloys: I. Model set-up and integration. Acta Mater 2006;54:3275-3289

[387] Schneider M. Modellierung und validierung zeitabhängiger mikrochemischer prozesse in aluminium knetlegierungen. PhD thesis, Rheinisch-Westfaelische Technische Hochschule, Aachen, Germany; 2006.

[388] Buken H, Sherstnev P, Kozeschnik E. A state parameter-based model for static recrystallization interacting with precipitation. Model Simul Mater Sci Eng 2016;24:035006

[389] L'Ecuyer JD, L'Espérance G. Precipitation interactions with dynamic recrystallization of a HSLA steel. Acta Mater 1989;37:1023-1031

[390] Kendig KL, Miracle DB. Strengthening mechanisms of an Al-Mg-Sc-Zr alloy. Acta Mater 2002;50:4165-4175

[391] Dadé M, Malaplate J, Garnier J, De Geuser F, Barcelo F, Widen P, Deschamps A. Influence of microstructural parameters on the mechanical properties of oxide dispersion strengthened Fe-14Cr steels. Acta Mater 2017;127:165-177

[392] Chokshi AH, Rosen A, Karch J, Gleiter H. On the validity of the hall-petch relationship in nanocrystalline materials. Scr Metall 1989;23:1679-1683

[393] Conrad H, Narayan. On the grain size softening in nanocrystalline materials. Scr Mater 2000 ;42 :1025-1030

[394] Lesuer DR, Syn CK, Sherby OD. Nano-subgrain strengthening in ball-milled iron. Mater Sci Eng A 2007;463:54-60

[395] Kuhlmann-Wilsdorf D. Theory of plastic deformation: - properties of low energy dislocation structures. Mater Sci Eng A 1989 ;113 :1-41

[396] Gladman T. Precipitation hardening in metals. Mater Sci Technol 1999;15:30-36

[397] Nie JF. Effects of precipitate shape and orientation on dispersion strengthening in magnesium alloys. Scr Mater 2003;48:1009-1015

[398] Ardell AJ. Precipitation hardening. Metall Trans A 1985 ;16 :2131-2165

[399] Hutchinson B. Critical Assessment 16 : Anisotropy in metals. 2015 ;31 :1393-1401

[400] Kocks UF, Tome CN, Wenk H-R. Texture and Anisotropy: Preferred orientations in polycrystals and their effect on materials properties. Cambridge University Press, Cambridge,1998

[401] Wang SC, Starink MJ. Precipitates and intermetallic phases in precipitation hardening Al–Cu–Mg–(Li) based alloys. Int Mater Rev 2005;50:193-215

[402] Pineau A, Benzerga AA, Pardoen T. Failure of metals I: Brittle and ductile fracture. Acta Mater 2016;107:424-483

[403] Babout L, Brechet Y, Maire E, Fougères R. On the competition between particle fracture and particle decohesion in metal matrix composites. Acta Mater 2004;52:4517-4525

[404] Gurland J. Observations on the fracture of cementite particles in a spheroidized 1.05% C steel deformed at room temperature. Acta Metall 1972;20:735-741

[405] Griffith AA. The Phenomena of Rupture and Flow in Solids. Phil Trans R Soc Lond A 1921;221:163-198

[406] Bae DH, Ghosh AK. Cavity formation and early growth in a superplastic Al–Mg alloy. Acta Mater 2002;50:511-523

[407] Bae DH, Ghosh AK. Cavity growth in a superplastic Al–Mg alloy: II. An improved plasticity based model. Acta Mater 2002;50:1011-1029

[408] Xu W, Ferry M, Humphreys FJ. Spatial morphology of interfacial voids and other features generated at coarse silica particles in nickel during cold rolling and annealing. Scr Mater 2009;60:862-865

[409] Goods SH, Brown LM. Overview No. 1: The nucleation of cavities by plastic deformation. Acta Metall 1979;27:1-15

[410] Liu G, Sun J, Nan CW, Chen KH. Experiment and multiscale modeling of the coupled influence of constituents and precipitates on the ductile fracture of heat-treatable aluminum alloys. Acta Mater 2005;53:3459-3468

[411] Liu G, Zhang GJ, Wang RH, Hu W, Sun J, Chen K. HHeat treatment-modulated coupling effect of multi-scale second-phase particles on the ductile fracture of aged aluminum alloys. Acta Mater 2007;55:273-284

[412] Dumont D, Deschamps A, Brechet Y. On the relationship between microstructure, strength and toughness in AA7050 aluminum alloy. Mater Sci Eng A 2003;356 :326-336

[413] Sanders TH. The fracture behavior of recrystallized Al-2.8% Li-0.3% Mn sheet. Mater Sci Eng 1980;43:247-260

[414] Movchan BA. Structural conditions for maximum ductility of two-phase polycrystalline materials. Mater Sci Eng 1985;72:109-117

[415] Meyers MA, Mishra A, Benson DJ. Mechanical properties of nanocrystalline materials. Prog Mater Sci 2006;51:427-556

[416] Wang Y, Chen M, Zhou F, Ma E. High tensile ductility in a nanostructured metal. Nature 2002;419 :912-915

[417] Ma E. Eight routes to improve the tensile ductility of bulk nanostructured metals and alloys. JOM 2006;58:49-53

[418] Pelleg J. Mechanical properties of materials. Springer, 2013

[419] Rösler J, Arzt E. A new model-based creep equation for dispersion strengthened materials. Acta Metall Mater 1990;38:671-683

[420] Pollock TM, Argon AS. Creep resistance of CMSX-3 nickel base superalloy single crystals. Acta Metall Mater 1992;40:1-30

[421] Arzt E, Grahle P. High temperature creep behavior of oxide dispersion strengthened NiAl intermetallics. Acta Mater 1998;46:2717-2727

[422] Arzt E. Size effects in materials due to microstructural and dimensional constraints: a comparative review. Acta Mater 1998;46:5611-5626

[423] Dieter GE. Mechanical metallurgy. SI Metric ed./adapted by Bacon D. McGraw-Hill Book Co.

[424] Thompson AW, Backofen WA. The effect of grain size on fatigue. Acta Metall 1971;19:597-606

[425] Peralta P, Laird C. Fatigue of metals. In: D.E. Laughlin, K. Hono (Eds.), Physical Metallurgy, fifth ed.Elsevier, Amsterdam 2014, 1765–1880.

[426] Harlow DG, Nardiello J, Payne J. The effect of constituent particles in aluminum alloys on fatigue damage evolution: Statistical observations. Int J Fatigue 2010;32:505-511

[427] Zhang J, Perez RJ, Wong CR, Lavernia EJ. Effects of secondary phases on the damping behaviour of metals, alloys and metal matrix composites. Mater Sci Eng R 1994;13:325-389

[428] Wang HY, Yu ZP, Zhang L, Liu CG, Zha M, Wang C, Jiang QC. Achieving high strength and high ductility in magnesium alloy using hard-plate rolling (HPR) process. Sci Rep 2015;5:17100

[429] Yang W, Yan D, Rong L. The separation of recrystallization and precipitation processes in a cold-rolled Al–Mg–Sc solid solution. Scr Mater 2013;68:587-590

[430] Watanabe H, Tsutsui H, Mukai T, Ishikawa K, Okanda Y, Kohzu M, Higashi K. Grain size control of commercial wrought Mg-Al-Zn alloys utilizing dynamic recrystallization. Mater Trans 2001;42:1200-1205

[431] Xu SW, Matsumoto N, Kamado S, Honma T, Kojima Y. Dynamic microstructural changes in Mg–9Al–1Zn alloy during hot compression. Scr Mater 2009;61:249-252

[432] Changizian P, Zarei-Hanzaki A, Abedi HR. On the recrystallization behavior of homogenized AZ81 magnesium alloy: The effect of mechanical twins and γ precipitates. Mater Sci Eng A 2012;558:44-51

[433] Troeger LP, Starke EA. Particle-stimulated nucleation of recrystallization for grain-size control and superplasticity in an Al–Mg–Si–Cu alloy. Mater Sci Eng A 2000;293:19-29

[434] Driver JH, Juul Jensen D, Hansen N. Large strain deformation structures in aluminium crystals with rolling texture orientations. Acta Metall Mater 1994;42:3105-3114

[435] Huang X, Winther G. Dislocation structures. Part I. Grain orientation dependence. Philos Mag 2007;87:5189-5214

[436] Zhang Z, Zhang Y, Mishin OV, Tao N, Pantleon W, Juul Jensen D. Microstructural Analysis of Orientation-Dependent Recovery and Recrystallization in a Modified 9Cr -1Mo Steel Deformed by Compression at a High Strain Rate. Metall Mater Trans A 2016;47:4682-4693

[437] Xing Q, Huang X, Hansen N. Recovery of heavily cold-rolled aluminum: Effect of local texture. Metall Mater Trans A 2006;37:1311-1322

[438] Albou A, Borbely A, Maurice C, Driver JH. Orientation-dependent recovery in strongly deformed Al–0.1% Mn crystals. Philos Mag 2011;91:3981-4000

[439] Hutchinson WB. Development of Textures in Recrystallization. Metal Sci 1974;8:185-196

[440] Hutchinson B. Practical aspects of texture control in low carbon steels. Mater Sci Forum 1994;157-162:1917-1928

[441] Sakai T, Jonas JJ. Overview no. 35 Dynamic recrystallization: Mechanical and microstructural considerations. Acta Metall 1984;32:189-209

[442] Sellars CM. Modeling of structural evolution during hot rolling processes. In: Hansen N, Juul Jensen D, Leffers T, Ralph B, editors. Annealing process—recovery, recrystallization and grain growth. Roskilde: GH-Tryk ApS Odense; 1986.

[443] Ponge D, Gottstein G. Necklace formation during dynamic recrystallization: mechanisms and impact on flow behavior. Acta Mater 1998;46:69-80

[444] Ion SE, Humphreys FJ, White SH. Dynamic recrystallisation and the development of microstructure during the high temperature. Acta Mater 1982;30:1909-1919

[445] Wusatowska-Sarnek AM, Miura H, Sakai T. Nucleation and microtexture development under dynamic recrystallization of copper. Mater Sci Eng A 2002;323:177-189

[446] Engler O, Vatne HE, Nes E. The roles of oriented nucleation and oriented growth on recrystallization textures in commercial purity aluminium 1996;205:187-198

[447] Hutchinson B. The cube texture revisited. Mater Sci Forum 2012;702-703:3-10

[448] Huang Y, Humphreys FJ. The effect of solutes on grain boundary mobility during recrystallization and grain growth in some single-phase aluminium alloy. Mater Chem Phys 2012;132:166-174

[449] Huang Y, Humphreys FJ. Measurement of grain boundary mobility during recrystallization of a single-phase aluminium alloy. Acta Mater 1999;47 :2259-2268

[450] Engler O. Control of texture and earing in aluminium alloy AA 3105 sheet for packaging applications. Mater Sci Eng A 2012;538:69-80

[451] Huang K, Li YJ, Marthinsen K. Factors affecting the strength of P{011}<566>-texture after annealing of a cold-rolled Al–Mn–Fe–Si alloy. J Mater Sci 2015;50:5091-5103

[452] Decker DF. Alloy design, using second phases. Metall Trans 1973;4:2495-2518

[453] Tsivoulas D, Robson JD, Sigli C, Prangnell PB. Interactions between zirconium and manganese dispersoid-forming elements on their combined addition in Al–Cu–Li alloys. Acta Mater 2012;60:5245-5259

[454] Totten GE, MacKenzie DS. Handbook of Aluminum Vol.1: Physical Metallurgy and processes

[455] Bae DH, Kim SH, Kim DH, Kim WT. Deformation behavior of Mg–Zn–Y alloys reinforced by icosahedral quasicrystalline particles. Acta Mater 2002;50:2343-2356

[456] Vervynckt S, Verbeken K, Lopez B, Jonas JJ. Modern HSLA steels and role of non-recrystallisation temperature. Int Mater Rev 2012;57:187-207

[457] Charleux M, Poole WJ, Militzer M, Deschamps A. Precipitation behavior and its effect on strengthening of an HSLA-Nb/Ti steel. Metall Mater Trans A 2001;32:1635-1647

[458] Simmons JW. Overview: high-nitrogen alloying of stainless steels. Mater Sci Eng A 1996;207:159-169

[459] Poddar D, Cizek P, Beladi H, Hodgson PD. Evolution of strain-induced precipitates in a model austenitic Fe–30Ni–Nb steel and their effect on the flow behavior. Acta Mater 2014;80:1-15

[460] Pollock TM, Tin S. Nickel-based superalloys for advanced turbine engines: chemistry, microstructrue, and properties. J Propul Power 2006;22:361-374

[461] Hofstetter J, Rüedi S, Baumgartner I, Kilian H, Mingler B, Povoden-Karadeniz E, Pogatscher S, Uggowitzer PJ, Löffler JF. Processing and microstructure–property relations of high-strength low-alloy (HSLA) Mg–Zn–Ca alloys. Acta Mater 2015;98:423-432

[462] Zhao YH, Liao XZ, Cheng S, Ma E, Zhu YT. Simultaneously increasing the ductility and strength of nanostructured alloy. Adv Mater 2006;18:2280-2283

[463] Cheng S, Zhao YH, Zhu YT, Ma E. Optimizing the strength and ductility of fine structured 2024 Al alloy by nano-precipitation. Acta Mater 2007;55:5822-5832.

[464] Vinogradov A, Patlan V, Suzuki Y, Kitagawa K, Kopylov VI.Structure and properties of ultra-fine grain Cu–Cr–Zr alloy produced by equal-channel angular pressing. Acta Mater 2002;50:1639-1651

[465] Ukai S, Fujiwara M. Perspective of ODS alloys application in nuclear environments. J Nucl Mater 2002;307-311:749-757

[466] Zhang L, Ukai S, Hoshino T, Hayashi S, Qu X. Y_2O_3 evolution and dispersion refinement in Co-base ODS alloys. Acta Mater 2009 ;57 :3671-3682

[467] Williams CA, Unifantowic P, Baluc N, Smith GDW, Marquis EA. The formation and evolution of oxide particles in oxide-dispersion-strengthened ferritic steels. Acta Mater 2013;61:2219-2235

[468] Lassance D, Fabrègue D, Delannay F, Pardoen T. Micromechanics of room and high temperature fracture in 6xxx Al alloys. Prog Mater Sci 2007;52:62-129

[469] Robson JD, Stanford N, Barnett MR. Effect of precipitate shape on slip and twinning in magnesium alloys. Acta Mater 2011;59:1945-1956

[470] Stanford N, Geng J, Chun YB, Davies CHJ, Nie JF, Barnett MR. Effect of plate-shaped particle distributions on the deformation behaviour of magnesium alloy AZ91. Acta Mater 2012;60:218-228

[471] Robson JD, Stanford N, Barnett MR. Effect of Precipitate Shape and Habit on Mechanical Asymmetry in Magnesium Alloys. Metall Mater Trans A 2013;44:2984-2995

[472] Bhatia MI. Recrystallisation—Some applied aspects. Prog Mater Sci 1997;42:59-77

[473] Pollock TM. Alloy design for aircraft engines. Nat Mater 2016 ;15:809-815

[474] Williams JC, Starke EA. Progress in structural materials for aerospace systems. Acta Mater 2003;51:5775-5799

[475] https://commons.wikimedia.org/wiki/File%3AJet_engine.svg

[476] Reed RC. The Superalloys. Cambridge Univ Press 2006.

[477] Mathur HN, Panwisawas C, Jones CN, Reed RC, Rae CMF. Nucleation of recrystallisation in castings of single crystal Ni-based superalloys. Acta Mater 2017;129:112-123

[478] Fecht H, Furrer D. Processing of Nickel-Base Superalloys for Turbine Engine Disc Applications. Adv Eng Mater 2000;2:777-787

[479] Sallez N, Boulnat X, Borbély A, Béchade JL, Fabrègue D, Perez M, de Carian Y, Hennet L, Mocuta C, Thiaudière D, Bréchet Y. In situ characterization of microstructural instabilities: Recovery,recrystallization and abnormal growth in nanoreinforced steel powder. Acta Mater 2015;87:377–389

[480] Huang L, Jiang L, Topping TD, Dai C, Wang X, Carpenter R, Haines C, Schoenung JM. In situ oxide dispersion strengthened tungsten alloys with high compressive strength and high strain-to-failure. Acta Mater 2017;122:19-31

[481] Liu G, Zhang GJ, Jiang F, Ding XD, Sun YJ, Sun J, Ma E. Nanostructured high-strength molybdenum alloys with unprecedented tensile ductility. Nat Mater 2013;12:344-350

[482] Levy GN, Schindel R, Kruth JP. Rapid manufacturing and rapid tooling with layer manufacturing (LM) technologies, state of the art and future perspectives. CIRP Ann Manuf Technol 2003;52 :589-609

[483] Gu DD, Meiners W, Wissenbach K, Poprawe R. Laser additive manufacturing of metallic components: materials, processes and mechanisms. Int Mater Rev 2012;57:133-164

[484] Frazier WE. Metal Additive Manufacturing: A Review. J Mater Eng Perform 2014;23:1917-1928

[485] Thijs L, Verhaeghe F, Craeghs T, Van Humbeeck Jan, Kruth JP. A study of the microstructural evolution during selective laser melting of Ti–6Al–4V. Acta Mater 2010;58:3303-3312

[486] Zhang LC, Attar H. Selective laser melting of titanium alloys and titanium matrix composites for biomedical applications: a review. Adv Eng Mater 2016;18:463-475

[487] Amato KN, Gaytan SM, Murr LE, Martinez E, Shindo PW, Hernandez J, Collins S, Medina F. Microstructures and mechanical behavior of Inconel 718 fabricated by selective laser melting. Acta Mater 2012;60:2229-2239

[488] Ding Y, Muniz-Lerma JA, Trask M, Chou S, Walker A, Brochu M. Microstructure and mechanical property considerations in additive manufacturing of aluminum alloys. MRS Bulletin 2016;41:745-751

[489] Li X, Kong C, Becker T, Sercombe T. Investigation of Interfacial Reaction Products and Stress Distribution in Selective Laser Melted. Adv Eng Mater 2016;18:1337-1341

[490] Li XP, Ji G, Chen Z, Addad A, Wu Y, Wang HW, Vleugels J, Van Humbeeck J, Kruth JP. Selective laser melting of nano-TiB_2 decorated AlSi10Mg alloy with high fracture strength and ductility. Acta Mater 2017;129:183-193

[491] Dehoff RR, Babu SS. Characterization of interfacial microstructures in 3003 aluminum alloy blocks fabricated by ultrasonic additive manufacturing. Acta Mater 2010;13:4305-4315

[492] Shimizu S, Fujii HT, Sato YS, Kokawa H, Sriraman MR, Babu SS. Mechanism of weld formation during very-high-power ultrasonic additive manufacturing of Al alloy 6061. Acta Mater 2014;74:234-243

[493] Li D, Soar RC. Plastic flow and work hardening of Al alloy matrices during ultrasonic consolidation fibre embedding process. Mater Sci Eng A 2008;498:421-429.

[494] Fujii HT, Sriraman MR, Babu SS. Quantitative Evaluation of Bulk and Interface Microstructures in Al-3003 Alloy Builds Made by Very High Power Ultrasonic Additive Manufacturing. Metall Mater Trans A 2011;42:4045-4055

[495] Palanivel S, Nelaturu P, Glass B, Mishra RX. Friction stir additive manufacturing for high structural performance through microstructural control in an Mg based WE43 alloy. Mater Des 2015;65:934-952

[496] Boegelein T, Dryepondt SN, Pandey A, Dawson K, Tatlock GJ. Mechanical response and deformation mechanisms of ferritic oxide dispersion strengthened steel. Acta Mater 2015;87:201-215

[497] Ventura AP, Wade CA, Pawlikowski G, Bayes M, Watanabe M, Misiolek WZ. Mechanical Properties and Microstructural Characterization of Cu-4.3 Pct Sn Fabricated by Selective Laser Melting. Metall Mater Trans A 2017;48:178-187

[498] Langdon TG. Seventy-five years of superplasticity: historic developments and new opportunities. J Mater Sci 2009;44:5998-6010

[499] Barnes AJ. Superplastic Forming 40 Years and Still Growing. J Mater Eng Perform 2007;16:440-454

[500] Krajewski PE, Schroth JG. Overview of quick plastic forming technology. Mater Sci For 2007;551-552 :3-12

[501] Markus H, Sulinski H, Waldman J. Processes for the fabrication of 7000 series aluminum alloys. US Patent 3847681, 1974

[502] Paton NE, Hamilton CH. Method of imparting a fine grain structure to aluminum alloys having precipitating constituents. US Patent 4092181, 1978

[503] Pérez-Prado MT, Gonzalez-Doncel G, Ruano OA, McNelley TR. Texture analysis of the transition from slip to grain boundary sliding in a discontinuously recrystallized superplastic aluminum alloy. Acta Mater 2001;49:2259-2268

[504] Troeger LP, Starke EA. Microstructural and mechanical characterization of a superplastic 6XXX aluminum alloy. Mater Sci Eng A 2000;277:102-113

[505] Mikhaylovskaya AV, Kotov AD, Pozdniakov AV, Portnoy VK. A high-strength aluminium-based alloy with advanced superplasticity. J Alloy Compd 2014;599:139-144

[506] Nieh TG, Hsiung LM, Wadsworth J, Kaibyshev R. High strain rate superplasticity in a continuously recrystallized Al–6%Mg–0.3%Sc alloy. Acta Mater 1998;46:2789-2800

[507] Mohamed FA, Ahmed MMI, Langdon TG. Factors influencing ductility in the superplastic Zn-22 Pct Al eutectoid. Metall Trans A 1977;8:933-938

[508] Langdon TG. Achieving superplasticity in ultrafine-grained metals. Mech Mater. 2013;67:2-8

[509] Rashid M, Kim C, Ryntz E, Saunders F, Verma R, Kim S. Quick plastic forming of aluminum alloy sheet metal. US. Patent 6253588, 2001.

[510] Deardo AJ. Niobium in modern steels. Int Mater Rev 2003;48:371-402

[511] Zhao Z, Mao W, Roters F, Raabe D. A texture optimization study for minimum earing in aluminium by use of a texture component crystal plasticity finite element method. Acta Mater 2004;52:1003-1012

[512] Hutchinson WB, Oscarsson A, Karlsson Å. Control of microstructure and earing behaviour in aluminium alloy AA 3004 hot bands. Mater Sci Technol 1989;5:1118-1127

[513] Hutchinson WB, Ekström HE. Control of annealing texture and earing in non-hardenable aluminium alloys. Mater Sci Technol 1990;6:1103-1112